1987

High cycle fatigue behavior of welded details under variable amplitude loading, PhD dissertation, September 1987, 192p.

Peter B. Keating

High Cycle Fatigue Behavior of Welded Details Under Variable Amplitude Loading

by

Peter B. Keating

A Dissertation

Presented to the Graduate Committee

of Lehigh University

in Candidacy for the Degree of

Doctor of Philosophy

in

Civil Engineering

Lehigh University

Bethlehem, Pennsylvania

September 1987

Approved and recommended for acceptance as a dissertation in partial fulfillment of the requirements for the degree of Doctor of Philosophy.

April 24, 1987
(date)

John W. Fisher
Professor in Charge

Accepted Sept. 11, 1987
(date)

Special committee directing
the doctoral work of
Peter B. Keating

Professor B.T. Yen
Chairman

Professor R.G. Slutter

Professor I.J. Kugelman
Chairman
Department of Civil Engineering

Professor R.W. Hertzberg

Acknowledgments

The analytical study reported herein was conducted at Fritz Engineering Laboratory, Lehigh University, Bethlehem, Pennsylvania. Dr. Irwin J. Kugelman is the Chairman of the Department of Civil Engineering.

The work for this study was performed while the author was a Research Assistant for Project 12-15(5) of the National Cooperative Highway Research Program conducted by the Transportation Research Board. The four years spent on the project and its scope allowed an unique exposure to a large number of aspects relating to the high cycle fatigue behavior of welded steel details. This includes the fatigue test review and the resulting revisions to the AASHTO fatigue design provisions in 1987.

The author is indebted to Dr. John W. Fisher, the supervisor of the doctoral work, without who's time, patience, and contributions, this work would not have been possible. The five years spent under his supervision provided a truely unique setting for the study of fatigue and it's practical application. This has included not only analytical and laboratory studies but also valuable field exposure to in-service fatigue problems. It has left the author with the realization that one must always take a few steps back and view research results in a more general sense when a practical solution to a problem is desired. All of this has given the author a broadly based view of fatigue and fracture that could not have been duplicated anywhere else.

The author is also grateful for the contributions made by the other members of the doctoral committee. This includes Dr. Ben T. Yen, Committee Chairman, for his unique sense of practicality. Dr. Roger G. Slutter for his knowledge of large-scale testing. And Dr. Richard W. Hertzberg and his ability

to convey research results in a lucid and meaningful manner. All three have made significant contributions to the professional and academic development of the author.

The author wishes to thank George R. Irwin for his views on fatigue and fracture and how they relate to this study. To Ian Smith of the Swiss Federal Institute, Lausanna; Chitoshi Miki of the Tokyo Institute of Technology; and J. Hartley Danials, Lehigh University for their time and views on various subjects pertaining to this research. In addition, thanks are extended to William Conway and Donald Sorgenfri of the New Orleans office of Modjeski and Masters for providing the valuable work experience prior to the start of the author's graduate study in Structures. And to Harry Roeker, also of Modjeski and Masters, for teaching the author the art of bridge inspection.

Various people have helped to manage the trials and tribulations of a graduate program at Lehigh. This includes Mrs. Ruth Grimes for her help with typing and administrative tasks. Jack Gera and Pedro Kaye for help in the drafting of figures, and Richard Sopko for his expertise on photography. Monica Newman, Dean Krause, and Ann Marie Matusa of the Lehigh University Computing Center for all their time and effort spent in providing assistance with the preparation of the final manuscript. And to all those who passed through Room 420, Fritz Lab while the author remained.

Finally, but most importantly, sincere thanks and gratification are extended to Sabrina Watkins who took the author out of the water and up on to the bridge. Without her subtle but timely influence on the life of the author, all of this would not have come about.

Table of Contents

List of Figures

List of Tables

Abstract

The fatigue behavior of full-scale welded steel bridge details subjected to variable amplitude loading is examined. This classification of structural details requires the evaluation of their fatigue behavior in a more general perspective than what has currently been done. While extensive variable amplitude fatigue testing has been conducted on small-scale specimens, few test programs have involved large-scale specimens. The fatigue behavior of full-scale welded details is dominated by the existence of residual tensile stresses. The magnitude of these stresses is such that they are at or near the yield stress, regardless of the steel type and do not redistribute under the cyclic loading that a bridge type structure is normally subjected to. Due to the presence of the local tensile residual stresses and the limited range of global dead load and live load stresses, fatigue crack propagation must be considered in terms of high effective stress ratios. Small-scale specimens seldom accurately simulate this stress state, nor do they provide a defect size and distribution compatible with those commonly found in actual bridge details.

Because of the existence of high stress ratios due to residual stresses at crack initiation sites, fatigue crack propagation can be considered to occur at an upper bound rate. Fatigue crack growth studies have shown that as the stress ratio increases, fatigue crack propagation increases towards a limiting upper bound. With crack growth at high stress ratios, crack tip closure is reduced to the degree that cycle interaction effects become negligible. This includes both crack growth delay from overload cycles and crack growth acceleration from underloads. When fatigue crack propagation occurs along a single growth curve, then the basic assumptions of Miner's cumulative damage law are satisfied. The

use of Miner's Rule with an upper bound fatigue crack growth rate will provide a lower bound, conservative estimate of fatigue damage resulting from variable amplitude loading.

In the high cycle region, a substantial portion of fatigue life is devoted to crack initiation or crack growth at low rates. In addition, only the portion of stress cycles in the variable amplitude stress spectrum that are above the fatigue limit will contribute to fatigue crack propagation. The use of Miner's Rule may seem to be invalid. However, uncertainties exist in the fatigue design and evaluation procedures. This includes the variability in the crack growth threshold values and the inability to predict future bridge loads. The straight-line extension of the fatigue design resistance curves below the constant amplitude fatigue limits, coupled with the use of Miner's Rule, provides a lower bound estimate of fatigue strength and is compatible with available test data.

The effects of stress range spectrum shape and low cycle truncation on fatigue life estimate were also studied. For typical highway bridge stress spectrums, it was found that fatigue life was generally overestimated as non-contributing stress cycles were introduced into the life calculation. However, the inclusion of relatively small stress cycles had no major effect on fatigue life and only represented a movement along the fatigue resistance curve. It was concluded that for fatigue design, the present AASHTO procedure of using an artificially high stress range with an artificially low number of stress cycles is entirely adequate and provide a reasonable estimate of fatigue life.

Chapter 1
Introduction

1.1 Problem Statement

Current bridge design specifications are based on constant amplitude fatigue test data, while the loading experienced by bridge structures is both variable and random in nature. Over the years, extensive research has been conducted in an effort to relate the damage done by variable amplitude loading to the fatigue resistance of welded steel details as defined by the constant amplitude fatigue test data. A number of hypotheses or methods have been proposed that deal with the estimation of fatigue damage due to variable amplitude loading. The most widely recognized and used method to date was proposed by Miner[1] in 1945 and is currently referred to as Miner's Cumulative Damage Rule, or simply Miner's Rule. Briefly, the rule states that the number of load cycles applied, as expressed as a percentage of the number to failure at a given stress level, would be the proportion of useful life expended. When the total damage reached 100 percent, the specimen or member should fail. This results in a relatively simple method to deal with the problem of variable amplitude loading.

With the development of the arc welding process and its eventual application to steel highway bridges in the early 1960's, there has been an increasing awareness of the variable amplitude problem and how it relates to welded steel bridge details. There has been continued concern as to the validity of Miner's Rule as applied to this type of loading in two respects. First and foremost, the validity of the rule has been questioned. Experimental fatigue

test programs by Gurney[2, 3] and others[4, 5] have shown Miner's Rule to be unconservative for certain load spectra. This has given rise to a number of non-linear cumulative damage rules. Secondly, there has always been the question of how to estimate fatigue damage from load spectra that have a portion of the stress cycles below the constant amplitude fatigue limit. Various methods have been proposed that range from ignoring those cycles below the limit to the assumption that all cycles in the spectrum contribute to growth. A number of methods have been proposed in between these bounds. Haibach[6] has suggested that the slope of the S-N curve be changed from -3.0 to -5.0 below the constant amplitude fatigue limit. Tilly[7] has proposed a similar method; using two exponents to represent the constant amplitude fatigue curve. Both Yamada[8] and Schilling[9] have proposed the use of a variable amplitude fatigue limit determined as a function of the constant amplitude fatigue limit and the stress range spectrum. The cycles that fall below this variable limit are assumed not to contribute to crack growth.

Over the past ten years fatigue cracks have developed in in-service bridge details. These details, designed in accordance with earlier fatigue specifications, were subjected to stress cycles that exceed the current AASHTO fatigue limit. The rate of exceedance in most cases was quite low, usually below ten percent. In several cases, cracks were found in beams of bridges where the exceedance rate of the fatigue limit was estimated to be only 0.1 percent of the total number of stress cycles.[10] Available experimental results have shown that if only a relatively small portion of the cycles in the spectrum exceed the constant amplitude fatigue limit, cracking will occur. The extent of the fatigue cracking appears to be such that nearly all cycles are contributing to fatigue crack

propagation. That is, the cycles which are below the fatigue limit as well as those which exceed it cause crack growth.

The observed behavior of crack growth under variable loading, both experimental and actual, suggests that fatigue damage in bridges is more severe than originally assumed or implied in the fatigue design codes. Over the years the magnitude of the loads which bridges are subjected to have increased. This has been due to the general increase in truck weights and the increase in the number of permits or overloads allowed. As bridges are subjected to heavier loads in the future, it can be anticipated that more critical fatigue problems will occur which will significantly reduce the assumed fatigue life of a given welded structure.

1.2 Objectives

The main objective of this study is to evaluate the fatigue life behavior and fatigue resistance of welded bridge details subjected to variable amplitude loading both above and below the constant amplitude fatigue limit. The fatigue limit being defined as the maximum constant amplitude stress range that a given detail can be cycled indefinitely without showing any evidence of fatigue crack growth.

For stress range spectra in which all cycles are above the constant amplitude fatigue limit, it will be shown that Miner's Rule provides a correct estimate for cumulative damage of full-scale welded steel details subjected to variable amplitude loading when used in conjunction with large-scale fatigue test data. Fatigue resistance curves derived from large-scale test data provide the lower bound estimate of fatigue resistance that is consistent with Miner's Rule. Anomalies that exist in the literature are primarily due to small-scale test data

and using that data to evaluate full-scale structures' fatigue behavior.

For high cycle fatigue, where a major portion of the stress spectrum falls below the constant amplitude fatigue limit, it will be shown that the straight-line extension of the fatigue resistance curve is the correct lower bound estimate for use in both design of new structures and the evaluation of existing structures. While for a single detail type and a known load spectrum, the straight-line extension provide an overly conservative estimate of fatigue resistance, the variability inherent in structural detail types and loading conditions for both design and evaluation, almost always, result in a decrease in fatigue resistance. It is this variability that necessitates the use of the straight-line extension below the constant amplitude fatigue limit to define the fatigue resistance of full-scale welded steel details subjected to variable amplitude loading.

1.3 Scope

It is important to emphasize that the focus of this research will be towards the study of welded steel bridge details or similar type structural elements. In addition to highway and railroad bridges, comparable type details can be found in cranes, large welded vehicular frames, ships, and offshore structures. This classification of details possesses a certain type of uniqueness that distinguishes it from other structural classifications such as riveted and bolted structures, and aircraft structures. The two significant parameters which result in this differentiation are: the actual loadings that bridges are subjected to and the magnitude of the residual stresses found in welded steel structures. The loads to which bridges are subjected, both dead and live, result in a narrow range for the value of the stress ratio that actually occurs at welded

bridge details. The welding of the steel components result in zones of high residual stress that have a dominating effect on fatigue behavior throughout most of the life of the structure. Due to these two influential parameters, the evaluation of experimental test data must be performed with this uniqueness in mind. This should result in the elimination of many unnecessary parameters that can easily complicate a study of the fatigue behavior of welded steel bridge details subjected to variable amplitude loading.

Extensive use of fracture mechanics principles will be used to help describe the fatigue behavior of welded steel details. Specifically, the application of principles will be viewed in light of the fact that fatigue crack growth occurs in a zone of high residual tensile stress. The combination of the loading and the welding residual stresses result in a high effective stress ratio. Crack growth studies have shown that as the stress ratio increases, fatigue crack propagation rates also increase. Other fatigue tests involving occasional overload cycles have shown an interaction effect between cycles resulting in crack growth retardation. A careful review of the data shows that the interaction effect, and thus the amount of growth delay, decreases as the stress ratio is increased. The crack closure concept can be used to explain these effects as well as the apparent unconservativeness of Miner's Rule when applied to fatigue crack propagation specimens and small scale specimens.

A review of pertinent fatigue test data will be conducted. When viewed with the effect of high residual stresses and high stress ratios, many of the anomalies in the conclusions that have been reached from the test data over the years can be resolved. Since fatigue testing of full-scale specimens in the high cycle region requires high load capacity equipment and inordinate amounts of

time, most fatigue testing in this region is performed on smaller scale specimens. But these test conditions seldom simulate actual conditions. The existing large-scale fatigue test results define the fatigue behavior of welded steel bridge details when proper consideration is given to the influence of high magnitude residual stress fields.

In order to examine the variability of parameters influencing high cycle fatigue behavior, a fatigue crack propagation model will be developed. This simulation model will be based on linear elastic fracture mechanics, using the range of stress intensity concept at the crack tip as the driving force of fatigue crack propagation. Variability in fatigue design enters into both sides of the load-resistance equation. On the resistance side, the variability in the constant amplitude fatigue limit, or in more general terms, the variability in the fatigue crack propagation threshold value, will affect the fatigue strength of welded steel details. For a given stress range spectrum loading at or near the constant amplitude fatigue limit, the actual fatigue crack propagation threshold value will govern the amount of cumulative damage. Conversely, on the other side of the equation, the variability in the load spectrum will be studied. As the resulting stress spectrum increases due to increasing loads, a greater portion of the stress cycles are above the crack growth threshold value, thus increasing fatigue damage. In addition, the fatigue crack propagation model will be correlated with existing fatigue test data in order to explain the high cycle behavior of the data and the influence of the constant amplitude fatigue limit on the test results.

Chapter 2
Background

2.1 Early Development of Fatigue Design Criteria

The use of welded structures significantly increased with the development and expansion of the interstate highway system beginning in the early 1960's. It eventually became evident in the mid 1970's that the welding of steel bridge components could result in details that had relatively short fatigue lives. There were several cases in which fatigue cracks developed in bridges due to an inadequate knowledge of low fatigue strength details. An early research program, commonly known as the AASHO Road Test, indicated that fatigue crack growth could be expected in welded details when subjected to high stress range conditions resulting from simulated truck traffic.[11] This particular research program formed the basis for much of the fatigue research that followed.

Early fatigue design specifications required a reduction in the allowable maximum stress when the structural member was subjected to load reversals. The allowable stress was expressed in terms of the maximum stress and varied with the stress ratio, defined as the algebraic ratio of minimum and maximum stress. The provisions were based on the available data at the time and consisted mainly of small-scale plate specimens. Two million cycles was generally assumed to be the run-out or infinite life condition.

A major revision to the bridge fatigue specifications occurred in 1965 when AASHO adopted new steel bridge fatigue provisions.[12] This new set of fatigue provisions was based on additional fatigue test data and a re-examination of

older data. Basically, there were nine separate classifications of fatigue life for various types of conditions and details. Although there was no differentiation between the various welded attachment details that were commonly used in bridge design and fabrication; the allowable fatigue stress for a given detail was based on the maximum stress, with provisions for stress ratio and the steel yield stress. Some details and members of high strength steels were permitted higher allowable stresses.

While fatigue research continued, there still did not exist a single comprehensive test program that allowed for the systematic analysis of a large database that would reveal the significant parameters important in describing the fatigue behavior of welded bridge details. Often, many variables were introduced into an experiment with a limited number of test specimens. This made it impossible to establish clearly the statistical significance that stress variables, types of details, steel type, and quality of fabrication had on fatigue life. Failure to properly control and measure the variables influencing the fatigue strength resulted in apparent conflicts and contradictory claims on the stress variables and material characteristics.

2.2 National Cooperative Highway Research Program Project 12-7

2.2.1 Test program

National Cooperative Highway Research Program (NCHRP) Project 12-7 was developed to provide a statistically designed experimental program under controlled laboratory conditions.[13, 14] The program involved the fatigue testing of some 530 test beams and girders with two or more welded details each. Large size specimens were used to overcome some of the limitations of smaller, simulated specimens, such as: residual stress fields, defect size and distributions, and shear size. The specimens were fabricated with various details that are common to steel bridges, including coverplates, web and flange attachments, and web stiffeners. Three different types of steels were used to study the influence of yield stress on fatigue life: A36, A441, and A514. This provided a range of nominal yield stress that varied from 36 to 100 ksi.

The principle design variables for the study were those associated with three major categories: type of detail, stress condition, and type of steel. Minimum stress, maximum stress, and the stress range were selected as the controlled stress variables. This permitted variation in one variable while the others were maintained at a constant level. This was the first program that effectively controlled the design factors that influenced fatigue behavior.

2.2.2 Findings

With all of the different variables studied in the NCHRP project 12-7, only two significantly influenced the fatigue strength of welded details: stress range and detail type. These findings were observed to be applicable to every beam and detail examined in the project. The major reason for this simplification was the fact that as-welded steel structures contain localized residual stresses from the welding process and are of such magnitude that other

stress parameters can be eliminated from consideration. All welding processes result in high residual stresses, which are at or near the yield stress in the weldment and adjacent base metal. Thus, in the initial stages of fatigue crack growth in an as-welded structure, most of the fatigue life occurs in regions of high tensile residual stress. Under cyclic loading, the material at or near the initial discontinuities will be subjected to a fully effective tensile cyclic stress, even in the case of stress reversal. As a result, the stress ratio does not play a significant role when describing the fatigue strength of welded details since the maximum stress at a point of fatigue crack initiation and growth is, almost always, at yield stress.

Fatigue test data for the welded beams are plotted in Figs. 2-1 and 2-2 using the logarithmic transformation of both stress range and the number of cycles to failure. In Fig. 2-1, the data has been differentiated by steel type (yield stress). The uniform scatter of the data points indicate that the steel type does not significantly affect fatigue life. Figure 2-2 gives the same set of welded beam data, but plotted to show the different minimum stress levels. Again, the uniform scatter indicates that the minimum stress parameter does not play an important role in describing fatigue behavior.

With the stress range being the only important stress parameter in determining fatigue life, a stress range (S), cycle life (N) relationship could be developed. Regression analysis showed that this relation was log-log in nature, with a constant slope. The S-N curves are defined in log form by:

$$\log N = \log A - B \cdot \log Sr \tag{2.1}$$

and in exponential form by:

$$N = A \cdot Sr^{-B} \tag{2.2}$$

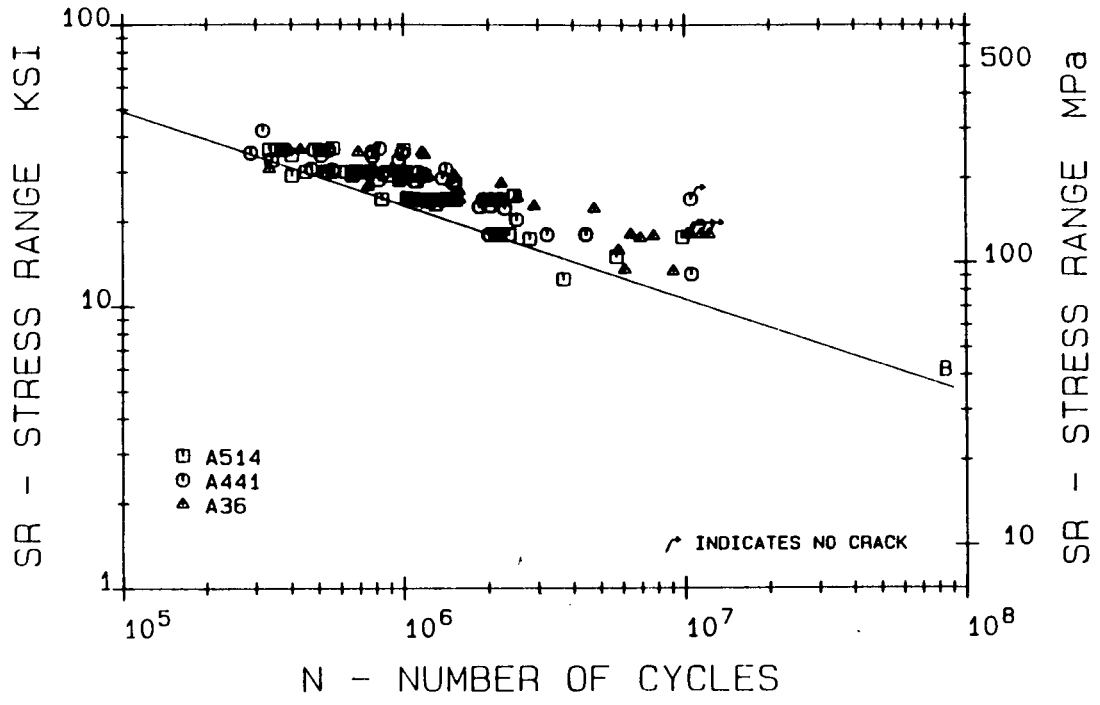

Figure 2-1: Effect of steel type on fatigue strength

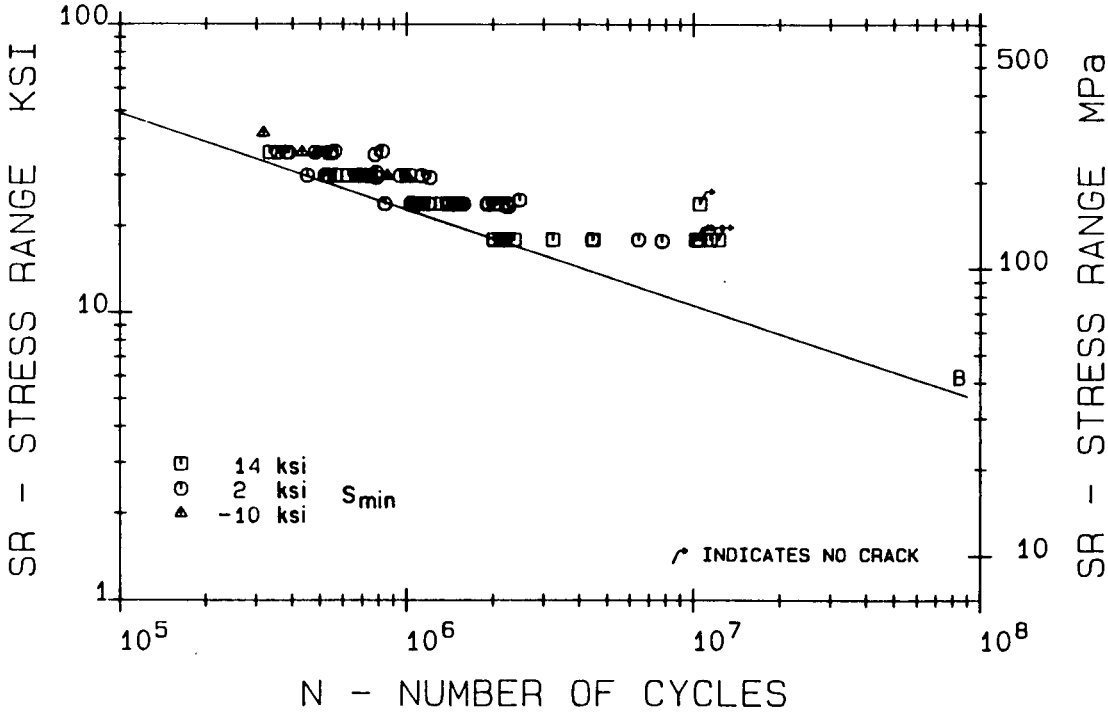

Figure 2-2: Effect of minimum stress on fatigue strength

where N is the number of cycles to failure, Sr is the nominal stress range, log A is the log-N-axis intercept of the S-N curve and B is the slope of the curve.

Six different categories were used to classify the fatigue strength of the details used in the test program. The categories were defined by the 95 percent confidence limits for 95 percent survival based on the regression analysis of the test data and are represented by a set of S-N curves. These fatigue design curves are shown in Fig. 2-3.

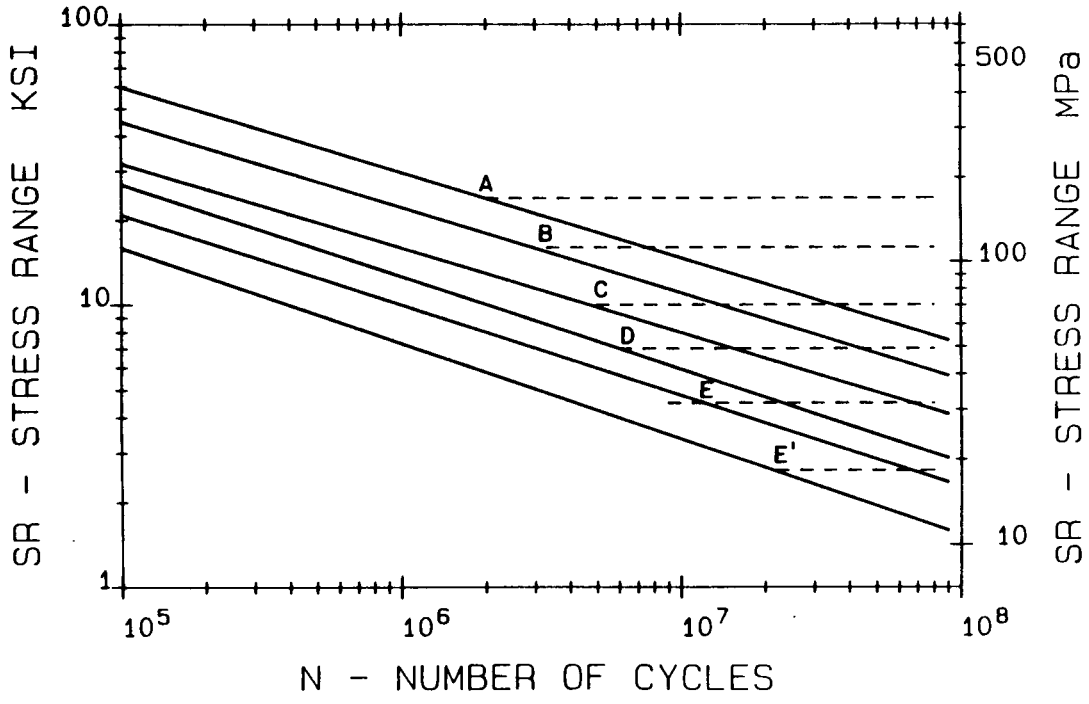

Figure 2-3: 1974 AASHTO Fatigue Design Curves

The linear regression analysis for each category yielded a unique value for the slope, which was then used to set the slope of the lower confidence limit used for the design curve. The slope, mean intercept value, standard deviation, and lower confidence intercept value for each design curve are shown in Table 2-1. All curves have similar slopes and have a slope of approximately -3.0. The stress range, cycle life relationships and corresponding curves were used to

Category	Slope	Intercept (mean)	Standard Deviation	Intercept (lower)
A	3.178	11.121	0.221	10.688
B	3.372	10.870	0.147	10.582
C	3.25	10.038	0.063	9.915
D	3.071	9.664	0.108	9.453
E	3.095	9.292	0.101	9.094
E′	3.000	------	------	8.610

Table 2-1: Regression analysis coefficients for 1983 AASHTO curves

provide the limits or bounds for all possible details that are normally encountered in the design of bridges and similar type structures. The curves and the detail classifications were adopted by AASHTO in 1973 and issued as *Interim Specifications - 1974*.[15]

2.2.3 Limitations of original NCHRP fatigue database

While the NCHRP Project 12-7 provided the most comprehensive test program to date and provided a more rational basis for fatigue design provisions, limitations in the fatigue test database still existed. These limitations can be summarized as follows:

- Limited types of details were evaluated in each design category.

- Constant Amplitude Fatigue Limit was not well defined. Few test specimens were cycled at a low enough stress range to clearly establish its value and no tests were carried out beyond 10^7 cycles.

- No test data in the high cycle, long life fatigue region.

- The database consisted of constant amplitude test data; whereas bridges are subjected to variable amplitude loading.

2.3 NCHRP Variable Amplitude Fatigue Test Programs

Several National Cooperative Highway Research Program projects have been conducted that studied the fatigue behavior of large-scale welded details subjected to random, variable amplitude loading. NCHRP Project 12-12 (NCHRP Report 188[9]) dealt with the applicability of constant amplitude fatigue data and the resulting resistance curves to variable amplitude loading. NCHRP project 12-15(4) (NCHRP Report 267[16])extended the findings of Project 12-12 into the high cycle, long life regime of fatigue. Both projects used beam specimens similar in size to those used in the original NCHRP test program. A current (1987) NCHRP project has the objective of extending the findings of Project 12-15(4) further into the long life region.[17] The specimens in this test program are large-size welded plate girders with web stiffeners, web attachments, and thick coverplated flanges.

The results of these studies have indicated that both the Root-Mean-Cube (RMC) (Miner's linear damage hypothesis) and the Root-Mean-Square (RMS) stress range provide a means of relating random variable stress cycles to constant cycle data. The effective stress range is defined by:

$$Sr_e = [\ \Sigma\, \alpha_i \cdot Sr_i^{-B}\ ]^{1/B} \tag{2.3}$$

in which Sr_i is the midwidth of the i^{th} bar, or interval, in a frequency-of-occurrence histogram defining the variable amplitude spectrum and α_i is the

fraction of stress ranges within that interval. If B is taken as 2.0, Sr_e from this equation is equal to the root-mean-square of the stress ranges in the spectrum. If B is taken as the reciprocal of the slope of the constant amplitude S-N curve, 3.0, the equation is equivalent to the root-mean-cube or Miner's Rule.

For fatigue assessments where the total fatigue life is required resulting from some specified load spectrum, Miner's Rule ($B = 3.0$) will give a more conservative estimate of the life. Conversely, in the evaluation of variable amplitude fatigue test results, the RMS average of the stress spectrum will result in a more conservative estimate for fatigue resistance. For the spectrum shapes used in the NCHRP test programs, the difference between the two methods was found to be approximately 11 percent.

For NCHRP Project 12-12, large scale welded beam test specimens were used, similar to those used in the original NCHRP program. Detail types studied were the longitudinal web-to-flange fillet weld and the coverplate detail. Four different stress spectrums were used to study the influence on fatigue life.

Figure 2-4 shows the plot of fatigue failures for the plain welded beams with the AASHTO Category B resistance curve. The results are well distributed and all plot above the allowable stress range curve. This indicates that variable amplitude test data can be reasonably related to constant amplitude results by the effective stress range. The results for the coverplate beams are given in Fig. 2-5. Again, the results are consistent with the constant amplitude allowable stress range curve, in this case, Category E. The data in Figs. 2-4 and 2-5 are plotted using the RMC effective stress range. Given the fact that the plotted results include three types of steel and four different stress

spectra, the scatter of the data is reasonable. No significant difference was observed in the data between the four stress spectra.

The main objective of Project 12-15(4) was to study the effect of the frequency of overloads on the fatigue strength of welded details. An overload was defined as a stress cycle of magnitude greater than the constant amplitude fatigue limit. Detail types studied were coverplates and web attachments. The test specimens, rolled beams with welded attachments, were subjected to a random variable amplitude load spectrum with most of the stress cycles below the constant amplitude fatigue limit. Exceedance rates of the constant amplitude fatigue limit ranged from approximately 12 to 0.1 percent.

For the coverplated beams, it was found that the data were bounded by the Category E and E′ curves (Fig. 2-6). The fatigue resistance of the coverplate detail used in this detail is classified as Category E with a flange thickness of 0.57 in. The attached coverplate thickness was 1.0 in. Only two failures occurred at the Category E′ curve, with the remainder falling between the two curves or above Category E. The results indicate that for variable amplitude loading, the fatigue resistance is more adequately defined by the Category E′ curve. Similar results were found for the web attachments and are plotted in Fig. 2-7. The results are reasonably scattered in the high cycle region with nearly all of the points falling above the the Category E′ fatigue life curve. The plate thickness of the web attachment detail was 1.0 in. and is therefore at the limit between Category E and E′. The test data are consistent with the Category E′ curve.

From the test results of NCHRP Project 12-15(4), it was concluded that if any of the stress cycles exceeded the constant amplitude fatigue limit, fatigue

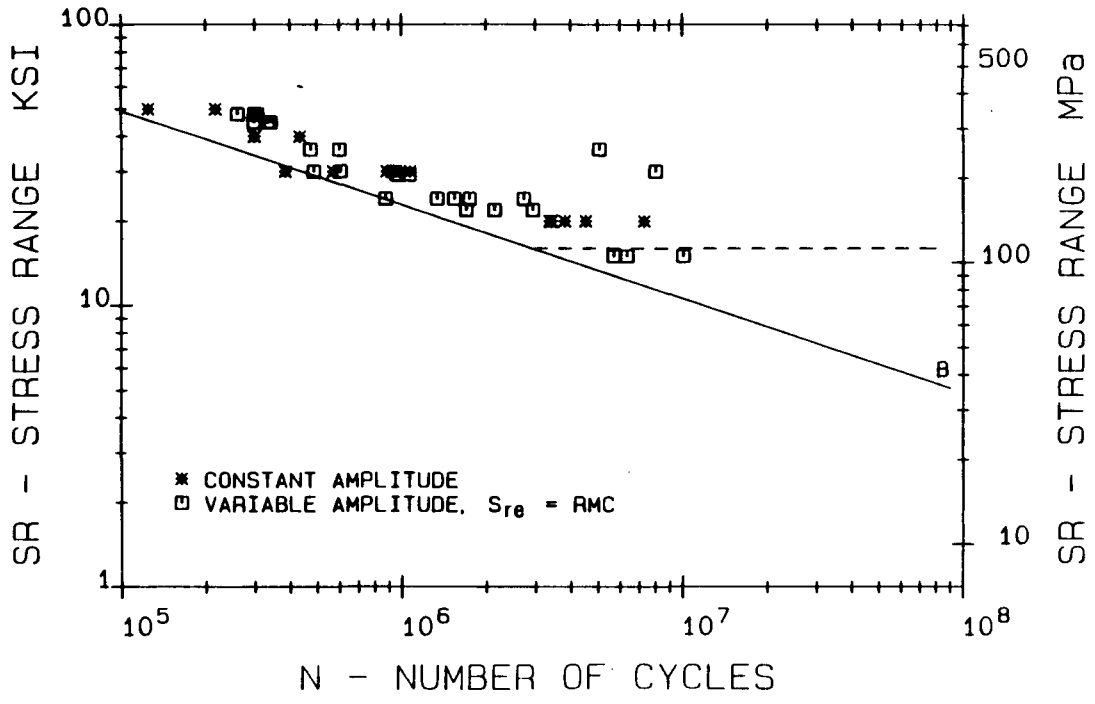

Figure 2-4: Test results for plain welded beams, NCHRP Project 12-12

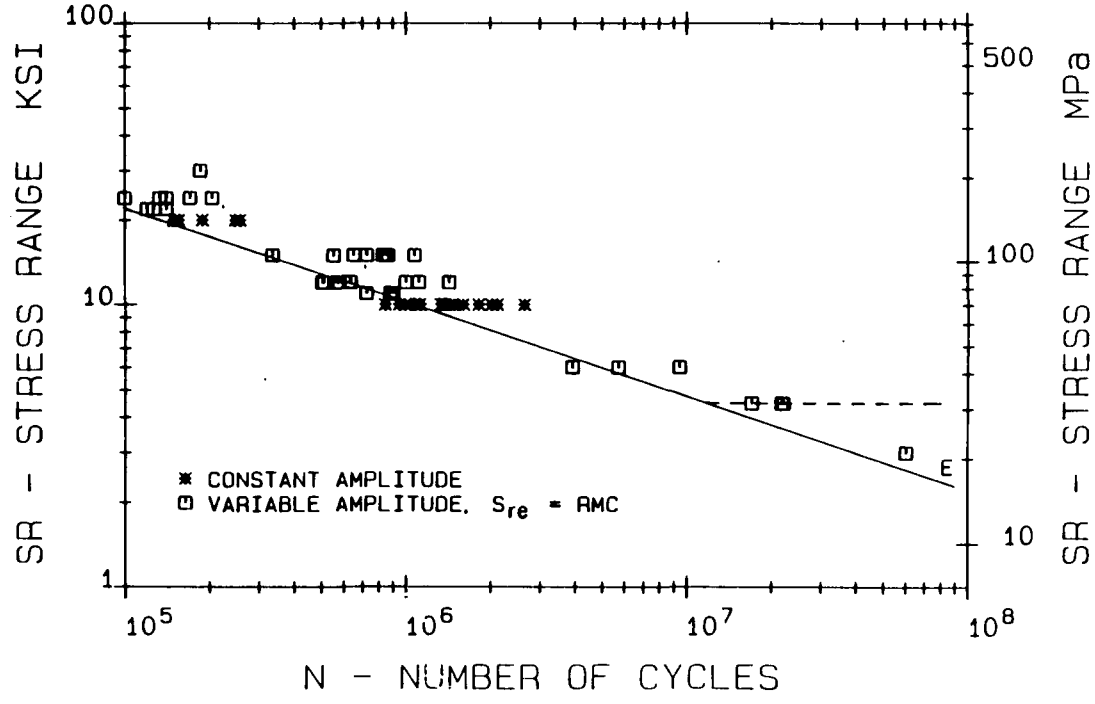

Figure 2-5: Test results for coverplated beam details, NCHRP Project 12-12

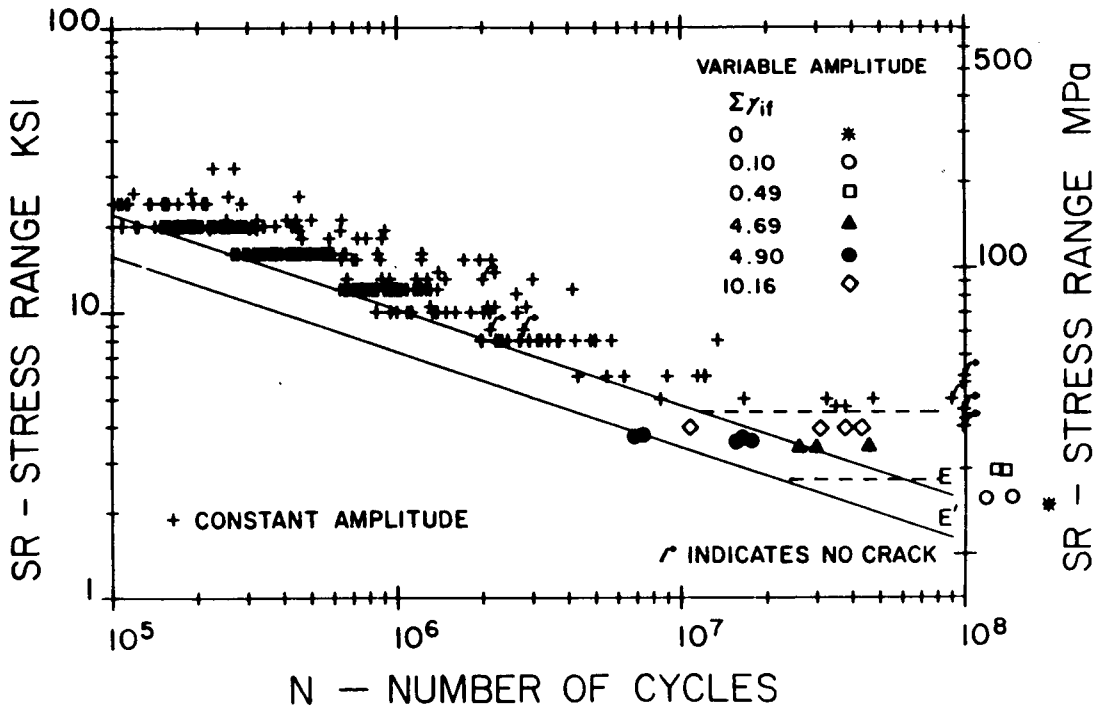

Figure 2-6: Test results for coverplated beam detail, NCHRP Project 12-15(4)

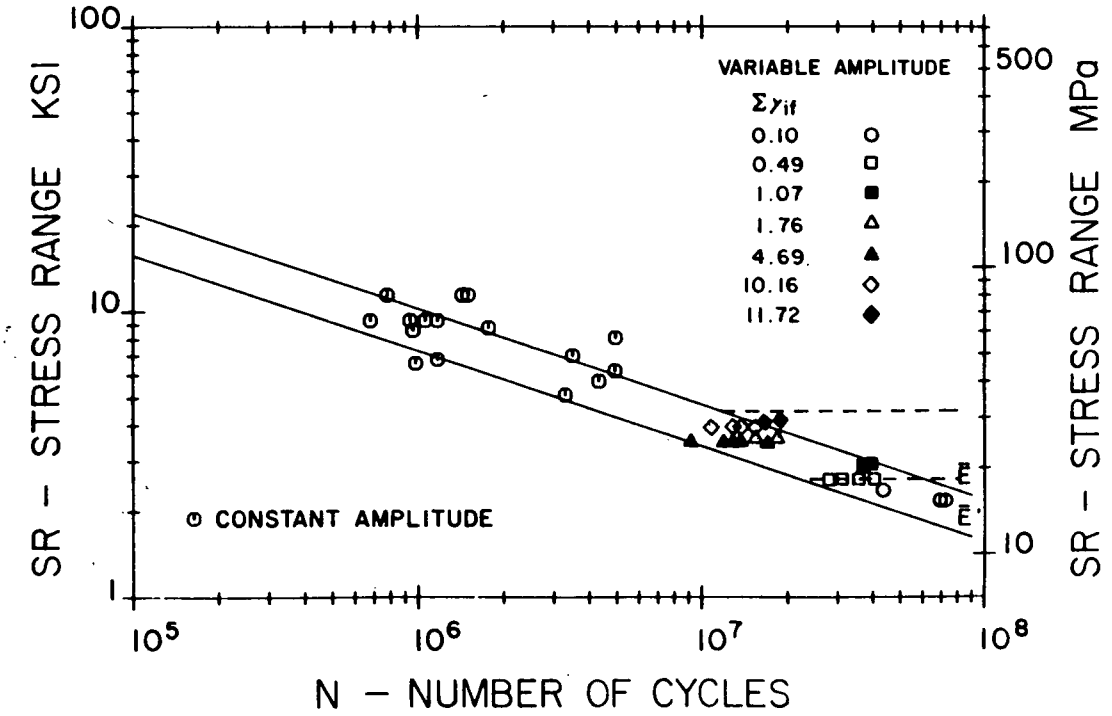

Figure 2-7: Test results for web attachments, NCHRP Project 12-15(4)

crack propagation would likely occur and fatigue life estimates should be based on the assumption that all stress cycles contribute to fatigue damage. This was found to hold for all exceedance rates. Therefore, the fatigue analysis of welded details subjected to variable amplitude loading requires that two stress parameters be considered: the effective stress range and the maximum stress range. Depending on the values of these two parameters and the value of the constant amplitude fatigue limit, three different cases can be encountered:

1. Effective stress range > Constant amplitude fatigue limit

2. Effective stress range < Constant amplitude fatigue limit
   Maximum stress range > Constant amplitude fatigue limit

3. Effective stress range < Constant amplitude fatigue limit
   Maximum stress range < Constant amplitude fatigue limit

For the first two cases, crack growth is defined by the S-N curve and it's straight line extension below the constant amplitude fatigue limit. Only for the situation represented by Case 3 is it assured that no crack growth will occur. The three cases are illustrated in Fig. 2-8.

The current NCHRP experimental program, Project 12-15(5), involves fatigue testing several bridge details at lower constant amplitude fatigue limit exceedance rates. A total of eight large-scale welded plate girders will be fatigue tested under a variable amplitude load spectrum for a minimum of 100 million cycles each. A randomized Rayleigh-type stress spectrum is used with the inclusion of an occasional overload above the constant amplitude fatigue limit. The frequencies of occurrence for the overloads are 0.1, 0.05, and 0.01 percent of the total stress range spectrum. The magnitude of the overload ranges from 7/6 of the constant amplitude fatigue limit for the 0.1 percent exceedance rate to 3/2 of the fatigue limit for the 0.01 percent exceedance rate.

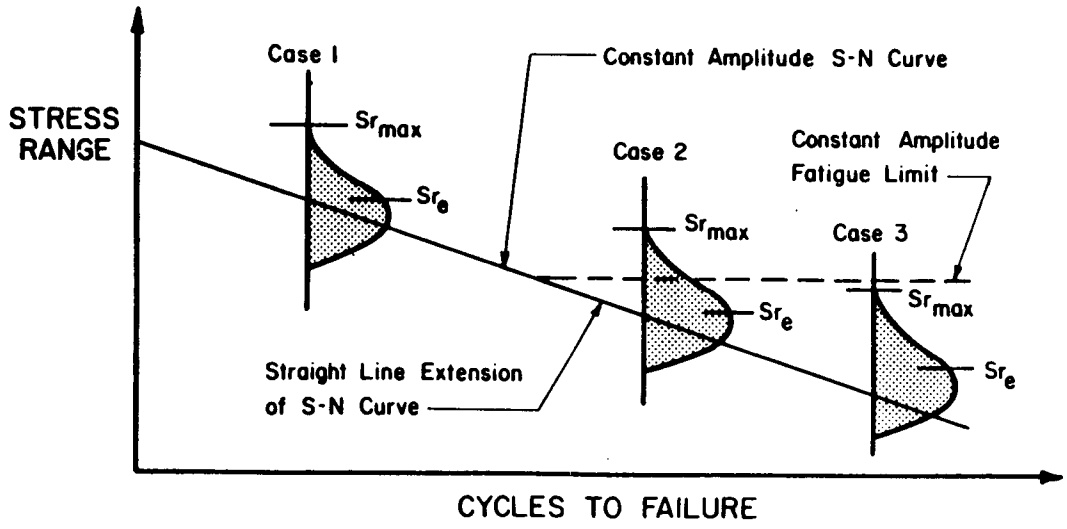

Figure 2-8: Three cases of variable amplitude stress spectrum

The test results from the first pair of test girders are given in Fig. 2-9 with the test results from NCHRP Project 12-15(4). Fatigue cracking occurred at three web attachment details. These attachments are 1.0 in. thick and are therefore classified as AASHTO Category E′. One detail, with an effective stress range of 2.4 ksi failed at 43.6 million cycles. While the constant amplitude fatigue limit of Category E′ is 2.6 ksi, the location of this particular detail gave an assumed fatigue limit of 4.2 ksi for a 0.1 percent exceedance rate. Using the Category E′ fatigue limit resulted in an exceedance rate of 14.6 percent. Fatigue crack growth was detected at a second web attachment detail at 81.7 million cycles. At this location, the load spectrum resulted in an effective stress range of 2.2 ksi with a peak value of 4.3 ksi. The third crack was detected at 100.7 million cycles, at an effective stress range of 1.4 ksi and a maximum stress range of 3.5 ksi. These data are plotted in Fig. 2-9 as open

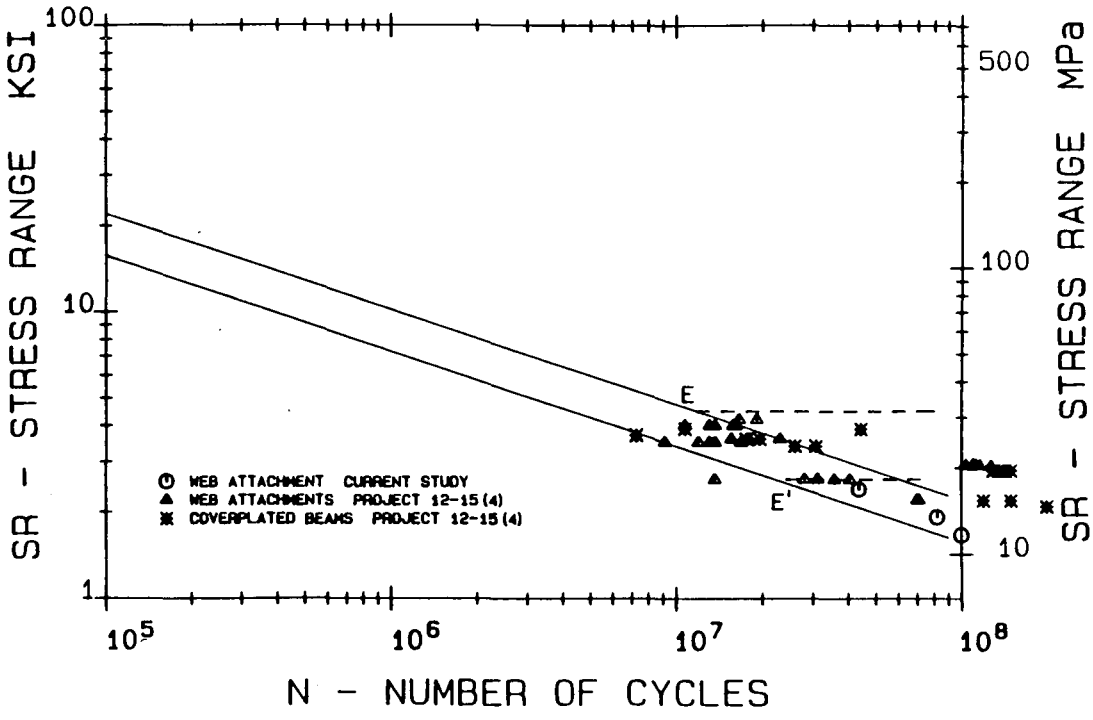

Figure 2-9: Fatigue test data, NCHRP Project 12-15(4) and 12-15(5)

circle symbols.

2.4 Other Variable Amplitude Fatigue Studies

The review of NCHRP sponsored variable amplitude fatigue test programs dealt with applied stress ranges that had a constant minimum stress level for all stress cycles, i.e., no cycle superposition. Ideally, each individual stress cycle represented the passage of a single truck. However, examination of stress histories for bridges under normal traffic loading shows the presence of complex stress cycles in which small amplitude or minor cycles are superimposed on a single, larger stress cycle. The minor cycles can be the result of dynamic effects, axle spacing, roadway surface condition, or multiple truck loading, and are all influenced by the span length of the bridge. A comparison between a simple stress cycle and a complex stress cycle is given in Fig. 2-10. Several

studies have been conducted to examine stress cycle superposition (complex stress cycles) and the ability of Miner's cumulative damage rule to accurately predict fatigue damage when there is stress cycle interaction.

A major difficulty in evaluating the fatigue damage caused by complex stress cycles is the determination of a single stress cycle. The individual component of a complex cycle must be transformed into an equivalent constant amplitude stress cycle. The generally accepted technique is commonly known as the rainflow cycle counting method.[18] The development of this technique is based on the compatibility between the stress history and the stress-strain diagram. An individual stress cycle is counted each time the stress strain hysteresis forms a closed loop. The cycle counting method is used to determine the basic cycle count (number and magnitude) in complex cycle fatigue studies as well as the experimental assessment of existing structures. Correction factors have been proposed to this estimate to correlate the fatigue damage caused by variable amplitude loading with the fatigue resistance exhibited by the constant amplitude test data.

Gurney performed fatigue tests on small-scale specimens using complex load histories to assess the validity of Miner's Rule.[2, 3] Several examples of the stress-histories used in the experimental program are given in Fig. 2-11. Each stress sequence consisted of a single maximum stress cycle, Sr, with a number of superimposed minor stress cycles of magnitude z. The test results from these complex load histories consistently gave cycle lives less than those predicted by Miner's Rule. Gurney noted that there existed a linear relationship between the minor cycle, z, and the fatigue life of the complex cycles such that:

$$N_B = N_C \times (v + 1)^{-\rho} \tag{2.4}$$

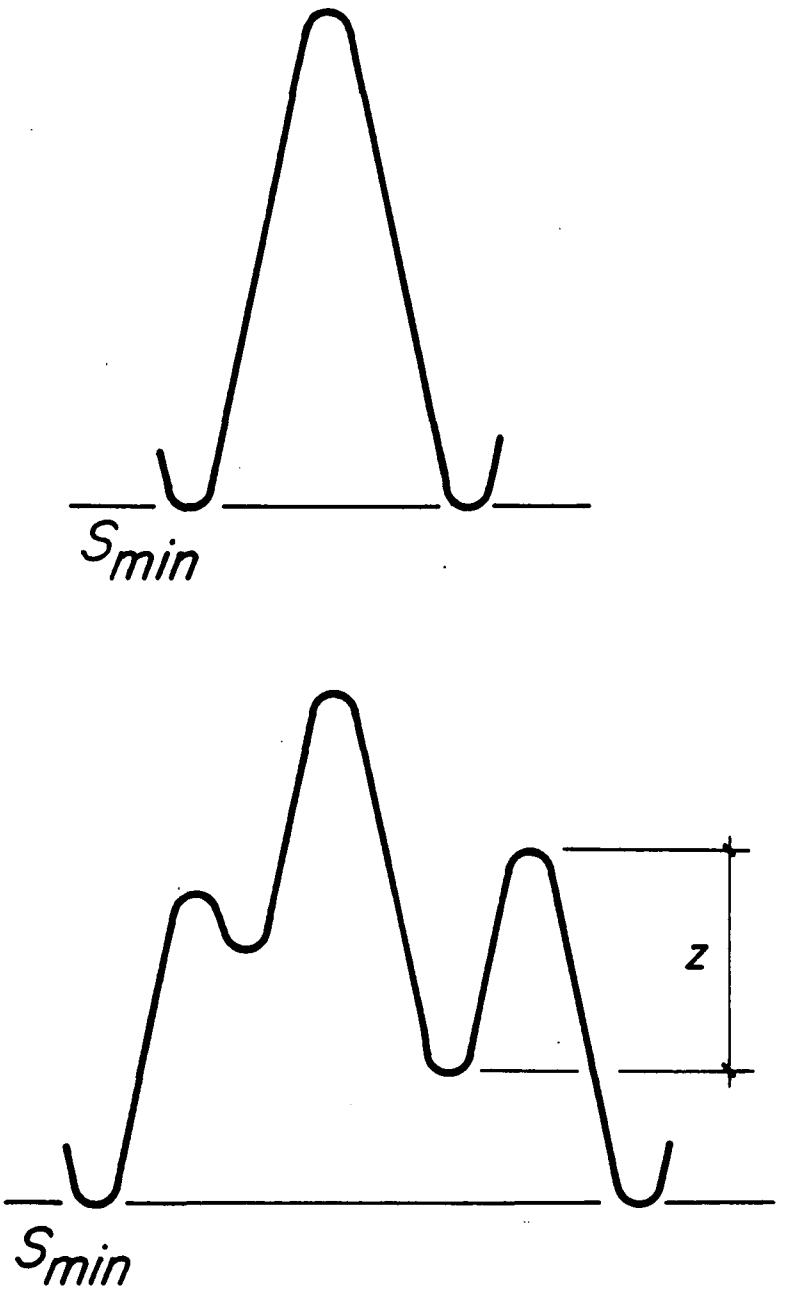

Figure 2-10: Comparison of simple and complex stress histories

where

N_B = number of complex cycles to failure

N_C = constant amplitude cycles to failure for Sr

v = number of minor cycles, z

ρ = ratio of minor cycle to primary cycle stress range

For complex cycle histories having n different magnitudes of minor cycles, the fatigue life can be estimated by:

$$N_B = N_C \left[\prod_{2}^{n} \left(\frac{E_{i-1}}{E_i} \right)^{\rho_i} \right] \tag{2.5}$$

where E_i is the total number of cycles per block with a stress range equal to or exceeding ρ_i times the maximum stress cycle, Sr.

Additional work by Gurney has shown the sensitivity of the damage model to the block length.[19] The block length is defined as the number of cycles between the inclusion of the peak or maximum stress cycle, Sr. As the block length was increased with the addition of lower magnitude stress cycles, cycle life estimates given by Eq. (2.4) became unconservative. It was suggested that the damage model only be used in designing structures subjected to short block type loading, whereas, Miner's Rule be used for long block loading.

Variable amplitude fatigue tests were also conducted by Joehnk[4] in order to assess the validity of Miner's Rule. Small-scale tee-shaped weldments were used as test specimens. The complex stress history used in this experimental program was formed by combining two sine waves cycling at two different frequencies and amplitudes. This gave a superimposed sine stress history similar to those used by Gurney. Joehnk also found Miner's Rule to be unconservative

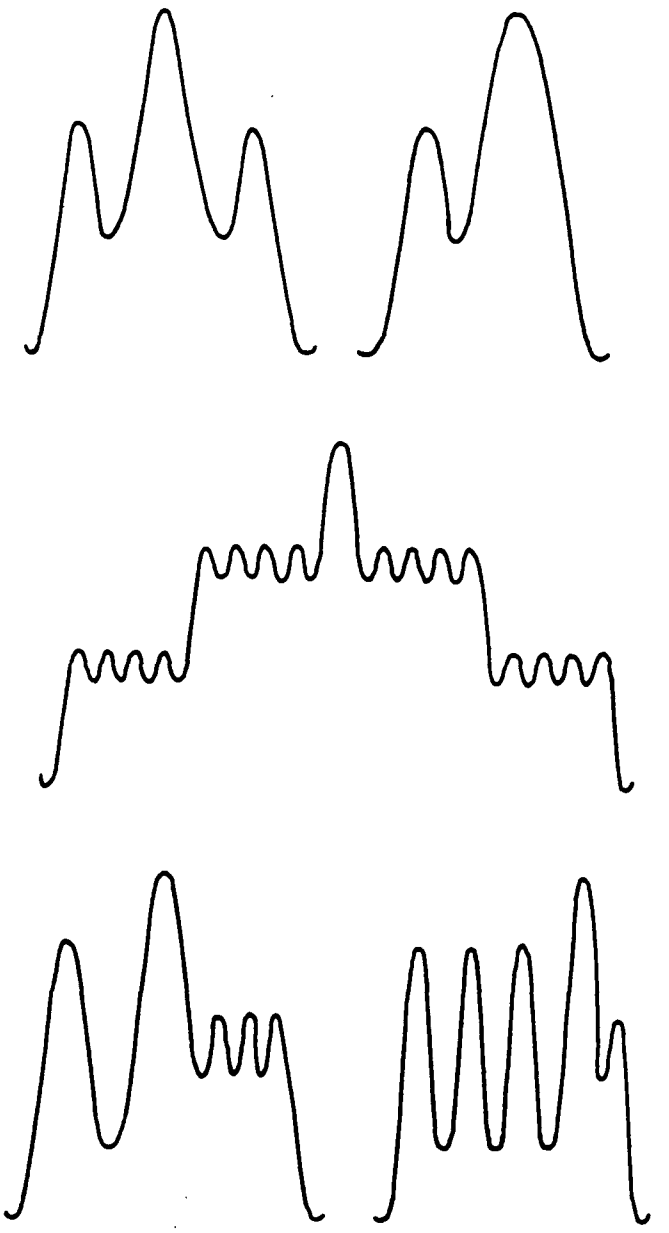

Figure 2-11: Complex stress histories used by Gurney

for complex stress cycles and concluded that the rule underestimated the fatigue damage caused by the minor cycles. Based on the test results, Joehnk developed a non-linear form of Miner's Rule to account for the increase in damage from the smaller amplitude stress cycles by modifying the effective stress range calculation:

$$Sr_e = [\ \Sigma\ (\alpha_i\ (\rho^{-0.5})\ Sr_i)^m\ ]^{1/m} \tag{2.6}$$

where

Sr_e = effective stress range

α_i = the factorial occurrence of Sr_i

ρ = ratio of minor cycle to major cycle

Sr_i = stress range interval i

m = slope of the log-log S-N curve

Subsequent work performed by Swensson[5] on identical type specimens with applied load histories developed from strain data obtained from in-service highway bridges, indicated minor cycles caused fatigue damage that was underestimated by Miner's Rule; even if the magnitude of the minor stress cycle was below that of the threshold stress range. A fatigue damage factor, I_f, was proposed to be used in the calculation of the major stress cycle produced by the passage of a single truck. The value of I_f was found to be dependent on the number and size of the minor cycles in the complex stress history. For the bridge used as the basis of the study, I_f was estimated as 1.15. In addition, the research indicated a need to modify the non-linear damage rule proposed by Joehnk (Eq. (2.6)) based on the mean stress level, magnitude, and the number of minor cycles of the complex stress cycle.

2.5 Current Review of Fatigue Test Data

Since the AASHTO specifications resistance provisions were introduced in 1974, several major fatigue studies have been conducted. Tests were conducted in East Germany, Japan, Switzerland, Office of Research and Experiments of the International Union of Railways - ORE (West Germany, Poland, England, and Holland), as well as in the United States. The additional studies evaluated the applicability of the NCHRP test program to fabrication conditions elsewhere in the world and were used to develop similar fatigue codes. The additional tests augmented the original NCHRP findings and often defined the fatigue resistance of details that were not previously tested.

A recent review and re-evaluation of the AASHTO fatigue specifications has been conducted using all available test data.[20] While the majority of the new test data is from constant amplitude loading, several studies dealt with the fatigue strength of large-scale details subjected to variable amplitude loading. A detailed discussion of these data is given in Sec. 2.3. Each data group was compared to the existing AASHTO fatigue design resistance provision in order to determine the adequacy of the resistance curves and to check for detail types whose fatigue strength deviated from these curves. While most of the data correlated well with the original database, the review indicated that minor adjustments to the fatigue provisions were required. A revised set of fatigue design curves has been proposed that better estimates the fatigue resistance of welded steel details and is shown in Fig. 2-12. Though similar to the existing AASHTO curves, the new curves are more uniform and parallel; each curve is set at a constant slope of -3.0. A new resistance category, B′, has been added to better estimate the fatigue resistance of partial penetration longitudinal

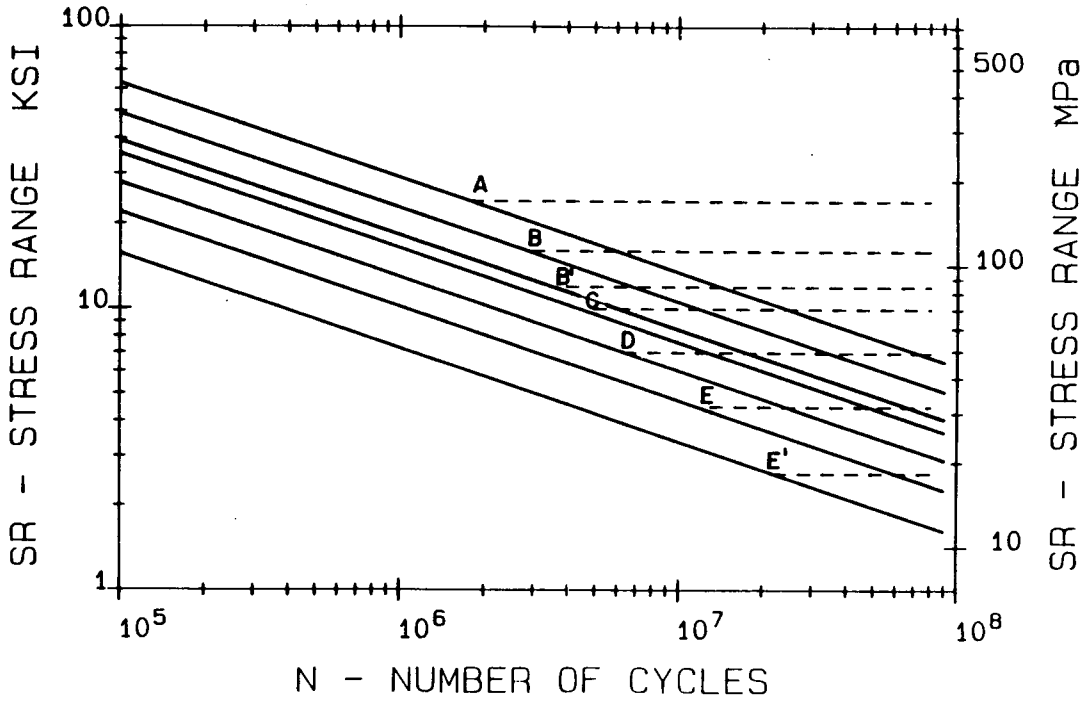

Figure 2-12: Revised AASHTO Fatigue Design Curves

groove welds and longitudinal welds with backing bars. Also, the constant amplitude fatigue limit for Category E has been lowered from 5.0 ksi to 4.5 ksi based on high cycle, constant amplitude fatigue tests of coverplated beams.[21]

Although the fatigue data review has significantly increased the database,[22] from 800 fatigue test failure results to over 2000, limitations still exist. Even though the number of types of details tested has increased, this still represents only a fraction of the number of types actually designed and fabricated in large scale welded structures. As will be extensively addressed in subsequent chapters, the size of the test specimen can have a significant effect on fatigue resistance. Almost all of the detail types tested in the reviewed programs do not approach the full size of actual details used. Constant amplitude testing to determine the constant amplitude fatigue limit still remains scarce for full-scale specimens. Currently, only two detail types have been studied in depth to determine this

value: the web stiffener detail (Category C) and the coverplate detail (Category E). In addition, fatigue test data for large-scale test specimens are still scarce in the high cycle region. Few test programs have dealt with the long life fatigue behavior under variable amplitude loading. Few test programs cycle a test specimen beyond ten million cycles. The constant amplitude fatigue limits for Categories E and E′ intersect their corresponding resistance curve at approximately 12 million and 22 million constant amplitude cycles, respectively. Because of these limitations in the test data there must be limitations placed on the application of the resulting fatigue design resistance curves.

Implied in the new AASHTO fatigue design curves, though not explicitly discussed in NCHRP Report 286,[20] is the fatigue behavior of welded steel details subjected to variable amplitude loading. As shown in Fig. 2-12, each curve has a constant slope of -3.0. This would imply that fatigue damage of variable amplitude loading is estimated through the use of Miner's linear cumulative damage law. Also, each curve extends below the constant amplitude fatigue limit with the same constant slope of -3.0. This would also imply that variable amplitude fatigue damage accumulates linearly, according to Miner's Rule, regardless of the values of the stress ranges in the spectrum. The remainder of this study will concern itself with these two aspects of fatigue resistance in the context of full-scale welded bridge details.

Chapter 3
Large-Scale Welded Bridge Details

Extensive research has been conducted in the area of fatigue growth in metal structures. Any structural or machine component that will be subjected to some type of cyclic loading during any or all of its intended life must also be designed on the basis of fatigue. While each industry or field of study concerns itself with the problem of fatigue, each deals with it differently owing to the variation in the parameters that influence fatigue behavior. These parameters include: material type (steel, aluminum, composites), joining methods (welding, bolting, riveting), loading (constant or variable, deterministic vs. probabilistic), and design life (finite and infinite). For example, the aircraft industry is concerned predominantly with fatigue crack initiation, primarily in aluminum alloys. Fatigue design of machinery is controlled by narrow band load spectra and crack initiation at stress concentrations.

Welded steel bridge details differ from other commonly used structural details in that their fatigue behavior is prescribed by two dominating factors: residual stresses, and the loading and resulting stress range spectrum. The influence of these parameters gives rise to many conditions that control the propagation behavior of fatigue cracks. The following describes in depth these important factors and how their interaction specifically affect fatigue crack propagation in welded steel bridge details.

3.1 Loading

The loading by which a bridge type structure is subjected to is normally complex and varied. The loading can be characterized as both variable and random. The determination of fatigue strength and fatigue damage is made difficult by this fact. But due to constraints inherent in the design process, limitations are placed on both the dead load and live load values, resulting in a narrowing range for fatigue loading.

The maximum design truck load for highway bridges has been the AASHTO HS20 load configuration. The total gross weight of this design vehicle is 72 kips. This load was first introduced into the AASHTO design specifications in 1944 and has remained essentially unchanged through the present 1983 AASHTO specifications. Various states have modified their design criteria to include higher design loads and overload provisions. For example, New York State and others design to a 80 kip load. However, to date, these higher loads have not been uniformly adopted by all state highway agencies nor by AASHTO. The current fatigue design specifications require the fatigue design of welded details on the basis of this design load.

Actual bridge loading differs greatly from the design loading in several respects. Trucks weights vary greatly as shown by the gross vehicle weight distribution in Fig 3-1. The obvious variability in bridge loading gives rise to the need to assess fatigue damage in terms of variable amplitude loading. The maximum design load does not correspond to the maximum weight of trucks found in use. The current (1987) legal weight limit for trucks is presently set at 80 kips. Often, this limit is exceeded, both legally and illegally. Special heavy loads or overloads are permitted on highways that are significantly above

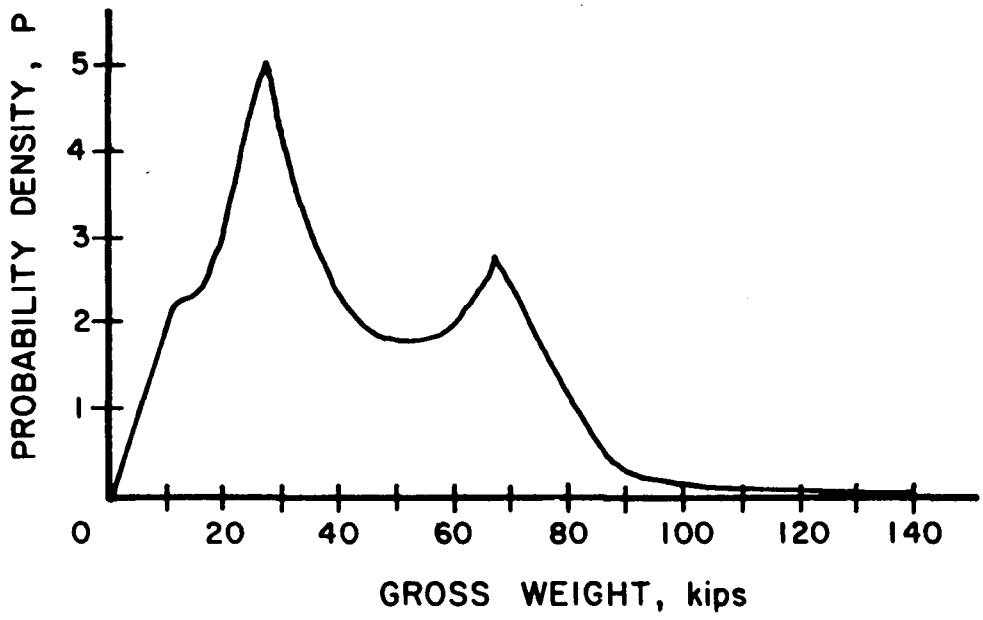

Figure 3-1: Gross vehicle weight distribution

the 80 kip gross weight. The maximum overload weight is governed by the strength capacity of the bridge along the intended route of the overload. Presently, no direct consideration is given to the fatigue damage that is caused by these overloads.

A recent investigation by Schelling[23] studied the effect of 90 kip container trucks on bridge structures along selected routes in the state of Maryland. While it was concluded that the container vehicle did not impose any greater hardship on the bridge structure than the AASHTO HS20 design vehicle, it was concluded that an increase in coverplate end stressing would occur. It was recommended that an increased inspection program be implemented and any cracked detail be retrofitted with a bolted connection.

Of greater occurrence is illegal overloads. Note that the maximum value in Fig. 3-1 is approximately twice that of the design load (120 kips vs. 72

kips). An annual inspection of one particular bridge has shown the trend of increasing the permanent set of camber in the roadway stringers due to illegal overloads. Enforcement of the legal load limit has continued to be difficult.

While the design load has remained constant over the last forty years, the general trend for actual loads is to increase. Advances in engine design have led to increased engine horsepower, resulting in the ability of trucks to haul greater loads. The legal load limit was 72 kips through 1976, when it was raised to 80 kips. Recent lobbying by the trucking industry has created pressure to increase this legal load limit above 80 kips. The overall average weight of trucks has increased in the pass decade due to the deregulation of the trucking industry in 1980. Prior to deregulation, a significant percentage of trucks were empty due to regulations prohibiting return transport between states. As a consequence of deregulation and increased competitiveness, the truck industry has become more efficient, with a greater portion of trucks running at or near capacity.

An increase in the actual loading has also occurred in the railroad industry.[24] Prior to the introduction of diesel locomotives, the steam locomotive and it's tender represented the heaviest load on a railroad bridge. A total gross weight of over 500 kips for the larger steam locomotives was not uncommon. (A present day six-axle diesel locomotive has an average gross weight of 420 kips.) Generally, the steam locomotive represented the only significant load for design. Individual car loads were low enough in weight so that for fatigue evaluation purposes, they could be ignored. The diesel units, though generally lighter in weight than steam units and with much less impact, allowed for the combining of engines in order to increase horsepower and load-

pulling capacity. This increased the number of fatigue load cycles per train and resulted in a significant increase in freight car loads. Present day freight cars can have individual axle loads of up to 80 kips, comparable to an E80 design engine axle load. Freight car axial loads of unit trains can be as high as 65 kips, which equals the axial loads for diesel locomotives. As with the trucking industry, there is pressure with the railroad industry to use ever increasing loads. The use of heavier freight cars and unit trains will have a significant effect on fatigue damage of railroad bridges.

3.2 Resulting Stress Distributions

Due to design constraints, mainly strength considerations, the magnitudes of the stress cycles that a bridge is subjected normally results in a limited range of stress levels. In bridge design codes, the principal consideration is the maximum stress produced by a particular combination of dead load and live load (including impact). For allowable stress design, the combination of dead load and live load stresses may not exceed a fraction of the yield stress. This value is $0.55F_y$ for flexural and tensile stresses. For Load and Resistance Factored Design (LRFD), both dead and live loads are factored upwards at the service load level. This value may not exceed a magnitude slightly lower than the yield stress. In both design procedures, limitations are placed on the possible maximum range of stress. For both dead load and live load, the resulting stresses may range from $0.1\sigma_y$ to $0.7\sigma_y$ depending on the bridge type. This results in a limited range for the stress ratio.

The value for stress range is further limited by the span length. For primary members, such as longitudinal girders and truss chords, as the span length is increased, a greater portion of the allowable maximum stress is due to

dead load. A greater portion of a member's capacity must be devoted to resisting its own weight. For short span bridges, the ratio of dead load to live load stress is 2 to 3. As the span length increases, this ratio increases. For long span bridges, the ratio can be as high as 4:1. Obviously, an efficient design with the least amount of material, would be one that minimizes this ratio. One way to accomplish this is to use a higher strength steel. While the dead load stress would decrease only slightly, a higher live load stress would be allowed providing details do not limit the stress range. All of these factors result in limiting the stress range values.

When these factors are taken into account, the possible values for the nominal stress ratio are limited. The stress ratio is defined as the ratio of minimum stress to maximum stress. In most cases, the minimum value can be taken as the dead load stress. In members where live load stress reversal occurs, this would not be the case since the minimum stress would be further lowered by the addition of a compressive live load. Consider two simplified cases: a dead load stress of $0.3\sigma_y$, and a live load stress of $0.3\sigma_y$ (values comparable to a short span). The stress ratio would be equal to $+ 0.5\sigma_y$. For a long-span bridge, the values would be equal to, in the order of, $0.5\sigma_y$ and $0.1\sigma_y$, for the dead load and live load, respectively. This results in a stress ratio of + 0.8.

Given that these two cases represent the upper and lower bounds for the stress ratios occurring in simple span bridges, it can be reasonably concluded that most bridges are subjected to high nominal stress ratios. Most fatigue tests on small-scale welded specimens is done at lower stress ratios; ranging in the order of -0.5 to 0.1.

It must be noted that these values represent nominal stress ratios. No consideration was given to other factors that can influence the local stresses at a welded detail. This includes residual stresses and stress concentrations. The effect of residual stresses on the stress ratio will be discussed in Section 3.3.

The stress history at a particular detail caused by the passage of a single truck across a bridge is strongly dependent upon several factors. These included: span length, bridge type, and member type and location. Generally, stress traces are composed of one or more primary cycles with superimposed smaller vibratory stresses. For spans between 30 ft and 60 ft, two individual stress cycles occur which correspond to the two axle groups for 4 and 5 axle trucks. For spans greater than 60 ft, a single complex cycle occurs. Figure 3-2 gives representative examples of the flexural stress histories of the primary longitudinal members for several types of bridges.

Studies have been conducted that analyzed the stress histories of a large number of bridge types in order to determine the number of cycles per truck crossing for fatigue design purposes.[25] This study showed that on average, a single truck passage resulted in one primary stress cycle with four to five secondary cycles of amplitude not exceeding 20 percent of the primary cycle. It was concluded that vibration stresses and closely spaced trucks had only a marginal effect on the cycle count and magnitude and that there was no adjustment necessary for the design values. Although superimposed vibration stress on the primary cycle increases the stress range, the design impact factor adequately adjusts for the effect. Schilling concluded that a complex stress history could be decomposed into a number of equivalent simple primary cycles. The number, being dependent upon the bridge type and span length, varied

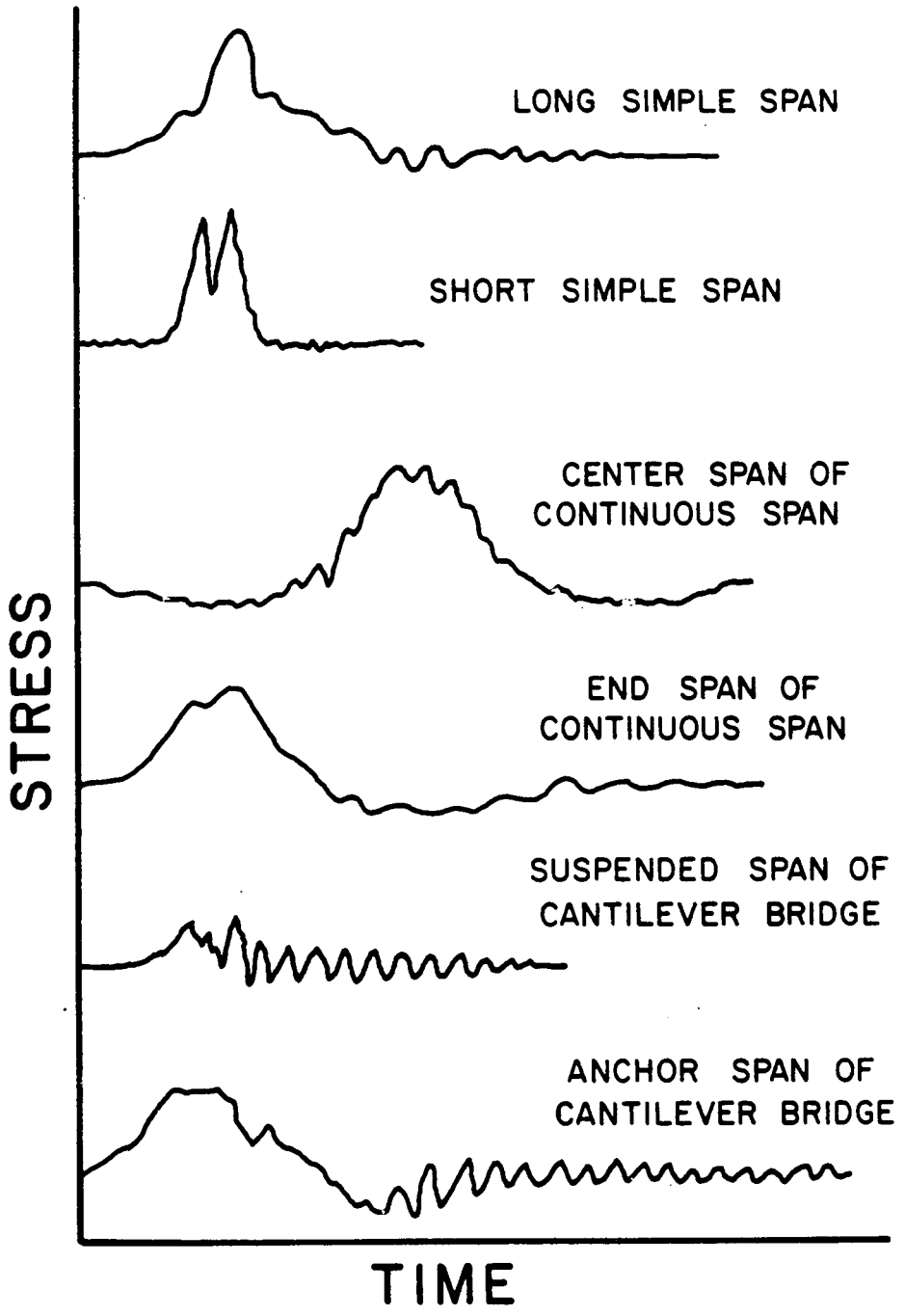

Figure 3-2: Typical stress histories for various bridge types

between one and two cycles per vehicle.

Numerous investigations have been conducted that deal with the measured response of bridges to truck traffic. Stress range histograms have been developed for individual bridge details as well as composite histograms of a number of bridges. Three general types of distributions have been observed as shown in Fig. 3-3: a) unimodal, b) bimodal, and c) continuously descending. The type of stress range histogram observed at a particular location is, in part, due to the cycle counting method used to reduce the data and the length of time measurements were taken. Review of the data from the measured bridge responses indicated that stress ranges seldom exceed 10 ksi and the effective stress range for a measured spectrum seldom exceeded 5 ksi.

3.3 Residual Stresses in Welded Details

3.3.1 Residual stress distributions

As shown in NCHRP Project 12-7 and numerous other studies, all welding processes result in high residual tensile stresses. The weldment and adjacent base metal are usually at or near the yield point of the base metal. As part of the NCHRP project, residual stresses were measured in several welded beams prior to and after cyclic loading.[13] These beams were destructively examined to determine their residual stress distributions using the method of sectioning.[26] Residual stresses were measured on both the inside and outside surfaces of the flange plates and on both sides of the web. Due to the finite size of the sectioned portion of the welded beam, only an average value of residual stress could be measured. Beams fabricated from all three steel types (A36, A441, and A514) used in the test program were examined.

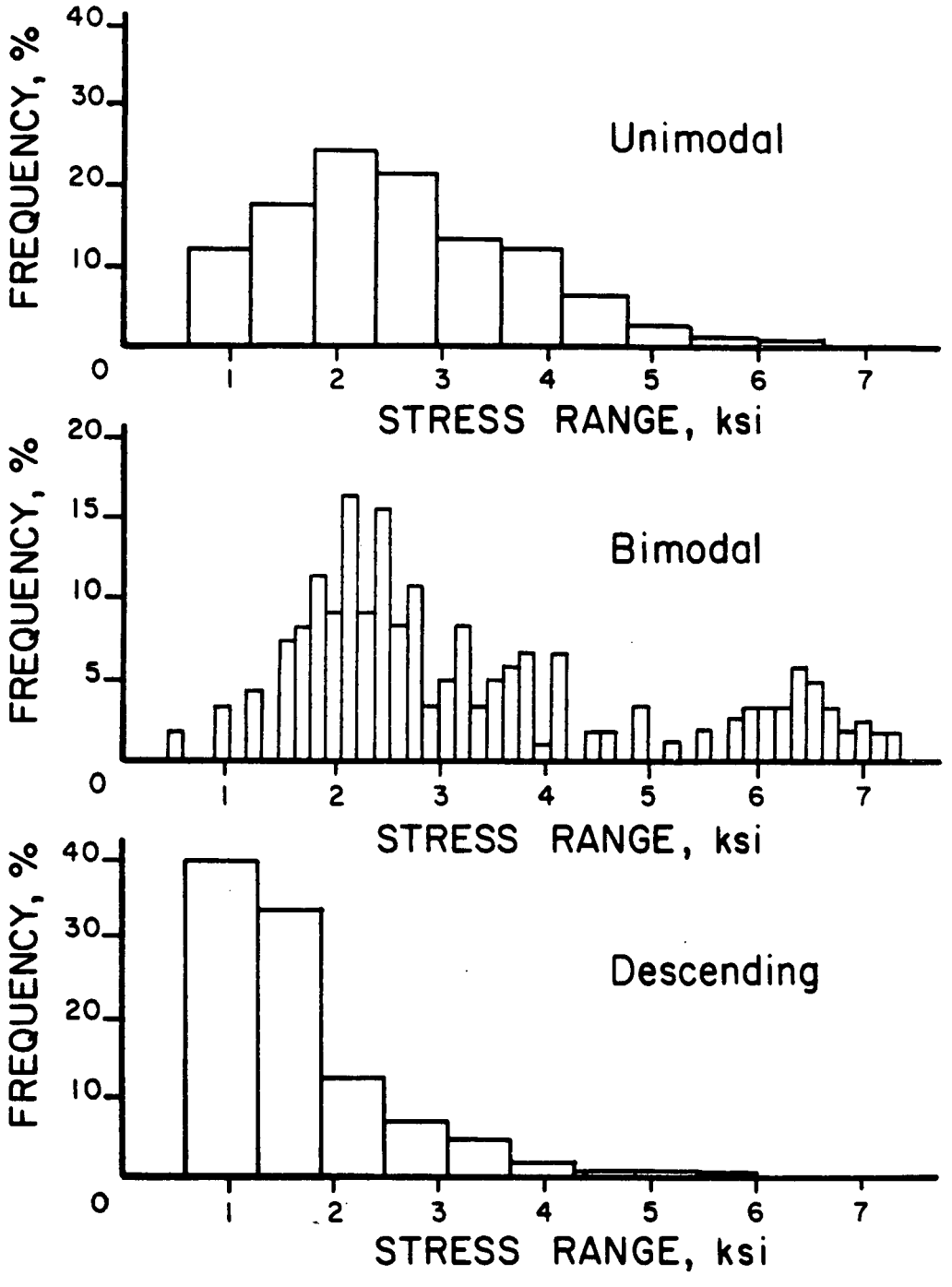

Figure 3-3: Typical measured stress range histograms for bridges

The results from some of the residual stress measurements[13] are shown in Fig. 3-4. These distributions correspond to the measured residual stresses in the flanges of the welded beam specimens and are in the longitudinal direction, parallel with the longitudinal axis of the web-to-flange fillet weld. As Fig. 3-4 illustrates, large tensile residual stresses were measured in the vicinity of the web-to-flange fillet welds. As the steel strength increased, the magnitude of the maximum tensile residual stress also increased and was near the yield point for the weld itself.

When a set of newly fabricated full-scale welded plate girder test specimens were shipped to the laboratory during inclement weather, it provided a unique opportunity to observe enhanced residual stress patterns qualitatively. Figure 3-5 is a view of a fillet welded web attachment. The attachment plate is 1.0 in. thick and 12 in. long. During welding, the expansion and contraction of the web plate from the heat input of the weld caused the mill scale to flake off (see Theory of Brittle-Coating Method) along lines perpendicular to the principal stress field. Corrosion of the exposed steel surface visually enhanced the pattern. The mill scale crack pattern runs both parallel and perpendicular to the weld axis, indicating the development of high residual stresses in both directions. The area of web plate affected by the welding heat input approximates 6 in. in all directions. Figure 3-6 shows similar patterns at a transverse web stiffener. Note the yield lines around the end of the stiffener, indicating significant development of residual stresses at this location. Also, note the yield lines due to the constraint of the upper flange plate and the adjacent web stiffener.

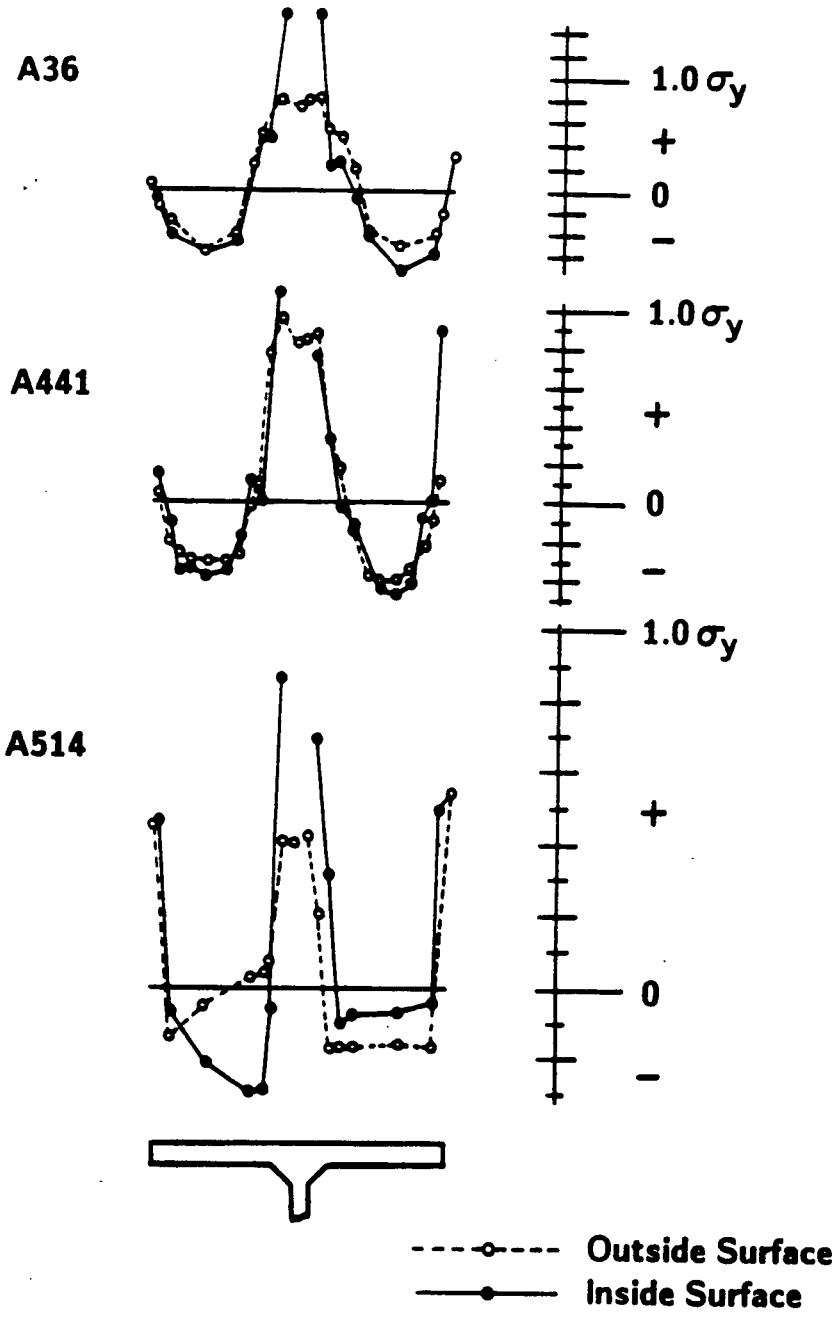

Figure 3-4: Measured residual stresses in the compression flanges of welded beams

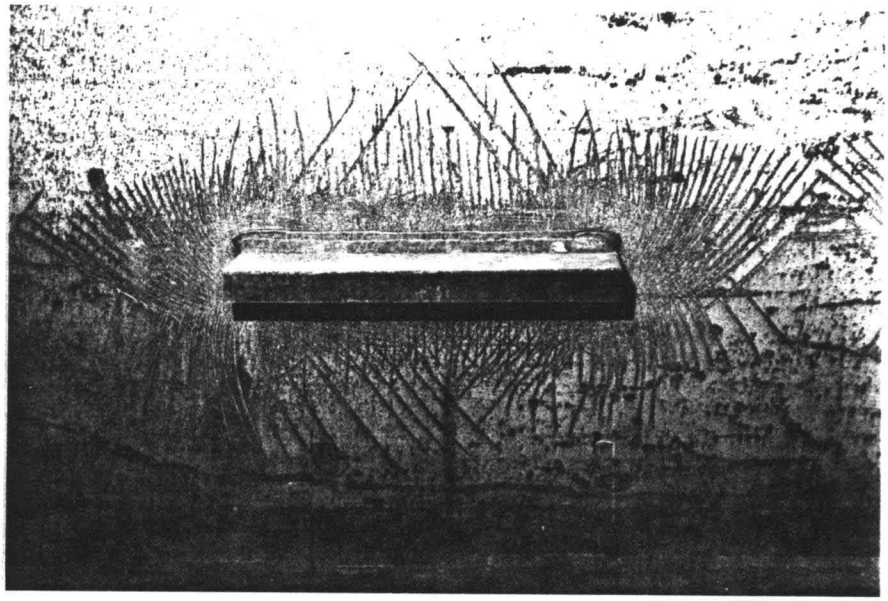

Figure 3-5: Residual stress pattern in mill scale at a web attachment

3.3.2 Redistribution under cyclic loading

The previous discussion involved the measurement of residual stresses in the as-welded state, prior to any type of loading. Loading that causes strains above yield will, upon unloading, result in a change in the initial state of stress. If redistribution is occurring in welded structures, then the fatigue behavior will be altered. An investigation was conducted to determine the degree of residual stress re-distribution from both high and low magnitude cyclic loading.[27]

Several welded beams used in NCHRP Project 12-7 were also used to study the residual stress redistribution due to cyclic loading incurred. During constant amplitude fatigue tests, strain gages mounted at various locations on the flange and web plates were monitored. In addition, upon completion of the fatigue tests, the final residual stress distribution patterns were determined by

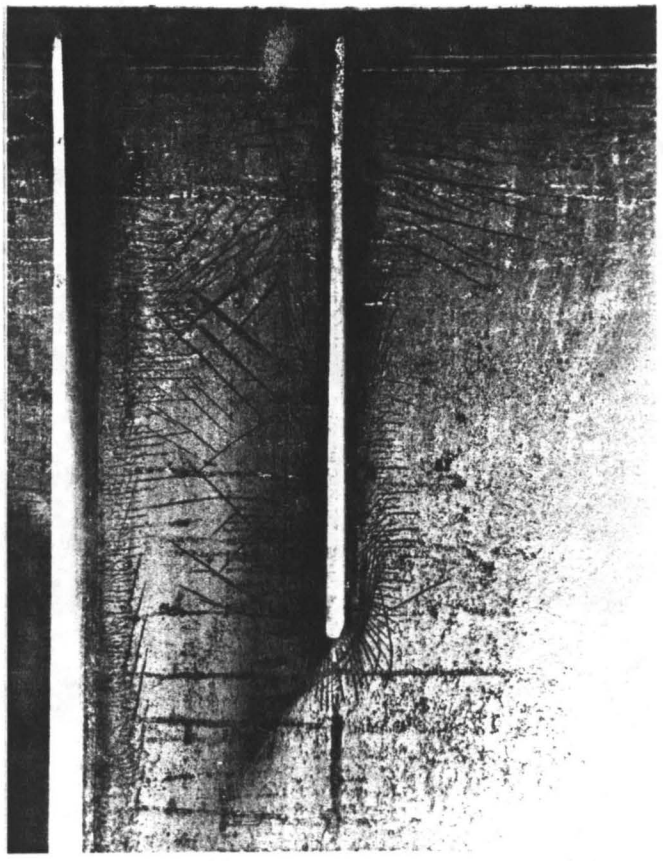

Figure 3-6: Residual stress patterns at a web stiffener

the method of sectioning. Sections from both the shear span and the constant moment region were examined. The residual stress patterns at mid-span for A514 beams are shown in Fig. 3-7. Since the method of sectioning is a destructive process, separate specimens were used for the before cycling and after cycling measurements. The loaded beam was constantly cycled at a stress range of 30 ksi with a maximum bending stress of 20 ksi in the flanges (approximately $0.2\sigma_y$). As Fig. 3-7 indicates, the average tensile residual stress at the weld decreases approximately $0.2\sigma_y$ and only minor redistribution occurred throughout the cross-section.

From the investigation of residual stress redistribution, the following

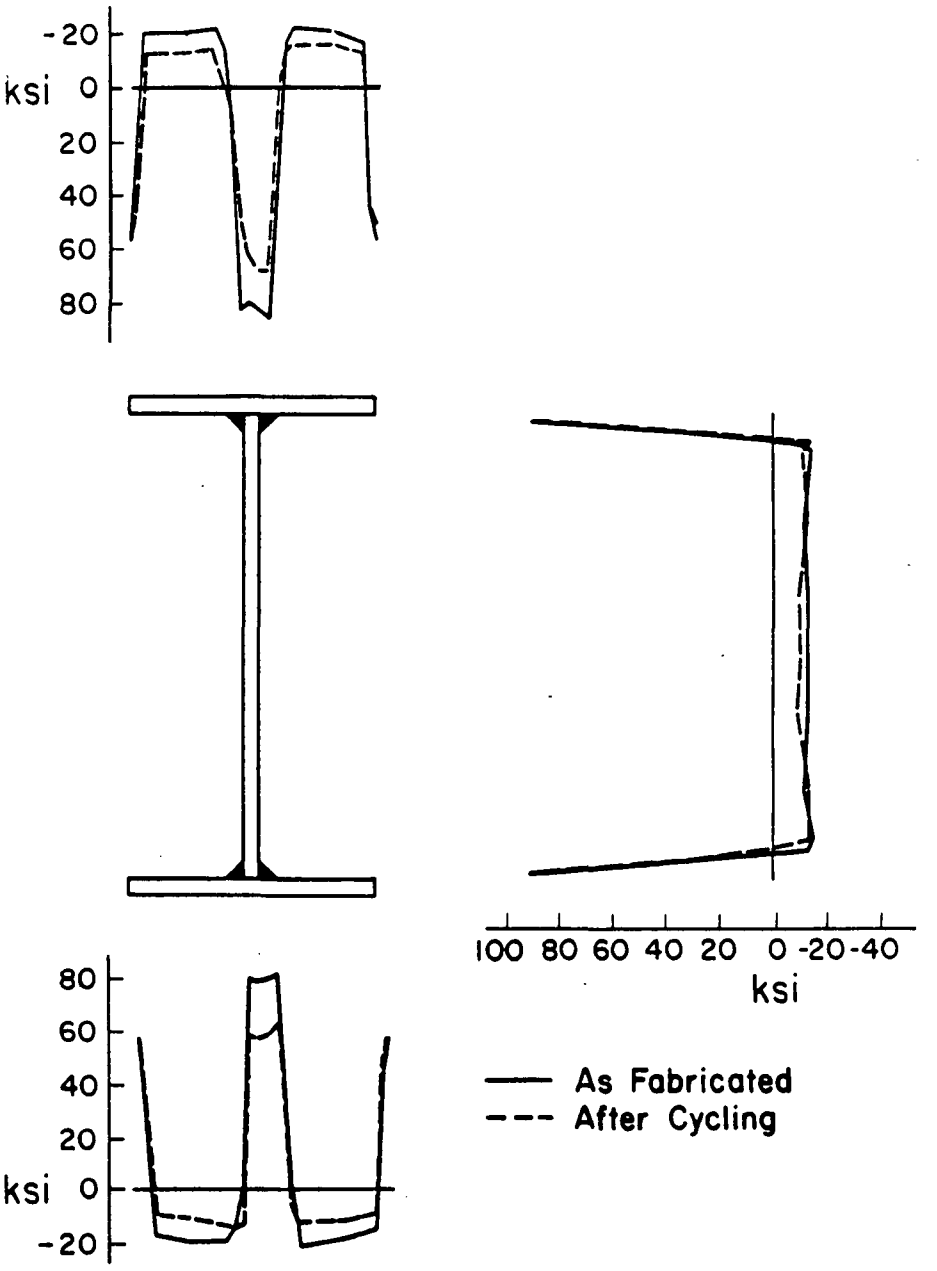

Figure 3-7: Comparison of uncycled and cycled residual stress distributions, mid-span, A514

observations and conclusions were drawn:

- Redistribution of residual stresses in a welded beam took place when the maximum applied stress plus the residual stress exceed the yield stress of the material.

- Redistribution is a function of initial residual stress and the applied load.

- For low magnitude cyclic loading (20 ksi maximum tensile or compression stress) the change in the residual stress distribution was not significant

3.3.3 Redistribution under simplified load cases

To give a simple example of the residual stress redistribution or degradation due to dead load and live load interaction, an idealized initial residual stress pattern prior to loading in a tension flange was assumed. This pattern is shown in Fig. 3-8 and is based on the residual stress measurements of NCHRP Project 12-7 (see Fig. 3-4) and on research performed by Tall.[28] The residual stress at the web-to-flange weld is assumed to be at the yield stress of the base metal. The maximum value of the compressive residual stress is taken as one-fourth of the yield stress. The tensile stresses in the weld are balanced by the compressive stresses in the flange plate. It is assumed that the stress is uniform through the thickness of the flange plate.

Loading for the example is taken such that the dead load results in a stress of one-fourth of the yield stress and the live load causes a maximum

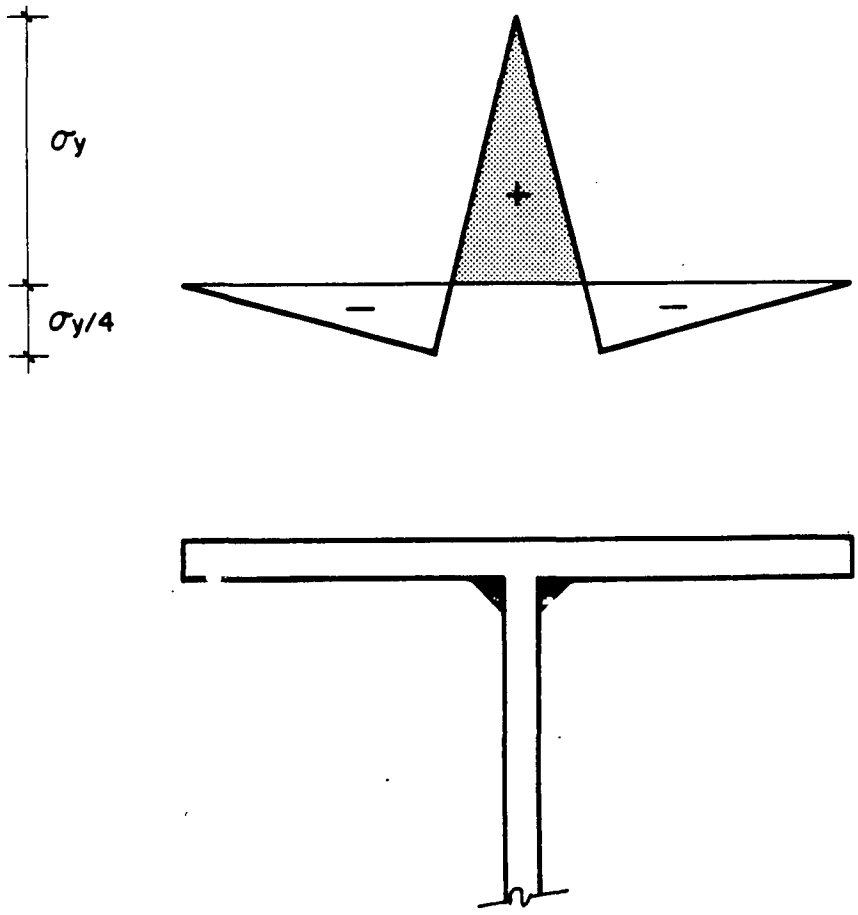

Figure 3-8: Assumed residual stress distribution in tension flange

stress range of one-half of the yield stress. Both the dead load and the live load can be either tensile or compressive, resulting in four different loading conditions (Table 3-1). For a continuous span bridge, the magnitude and the ratio of dead load to live load will vary greatly. In addition, the types of weld details will place a limiting factor on the live load stress range. The first two load cases are for tensile dead load stresses and are shown in Figs. 3-9 and 3-10 for tensile live load and compressive live load respectively. The compressive dead load Cases 3 and 4 are shown in Figs. 3-11 ad 3-12.

The results of the four cases are summarized in Table 3-2. To keep the

Load Case	Dead Load	Live Load
1	$+ \sigma_y/4$	$+ \sigma_y/2$
2	$+ \sigma_y/4$	$- \sigma_y/2$
3	$- \sigma_y/4$	$+ \sigma_y/2$
4	$- \sigma_y/4$	$- \sigma_y/2$

Table 3-1: Four dead load and live load loading conditions

example simple, any loss of tensile residual stress due to overload has not been balanced with a corresponding reduction in the compressive zone. Though this violates the cross-section equilibrium, the effect on the final maximum value of tensile residual stress is insignificant. Reduction in the tensile residual stress at the weld is predicted for tensile live loading only. The maximum reduction corresponds to the value of the live load stress range of $0.5\sigma_y$, though the resulting residual stress remains at a relatively high level of $0.5\sigma_y$. Compressive live loads do not degrade the residual stress at the weld. It should also be noted that the tests carried out on A36, A441, and A514 steel beams had maximum applied stresses up to 50 ksi. None of these members exhibited significantly different fatigue resistance at a given stress range level.

Since crack growth propagation is dependent upon local stress conditions in the vicinity of the weld, it is more appropriate to use an effective stress ratio. The nominal minimum and maximum stress values are superimposed on the residual stresses and reduced to consider the effect of degradation from cyclic loading. As shown in Table 3-3, even though the nominal stress ratios vary

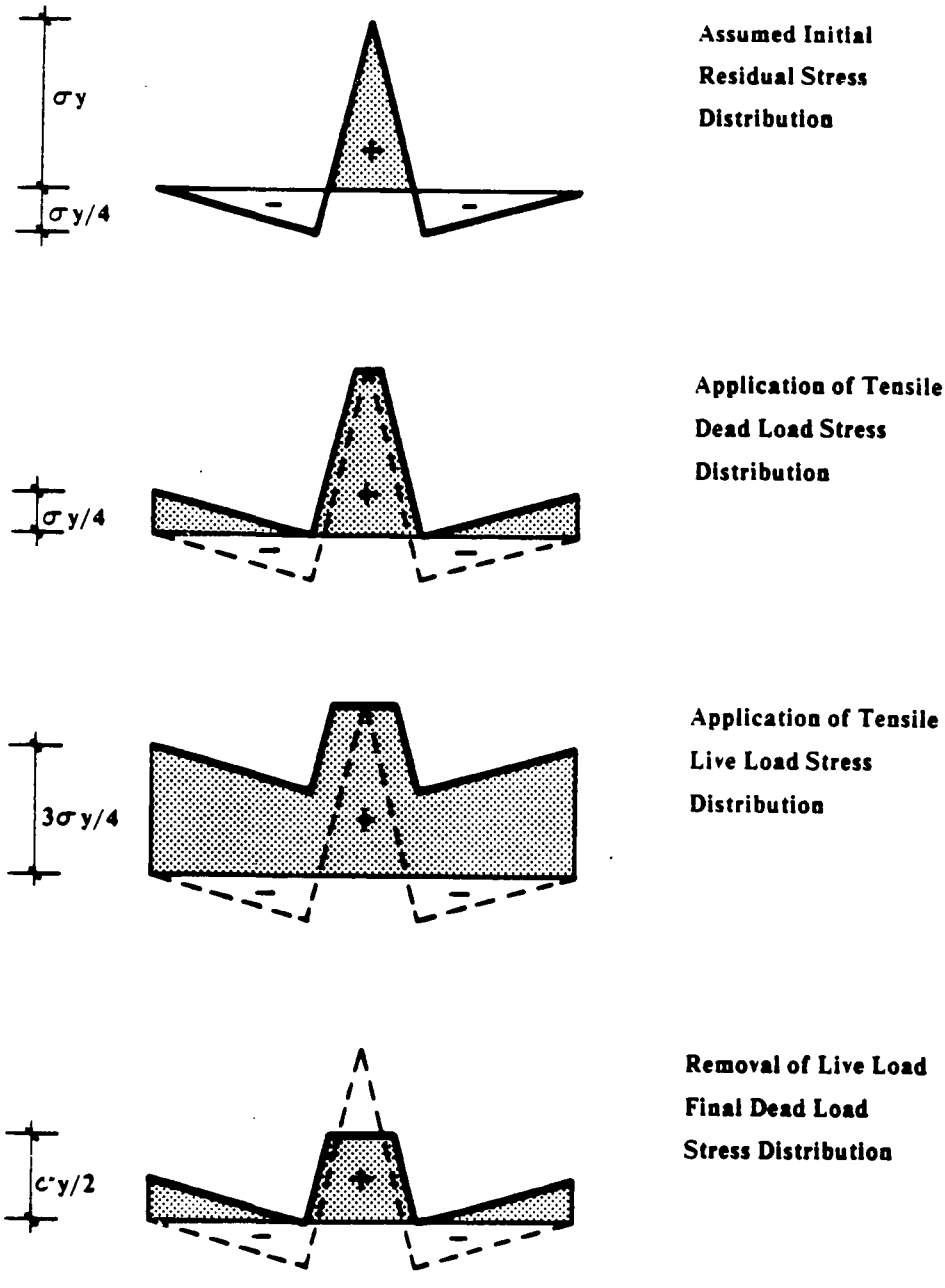

Figure 3-9: Case 1, tensile dead load and tensile live load

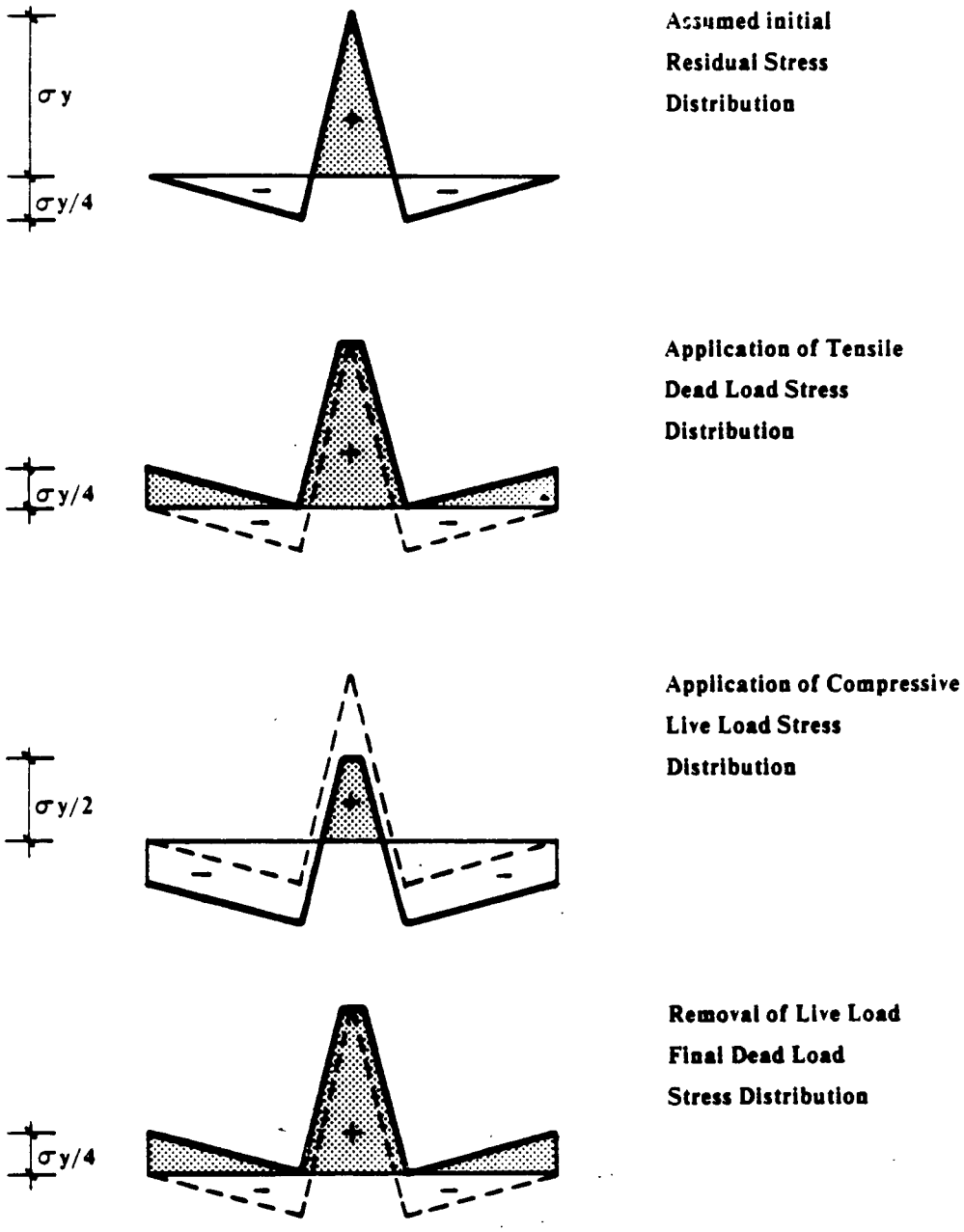

Figure 3-10: Case 2, tensile dead load and compressive live load

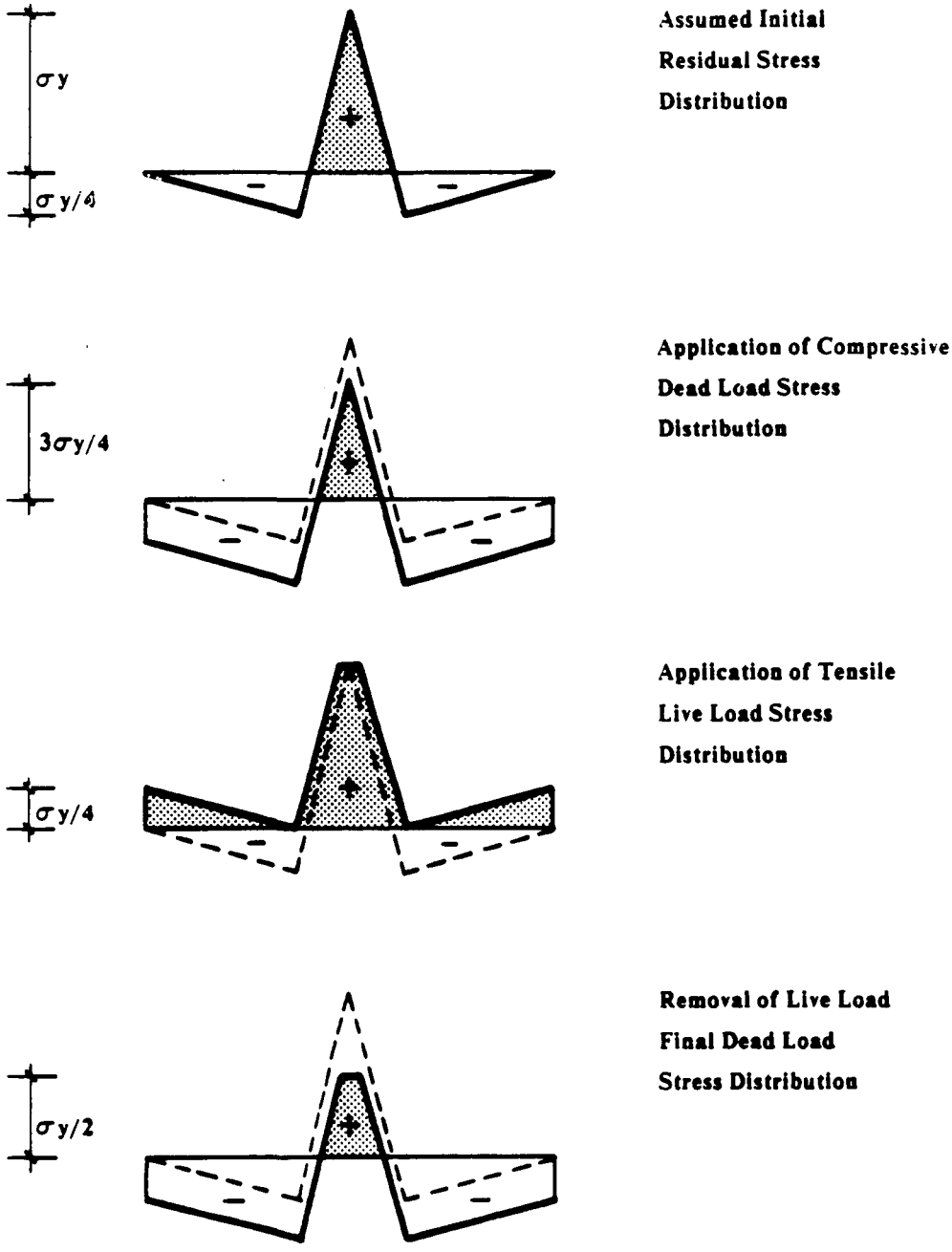

Figure 3-11: Case 3, compressive dead load and tensile live load

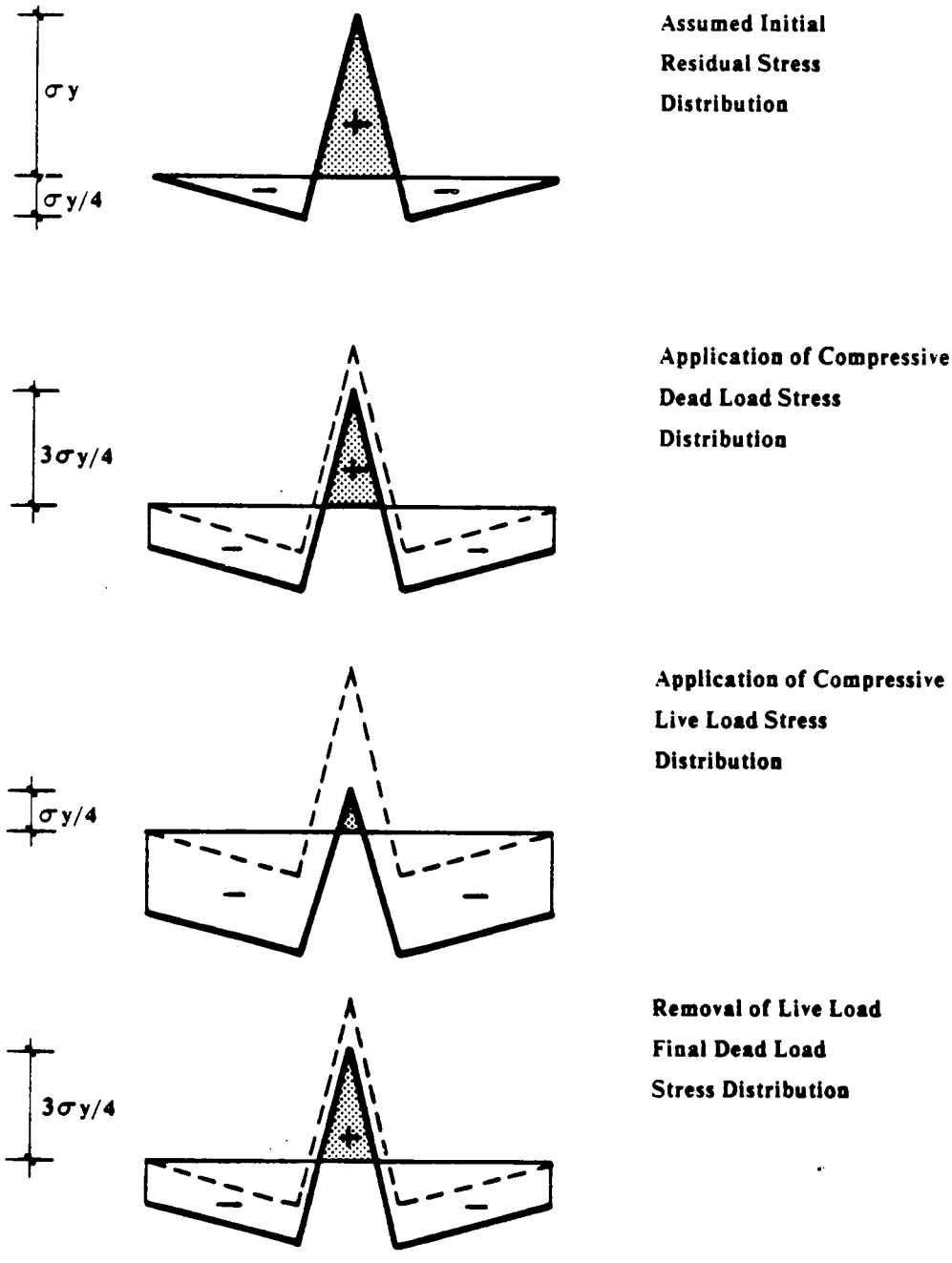

Figure 3-12: Case 4, compressive dead load and compressive live load

Load Case	Maximum Tensile Residual Stress at Weld		Reduction in Residual Stress at Weld
	Initial	Final	
1	σ_y	$\sigma_y/2$	$\sigma_y/2$
2	σ_y	σ_y	0
3	$3\sigma_y/4$	$\sigma_y/2$	$\sigma_y/4$
4	$3\sigma_y/4$	$3\sigma_y/4$	0

Table 3-2: Summary of four load cases

from -1.0 to 0.5 for the four load cases, the effective stress ratios result in a significantly smaller range of values: from 0.33 to 0.50. Therefore, for these idealized load cases, fatigue crack growth always occurs at a relatively high stress ratio.

Load Case	Nominal Stress Ratio R_{nom}	Effective Stress Ratio R_{eff}
1	0.33	0.50
2	-1.0	0.50
3	-1.0	0.50
4	0.33	0.33

Table 3-3: Comparison of nominal and effective stress ratios for four load cases

From the above example, several conclusions can be drawn with regard to

fatigue crack propagation in full-scale welded details:

- The higher the yield stress of the base metal, the less residual stress redistribution or degradation occurs since the allowable stress range for a given detail is independent of yield stress.

- The maximum reduction from the initial tensile residual stress occurs under tensile live loading. Therefore, as the detail severity increases and the allowable stress range decreases, residual stress degradation also decreases.

- The maximum reduction in the tensile residual stress is a function of the maximum live load stress range in the stress range spectrum and the level of dead load.

- For compressive live loading, fatigue crack propagation occurs during unloading.

3.4 Summary

For the fatigue behavior of large-scale welded structures to be properly understood and modeled, fatigue testing must be performed within the stress state limits that these structures are subjected to. A high effective stress ratio must exist at the weldment of a test specimen in order for crack propagation to occur in realistic stress field conditions. In addition, the range of stress must be limited in magnitude to simulate the load conditions experienced by bridge type structures.

Chapter 4
Fracture Mechanics Concepts

Crack propagation behavior can be described mathematically (quantitatively) through the use of the principles of linear elastic fracture mechanics. This includes both fatigue crack propagation (stable growth) and rapid fracture (unstable growth). Fracture mechanics will be used for the examination of the fatigue behavior of welded steel details on a microscopic level that is not obtainable with specimen testing; both small-scale and large-scale. However, this must all be done in light of the conditions and limitations discussed in Chapter 3 for the proper conclusions and applications to be drawn with regard to welded steel bridge details.

4.1 Linear Elastic Fracture Mechanics

The presence of a crack or similar type discontinuity in an otherwise isotropic and homogeneous material causes a local disruption of the stress (strain) field at the crack tip. For plane strain conditions (welded steel bridge details), Irwin[29] and Westergaard[30] showed that the elastic stress field near the crack tip can be described by the following expressions:

$$\sigma_y = \frac{K_1}{\sqrt{2\pi r}} \cos\frac{\theta}{2} \left[1 + \sin\frac{\theta}{2} \sin\frac{3\theta}{2} \right] \tag{4.1}$$

$$\sigma_x = \frac{K_1}{\sqrt{2\pi r}} \cos\frac{\theta}{2} \left[1 - \sin\frac{\theta}{2} \sin\frac{3\theta}{2} \right] \tag{4.2}$$

$$\tau_{xy} = \frac{K_1}{\sqrt{2\pi r}} \left[\sin\frac{\theta}{2} \cos\frac{\theta}{2} \cos\frac{3\theta}{2} \right] \tag{4.3}$$

where K_1 is a scaler amplitude factor known as the stress intensity factor where:

$$K_1 = \sqrt{\frac{E\mathcal{G}}{\pi}} \tag{4.4}$$

in which $\mathcal{G}$ is the energy associated with the unit crack extension and E is Young's Modulus of Elasticity. The parameters r and θ in Equation (4.1) to (4.3) are the polar coordinates describing the surrounding crack tip region as shown in Fig. 4-1.

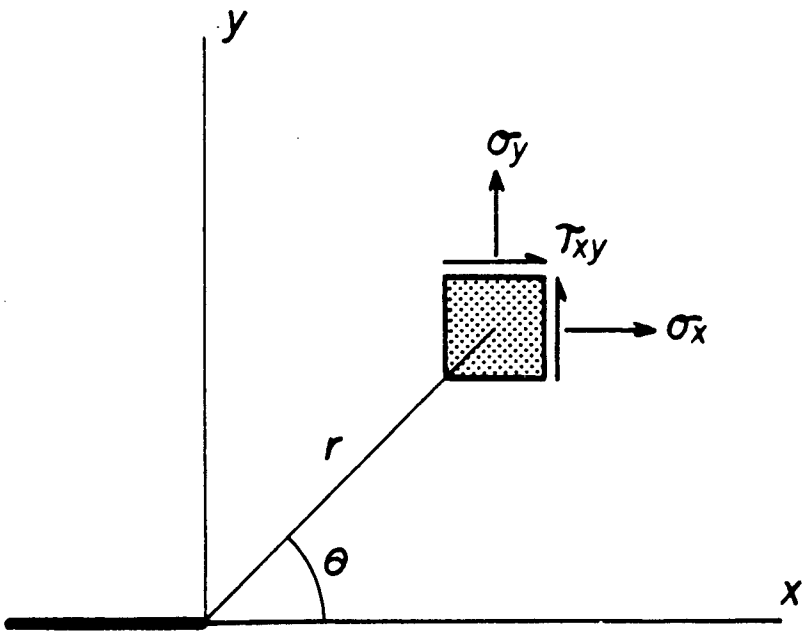

Figure 4-1: Two-dimensional polar coordinate system and stress components at a crack tip

The subscript 1 in the stress intensity factor term K_1 refers to a tensile opening load condition, commonly called Mode I. Similar solutions to Equations (4.2) and (4.3) exist for other load conditions. Mode II is for in-plane shear

and Mode III for out-of-plane shear load conditions, as shown in Fig. 4-2. However, in the study of the fatigue behavior of large-scale welded bridge details with specific application to design, Mode I represents the relevant loading condition. A deviation from a Mode I loading condition to either a Mode II or Mode III would represent an extreme or unusual loading situation not considered by the basic fatigue design philosophies.

The stress intensity factor may be expressed in a more general form as:

$$K = Y \sigma \sqrt{a} \tag{4.5}$$

where Y is a dimensionless quantity, determined by the body geometry and crack configuration. The stress intensity factor, K, has the units of stress times the square root of length. Equation (4.5) represents an idealized case of an internal thru thickness crack in an infinite plate. By modifying the parameter Y to incorporate the effects due to boundary conditions, non-uniform stress fields, etc, Equation (4.5) may be used to define the stress intensity factors for a wide range of cracks and geometrical conditions.

The stress intensity factor, K, provides a description of the magnitude of crack tip deformation fields and can therefore be considered as a crack driving force parameter under cyclic loading conditions. The fatigue crack growth rate, da/dN, has been related to the cyclic range of stress intensity factor ΔK, where ΔK represents the difference between the maximum and minimum stress levels.[31, 32] Therefore, in terms of Equation (4.5), the range of stress intensity factor can be taken as:

$$\Delta K = \Delta \sigma \; Y \sqrt{a} \tag{4.6}$$

where

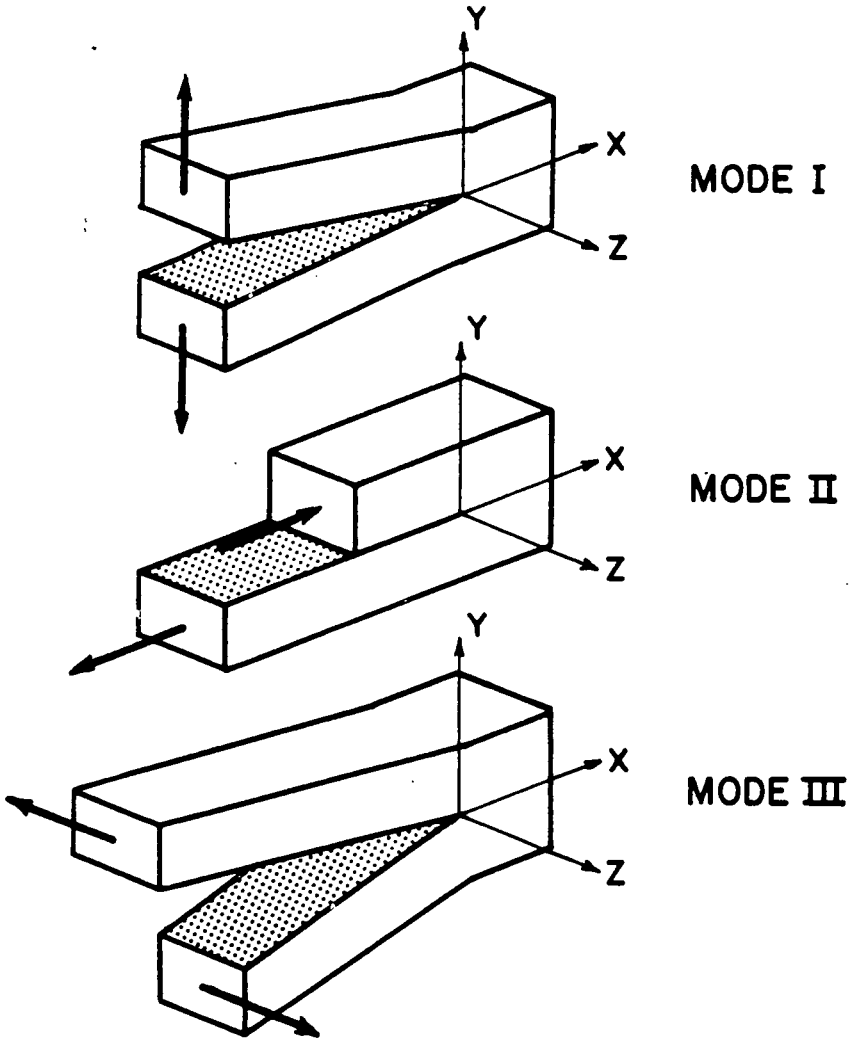

Figure 4-2: Three modes of crack front displacement under different loading conditions

$$\Delta\sigma = \sigma_{max} - \sigma_{min}$$

Stable fatigue crack propagation is commonly divided into three growth rate regimes depending upon the level of the range of stress intensity, ΔK, as shown in Fig. 4-3. The intermediate growth rate regime (Region II) can be described by a power-law relationship[33] in the form of:

$$\frac{da}{dN} = C\ \Delta K^n \tag{4.7}$$

where

a = crack length

N = number of cycles

ΔK = range of stress intensity

and C and n are: functions of material properties, environment, temperature, minimum and maximum stress levels, and frequency of loading. At the two extreme regimes of ΔK, deviations occur from the linear power-law relationship of the growth rate curve. In Region III, as ΔK increases, growth rates accelerate until a limiting maximum value of ΔK is reached. This value is a function of the material's fracture toughness, K_{1C}. In this region, an ever increasing amount of plasticity occurs at the crack tip until a critical crack tip state of stress is reached and rapid, unstable crack propagation occurs, culminating in fracture of the cross-section. While this obviously results in catastrophic failure of the specimen or structural member, this region of crack growth is "after the fact" as far as high cycle fatigue crack growth is concerned. By the time Region III is reached in the life of a full-scale, in-service welded steel detail, over 95 percent of the total fatigue life has been exhausted.

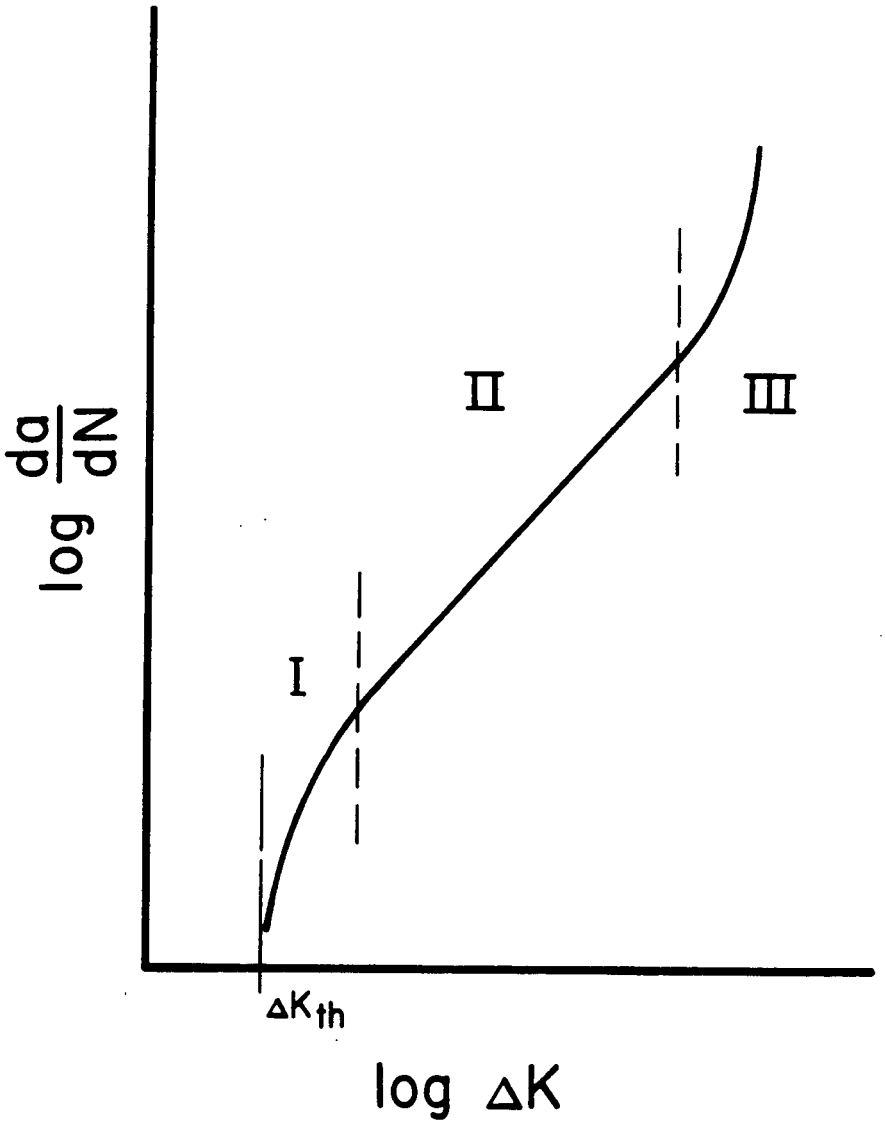

Figure 4-3: Fatigue crack propagation curve

Fatigue crack propagation is influenced mostly by Region I. For it is in this regime where a growth - no growth situation exists. At low ΔK levels, the crack growth rates diminish as the ΔK decreases to an asymptotic limit. This minimum value of ΔK is referred to as the threshold range of stress intensity, ΔK_{th}. For stress range cycles that result in a ΔK below the ΔK_{th} at the crack tip, no crack tip extension occurs.

With reference to Equations (4.1) to (4.3) and Fig. 4-1, the distance r is measured from the crack tip. As r approaches zero, the crack tip stress become infinite. However, most all engineering materials exhibit plastic flow at an elevated stress state, as defined by the material's yield stress, σ_{ys}. This places a limiting value on the stress field at or near the crack tip since yielding will occur. An estimation for an idealized circular plastic zone was proposed by Irwin[34] for Mode I loading conditions as shown in Fig. 4-4. The plastic zone radius, r_p, is determined by solving Equation (4.1) for r with the local stress, σ_y, equal to the yield stress, σ_{ys}, at $\theta = 0$. The plastic zone radius can be approximated by

$$r_p = \frac{1}{c\pi}\left[\frac{K_1}{\sigma_{ys}}\right]^2 \tag{4.8}$$

where the parameter c is used to take into account the degree of elastic constraint at the crack tip. For plane-stress conditions, c is taken as 2. For the plane-strain condition (applicable to large-scale welded details with cracks), c is taken as 6. Therefore, the plane-strain condition results in a smaller plastic zone size (by a factor of 3). It should be recognized that the value of σ_{ys} obtained experimentally from coupon tension tests would be less than that exhibited at a crack tip. At the crack tip, a plane-strain condition exists,

resulting in a multi-axial state of stress, thus elevating the commonly found uniaxial yield stress. The concept of the idealized circular plastic zone is useful in describing additional fracture mechanics principles such as crack closure and overload induced fatigue crack propagation.

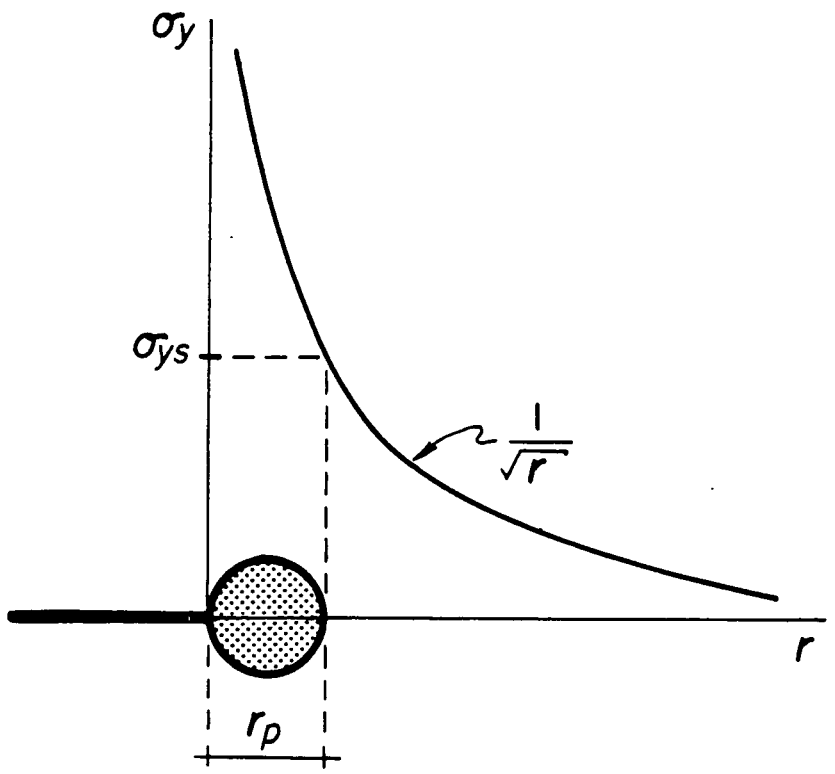

Figure 4-4: Schematic of elastic stress distribution near a crack tip

4.2 Crack Closure Concept

The range of stress intensity, by itself, is inadequate in describing fatigue crack propagation. From an examination of Eq. (4.6), it is apparent that the range of stress is the only stress parameter. No consideration is given to the mean stress level, or similarly, the stress ratio. The crack closure concept, as proposed by Elber,[35, 36] can be used successfully to correlate constant cycle fatigue crack propagation rates at different stress ratios. The underlying principal behind the the concept is that as a consequence of the permanent tensile deformation of the plastic zone left in the wake of a propagating crack during cycling, partial crack closure will occur during the unloading portion of the load cycle. Therefore, the strain required to open a fatigue crack is greater than the strain required to close the crack. Elber concluded that an effective stress intensity range, ΔK_{eff} (where $\Delta K_{eff} = K_{max} - K_{op}$), would better describe the fatigue crack process than the nominal or applied ΔK ($\Delta K = K_{max} - K_{min}$) as shown in Fig. 4-5. At a stress intensity below ΔK_{eff}, no fatigue crack propagation occurs since the crack tip is essentially closed and the actual value of K is zero.

Since the crack closure concept is based on the permanent deformations in the plastic zone, the degree of constraint at the crack tip will influence ΔK_{eff}. It can be argued that since the plastic zone size for the plane-strain load condition is less than that of plane-stress (Eq. (4.8)); less permanent plastic deformation is possible, hence, ΔK_{eff} is closer in value to ΔK.

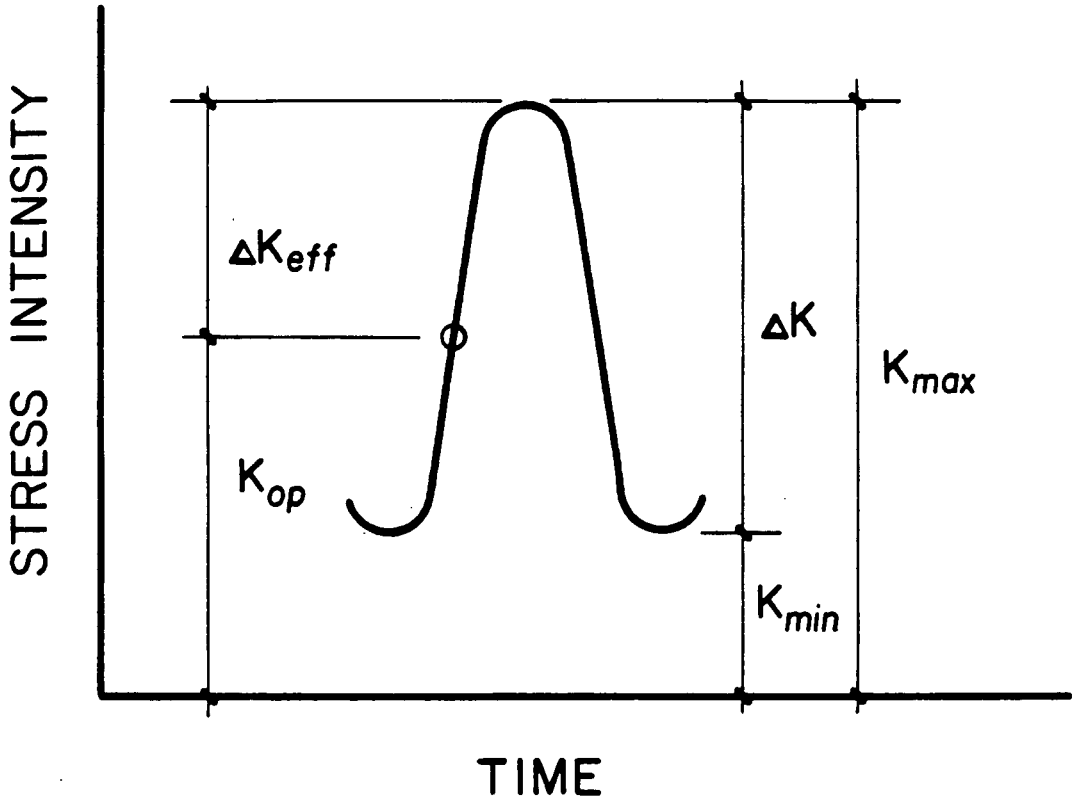

Figure 4-5: Schematic of effective stress intensity range concept

4.3 Fatigue Crack Propagation Rates

In the context of full-scale welded bridge details, fatigue crack propagation rates will only be considered for structural steels normally used in this type of application. A host of data exists for fatigue crack propagation in Region II, as defined by Equation (4.7). This includes a study sponsored by the National Cooperative Highway Research Program that examined subcritical crack growth and the fracture characteristics of bridge steels.[37] The steel types examined were American Society for Testing and Materials (ASTM) designations A36,

A588 Grades A and B, and A514 Grades E and F. Both constant amplitude and variable amplitude load test data will be reviewed for the different steel types with specific attention given to the effect of the stress ratio or mean stress level on the propagation rates. In addition, an examination will be made of the influence of specimen type used to obtain the test results, especially in the slow growth regime of Region I (Fig. 4-3).

4.3.1 Constant amplitude growth rates

The fatigue crack propagation test results of NCHRP Project 12-14 indicated that steel type does influence fatigue crack growth rates when classified according to grain structure. For high strength martensitic steels, yield strength greater than 80 ksi, Region II fatigue crack propagation rates in an air environment were conservatively (upper bound) estimated by the equation:

$$\frac{da}{dN} = 0.66 \cdot 10^{-8} \ \Delta K^{2.25} \tag{4.9}$$

As indicated by summary of test data shown in Fig. 4-6, the data for this type of structural steel fall within a single distribution band. The stress intensity range varied from 6.0 to 150 ksi$\sqrt{\text{in.}}$ Loading of the specimens resulted in an average stress ratio of only 0.1.

For the lower strength ferrite-pearlite steels, yield strength less than 80 ksi, the Region II growth rates were found to be best estimated by the equation:

$$\frac{da}{dN} = 3.6 \cdot 10^{-10} \ \Delta K^{3.0} \tag{4.10}$$

The test data for this type steel are plotted in Fig. 4-7. As with the martensitic steel data, only a stress ratio of 0.1 was used.

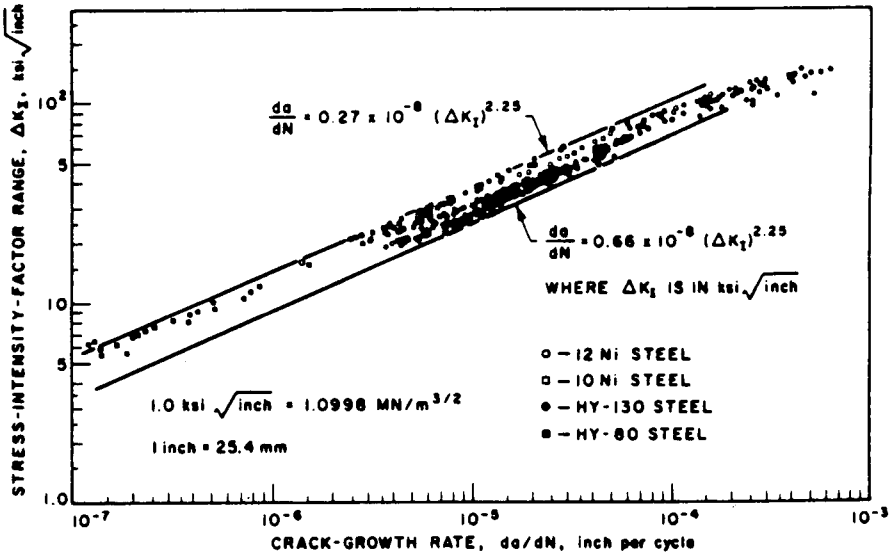

Figure 4-6: Summary of fatigue crack propagation data for martensitic steels[37]

A comparison of Equation (4.9) and (4.10) reveals that although the stress intensity range, ΔK, exponent is smaller for martensitic; the constant C (Eq. (4.7)) is smaller for the ferrite-pearlite steels than that of the martensitic steels (Fig. 4-8). In the higher growth rate regime of Region II, the propagation rates for martensitic steels provide the upper bound (of growth rate) value. However, at lower values of ΔK, the growth rates calculated from Eq. (4.10) for ferrite-pearlite steels provide a better estimation. The higher growth rates in ferrite-pearlite steels at low ΔK values can be contributed to the composition character of the microstructure of this type of steel.[38]

Growth rate experiments performed by Bucci et al.[39] revealed the influence of the stress ratio on fatigue crack propagation. All tests were conducted with

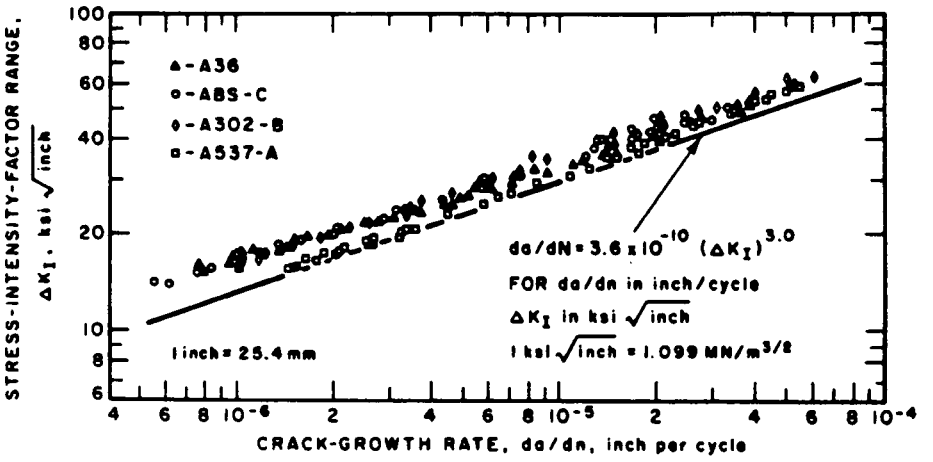

Figure 4-7: Summary of fatigue crack propagation data for ferrite-pearlite steels[37]

ASTM A517 Grade 7 steel with a nominal yield strength of 100 ksi. As illustrated in Fig. 4-9, at low fatigue crack growth rates, the stress ratio affects the fatigue crack growth rates. As the stress ratio increases, the growth rate also increases. This behavior has been observed by other investigators as well. This behavior can be contributed to crack closure effects (Sec. 4.2) as set forth by Elber. Due to crack closure during a portion of the stress cycle, the actual stress intensity range at the crack tip is less than the computed or nominal value.

The crack growth data for steels in Region II under constant amplitude loading show only a secondary effect of the stress ratio on fatigue crack propagation rates. While closure models would seem to predict an increase in

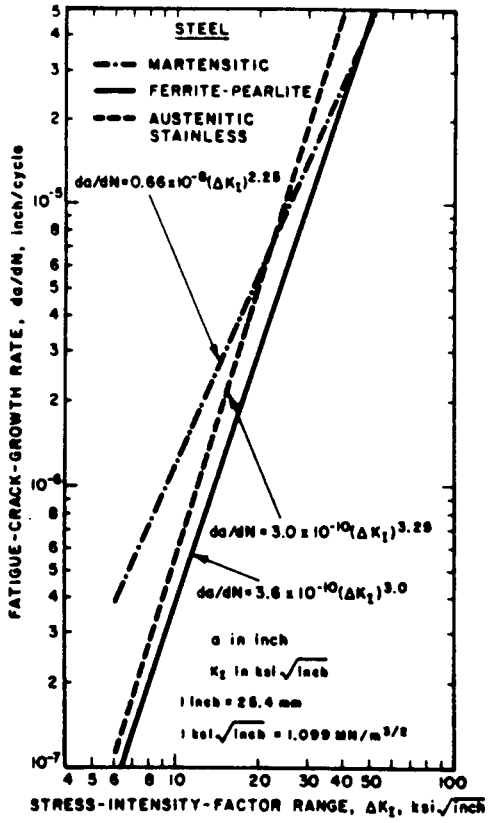

Figure 4-8: Comparison of fatigue crack propagation rates for ferrite-pearlite and martensitic steels

the growth rates with an increase in the stress ratio due to the increased crack tip opening, observed growth rate are not significantly higher. However, with the increased crack tip opening with increased stress ratio comes an increase in the plastic zone size as defined by Eq. 4.8. This leads to an increase in the residual plastic zone wake behind the advancing crack, thus decreasing the crack tip opening.

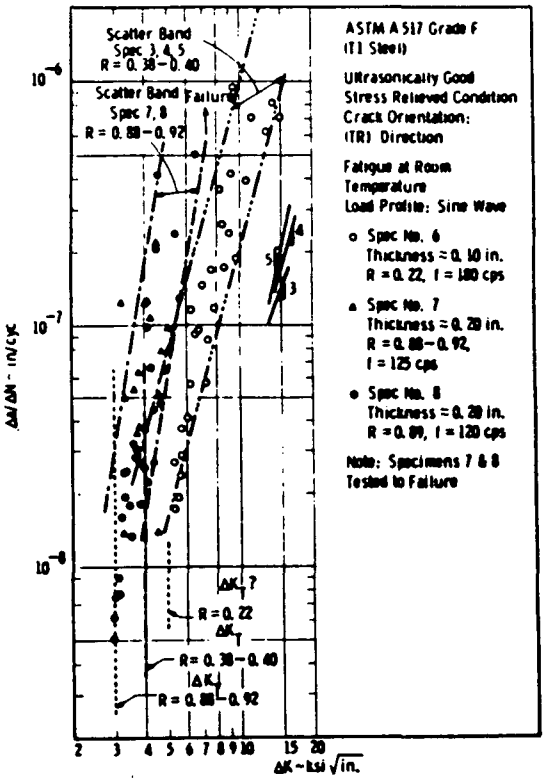

Figure 4-9: Comparison of crack growth rate behavior for varying stress ratio, ASTM A517 Grade F steel[39]

4.3.2 Variable amplitude growth rates

Also studied in NCHRP Project 12-14 was the effect of variable amplitude loading on fatigue crack propagation rates. The results of the study indicated that for all steels tested, the average rate of fatigue crack growth under random sequence, variable amplitude loading could be related to the constant amplitude growth data through the use of a root-mean-square average of the stress

intensity range, ΔK_{rms}. Thus, fatigue crack propagation rates could be estimated by the equation:

$$\frac{da}{dN} = C\ (\Delta K_{rms})^n \tag{4.11}$$

where C and n are material constants. Comparison of constant amplitude and variable amplitude growth rates for A36 steel and A588 Grade A steel are shown in Figs. 4-10 and 4-11, respectively.

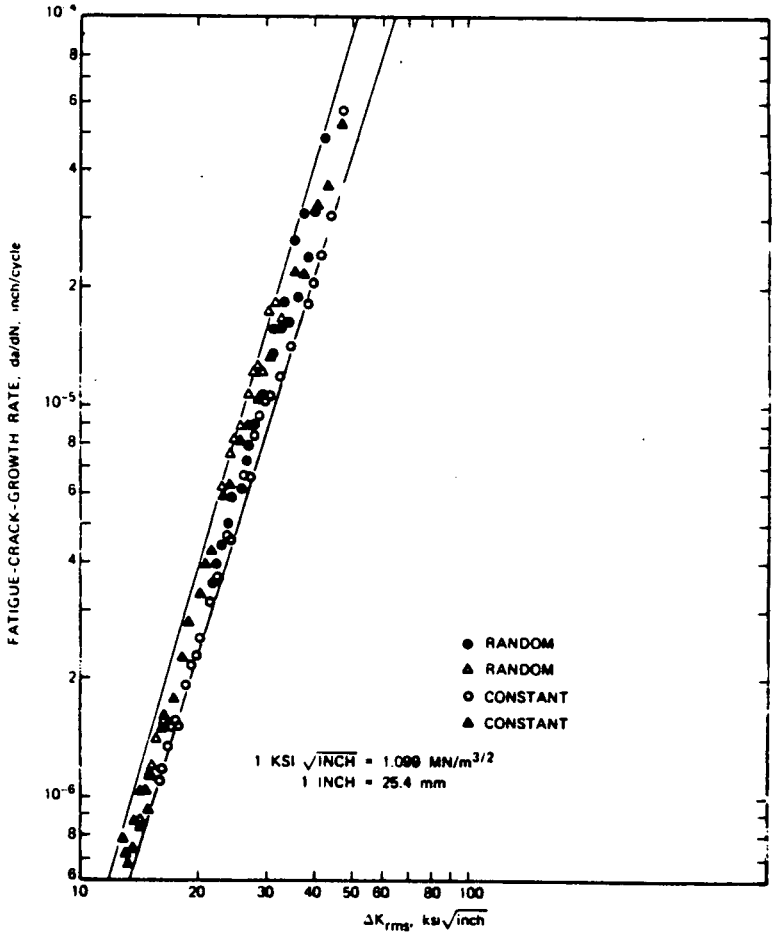

Figure 4-10: Crack growth rates for A36 steel[37]

As part of NCHRP Project 12-15(4), variable amplitude crack growth studies were conducted in the high cycle regime (Region I) using 1/4 in. thick

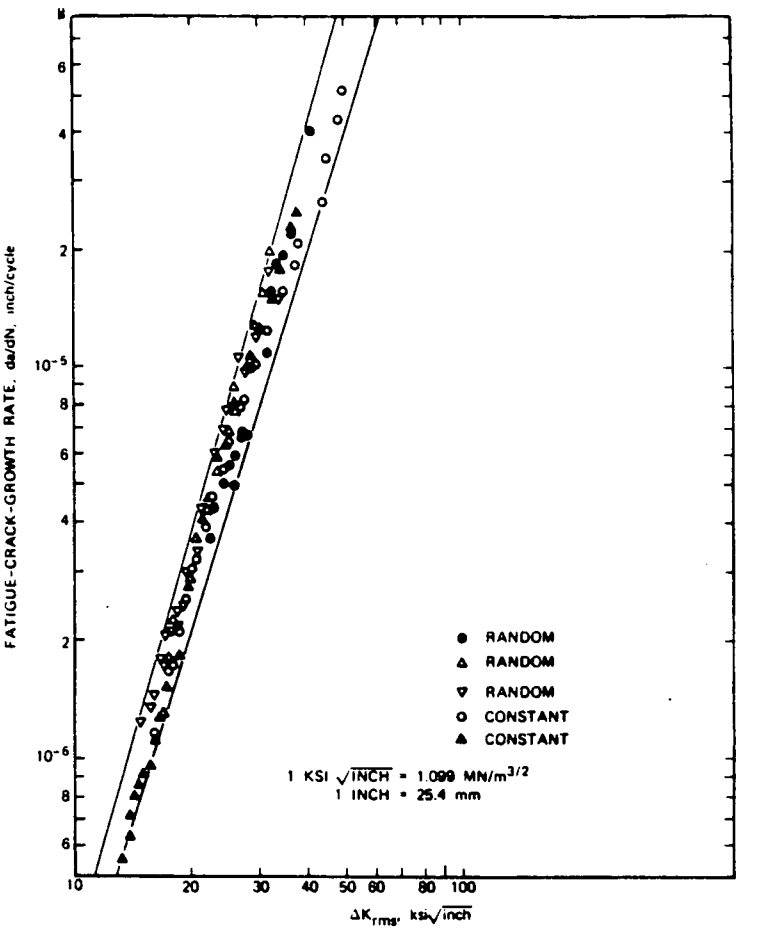

Figure 4-11: Crack growth rates for A588, Grade A steel[37]

center-crack A36 steel plate specimens. The specimens were tested under a random variable amplitude load sequence. Eight different block load levels were randomized in a Rayleigh-type distribution of 150 total blocks with each block having approximately 950 constant amplitude cycles. Three different stress ratios were studied: 0.3, 0.55, and 0.8. The highest ratio corresponds to the stress condition that exists in welded joints due to the tensile residual stresses.

The crack growth rates from the study are plotted in Fig. 4-12 with the upper bound crack growth rate curve suggested by Barsom (Eq. 4.10). These results were evaluated by relating the average crack growth rate under the

variable amplitude loading to the Root-Mean-Cubed of the stress intensity range. As the plot of data indicates, the growth rates are sensitive to the stress ratio, R. As the stress ratio was increased to 0.8, the growth rates coincide with the upper bound estimate. This was most evident in the low stress intensity range or near the crack growth threshold level.

4.4 Fatigue Crack Growth Thresholds

As the data from the previous section indicated, the fatigue crack growth rates are sensitive to the stress ratio. As R increases, crack growth thresholds have been found to decrease. A lower bound estimate of ΔK_{th} in austenite, banite, ferrite-pearlite, and martensite steels can be given as[40]

$$\Delta K_{th} = 6.4\,(\,1 - 0.85\,R) \tag{4.12}$$

where ΔK_{th} is given in ksi$\sqrt{\text{in}}$ and the stress ratio, R, is greater than +0.1.

Traditionally, crack growth threshold values are obtained from pre-cracked compact tension specimens in which the cyclic loading is reduced, decreasing ΔK, until a ΔK_{th} state is reached.[41] Recent re-evaluations of this test procedure have shown its sensitivity to the applied stress ratio. As the stress ratio is increased (increasing K values), it has been observed that the ΔK_{th} occurred at progressively lower stress intensity ranges.[42] This behavior can be related to the crack closure concept discussed previously. The pre-existing long crack in the specimen has increased crack closure due to the development of the residual plastic wake from the pre-cracking cycling. Hertzberg et al. has suggested a K_{max}, ΔK-decreasing test procedure be used to obtain a more realistic value of ΔK_{th} associated with engineering components. The high K_{max} value will reduce the influence of closure effects at the crack tip and will result

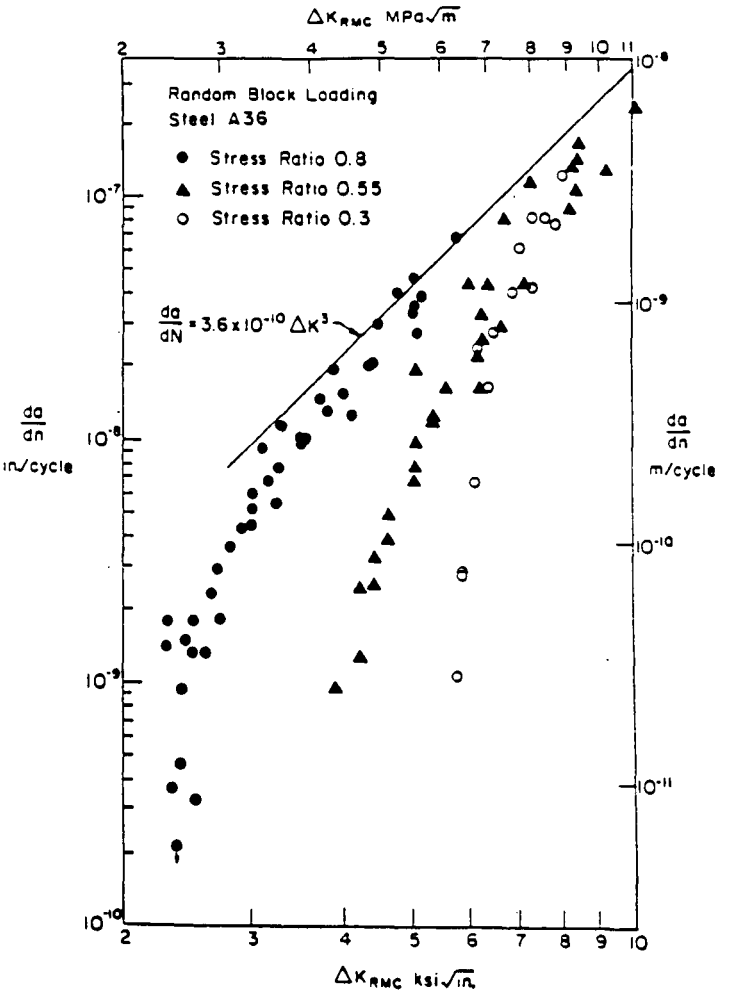

Figure 4-12: Variable amplitude block loading growth rates[16]

in lower observed values of ΔK_{th}.

The variable amplitude crack growth data will exhibit crack growth below ΔK_{th} obtained from constant amplitude crack growth data when an averaged stress intensity range is used to describe the load spectrum, such as ΔK_{RMS} or ΔK_{RMC}. While the average value of ΔK is below ΔK_{th}, the higher stress intensity ranges in the load spectrum will cause the initiation of crack propagation. Crack growth tests were carried out on similar specimens under both constant and variable amplitude loading near the crack growth threshold.[16] Only a small percentage of the variable load cycles resulted in stress intensity ranges above the constant cycle crack growth thresholds. At a stress ratio of 0.8, the threshold was reduced from 3.5 ksi$\sqrt{\text{in}}$ for constant cycling to approximately 2.0 ksi$\sqrt{\text{in}}$ for variable amplitude cycling. At a stress ratio of 0.55, the reduction of the threshold was from 5.5 ksi$\sqrt{\text{in}}$ to about 3.5 ksi$\sqrt{\text{in}}$.

A consequence of the higher load cycles resulting in stress intensity ranges above the threshold is crack tip advancement. The increase in crack size causes an increase in the stress intensity range for the entire load spectrum. Therefore, as crack growth is driven by the higher load cycles, an ever increasing number of lower load cycles will result in stress intensity ranges above the threshold. Eventually, all stress intensity ranges will be above the threshold and, therefore, contribute to crack propagation. This principle will form the basis of a variable amplitude crack propagation model to be developed in the next chapter.

4.5 Overload Induced Fatigue Crack Propagation

One of the most extensively studied and documented aspects of fatigue crack propagation has been the effect of overloads on crack growth rates.[43, 44, 45, 46, 47] If an isolated load is sufficiently large enough in magnitude, crack growth rates will decrease. This effect on crack propagation is shown schematically in Fig. 4-13. Several models have been set forth to explain the behavior, such as: crack tip blunting,[48] residual stresses,[49] and crack closure. Both the crack tip blunting model and the residual stress model suggest that the mechanism for delay will occur immediately upon application of the overload. However, von Euw observed that the retardation of the crack growth rate did not occur immediately, but rather required a number of additional cycles to decrease to a minimal level.[50] The delay retardation is caused by the formation of a zone of residual tensile deformation left in the wake of a propagating crack and is therefore supportive of the crack closure model.

Crack growth studies by Zwerneman[51] examined the effect of closely spaced overload stress cycles on fatigue crack propagation rates. When the high stress cycles were closely spaced (every 10 cycles) around smaller, single amplitude stress cycles, a mean stress effect caused growth rate acceleration. Retardation effects were only observed when the application of the overload was separated by thousands of smaller stress cycles. The spectrums used in the experimental program were highly programmed. It was concluded that for highway bridge loadings, the stress range spectrum is sufficiently random in nature such that crack growth acceleration would not occur. However, the fatigue damage should never be estimated to be greater than that provided by

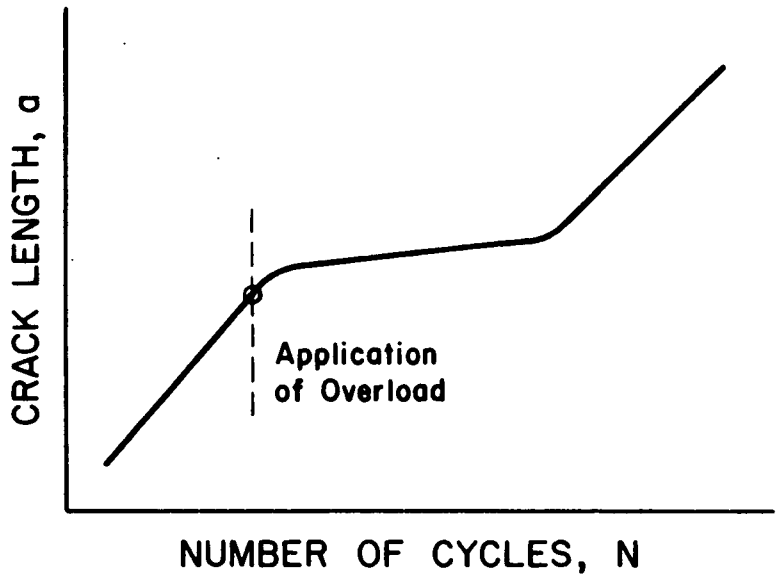

Figure 4-13: Influence of stress cycle overload on fatigue crack propagation

Miner's Rule in conjunction with the rainflow cycle counting method.

Although available crack growth data is lacking in this area, it can be speculated that overload/underload effects on propagation rates would decrease as the stress ratio is increased. This hypothesis is supported by the crack closure concept. The development of any crack growth acceleration or retardation is highly dependent on the formation of the residual crack tip plastic zone and the subsequent crack advancement through this zone with closure. An increase in the stress ratio would decrease the crack closure effects and minimize any acceleration or retardation effects on the crack growth as schematically shown in Fig. 4-14. This behavior would also be minimized by any randomness occurring in the load spectrum since this would have a tendency to "wash out" any isolated plastic zone resulting from an overload. Most crack propagation studies involving overloads have used programmed load spectrum with the overload stress cycles separated by smaller, constant stress cycles. To date, no crack growth studies have been performed under random loading at high stress ratios and with stress fluctuations within the ranges similar to those experienced by bridge details.

4.6 Summary

The current chapter has provided a brief summary of linear elastic fracture mechanics concepts with specific emphasis on fatigue crack propagation. While fatigue cracks are influenced by a wide range of factors resulting in an even greater range of behavior; any application of test results must be done within certain constraints. For welded steel bridge details this means crack growth in a zone of high tensile residual stress, stress fluctuations that are both variable and random, and within limited ranges of stress.

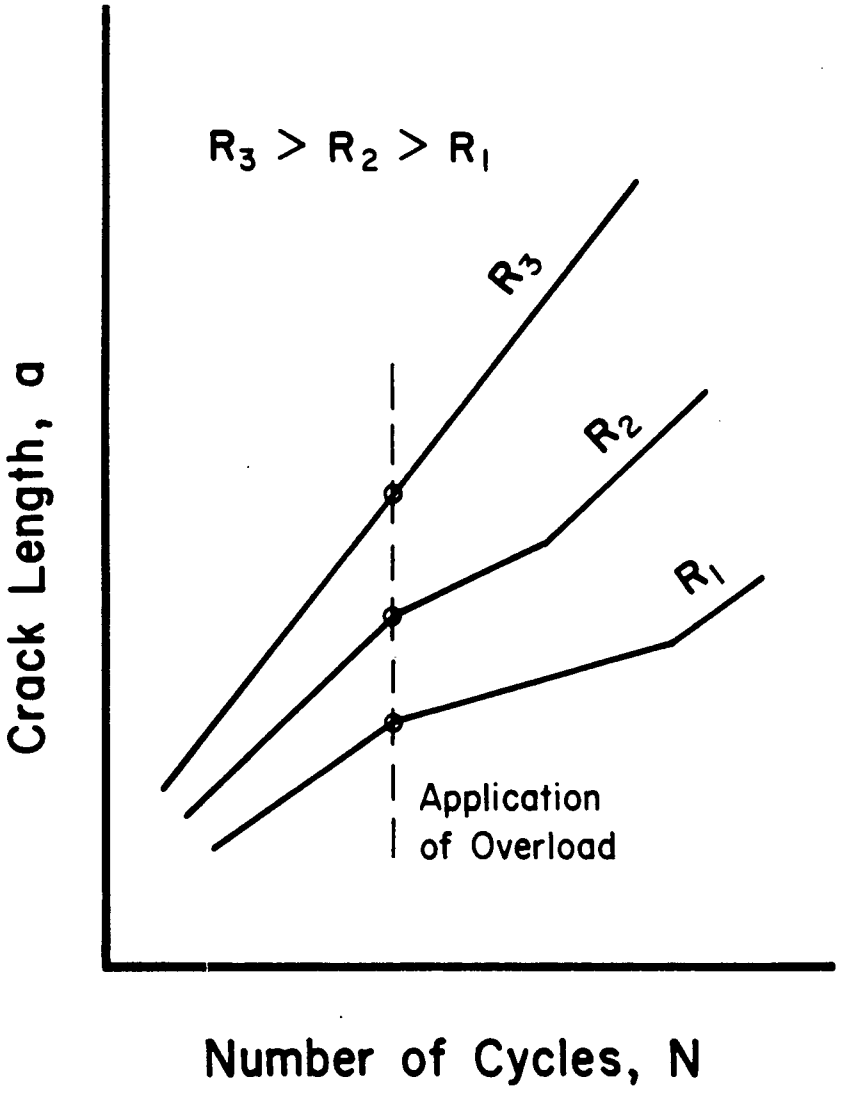

Figure 4-14: Schema of the effect of stress ratio on overload induced fatigue crack propagation

Given the preceding discussion on several aspects of fatigue crack propagation, the following conclusions can be drawn with regard to the fatigue behavior of large-scale welded steel details and the influence of crack propagation at high stress ratios:

- As the stress ratio increases, fatigue crack propagation rates increase. This effect is more pronounced at lower stress intensity range values. A schematic presentation of this effect at relatively low values of ΔK is shown in Fig. 4-15.

- As the stress ratio increases, fatigue crack threshold values, ΔK_{th}, decrease. For ferrite-pearlite steels, a fatigue crack threshold value as low as 1.8 ksi$\sqrt{\text{in}}$ has been observed under variable amplitude loading.

- As the stress ratio increases, it can be speculated that the effect of a single overload stress cycle on fatigue crack growth retardation is decreased. At high stress ratios, this effect is negligible.

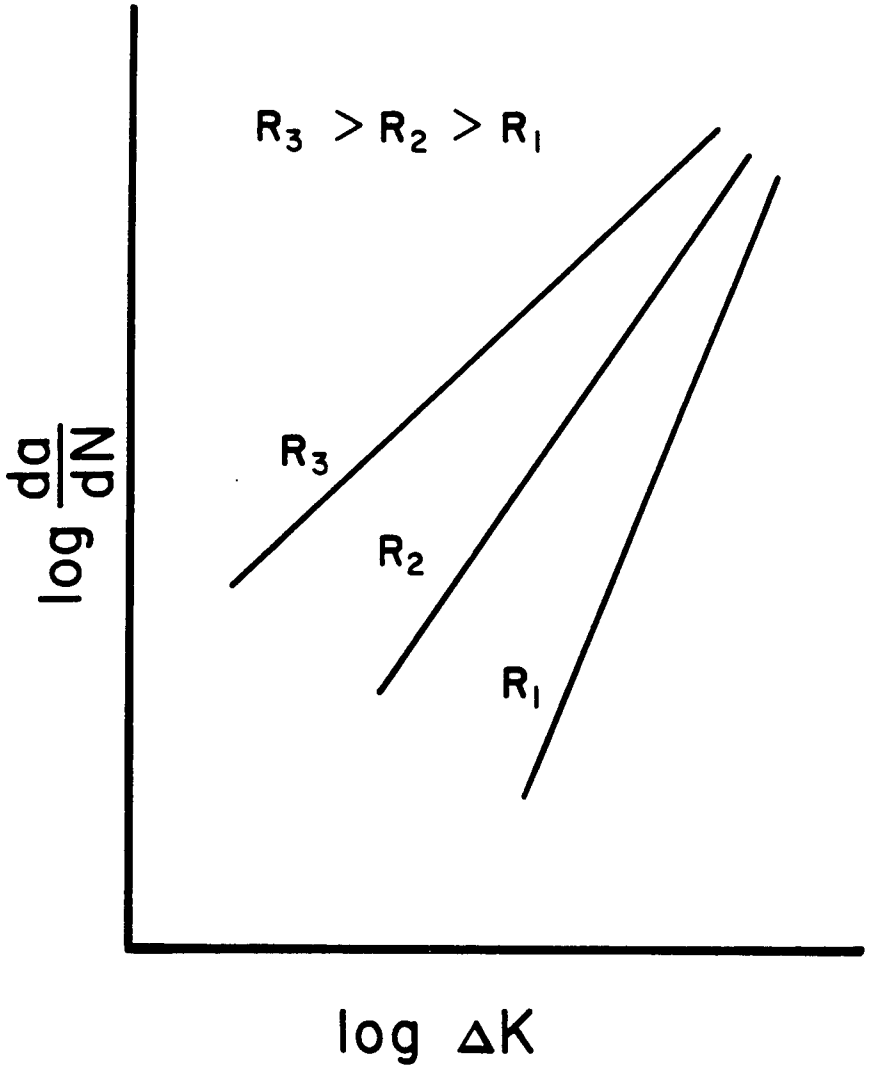

Figure 4-15: Schema of the effect of stress ratio on fatigue crack propagation rates

Chapter 5
Fatigue Crack Propagation Model

The development of linear-elastic fracture mechanics has allowed for its practical application to fatigue crack growth in steel bridge members. In this chapter, these principles will be used to evaluate the welded details of test specimens from NCHRP Projects 12-15(4) and 12-15(5). This includes the variable amplitude test results with regard to the variability that exists in fatigue behavior of welded details. In addition, the effect of stress cycle truncation is studied for both fatigue testing and fatigue life estimates.

5.1 Fatigue Crack Growth Model

The Paris Power Law (sec 4.1) is used to relate fatigue crack extension, da/dN, to the range of stress intensity factor, ΔK, and is given by:

$$\frac{da}{dN} = C\ \Delta K^n \tag{5.1}$$

The best estimate for the upper bound for fatigue crack growth rate in bridge steels and weldments is given by:

$$\frac{da}{dN} = 3.6{\cdot}10^{-10}\ \Delta K^{3.0} \tag{5.2}$$

This relationship will be used in the fatigue crack growth model. With the use of this crack growth rate as a constant value, the assumption is made that cycle interaction does not occur. This implies that crack acceleration or retardation does not result from cycle overloads or underloads to the degree that the crack growth rate changes significantly from the assumed values over the life of the detail. The experimental programs from which the test results are to be modeled have load cycles applied from a constant minimum load level

and as individual load cycles. No cycle addition or superposition of smaller stress cycles occurred. In addition, the load cycles were applied in a random fashion.

The calculation of the stress intensity range, ΔK, for welded bridge details, such as coverplate terminations and web attachments, can be related to the idealized case of a central through crack in an infinite plate by the application of appropriate stress field correction factors.[52, 53, 54] The generalized stress intensity range is given by:

$$\Delta K = F(a)\ Sr\ \sqrt{\pi a} \tag{5.3}$$

where $F(a)$ is the product of all applicable correction factors as a function of crack length, a, and is given by:

$$F(a) = F_e \cdot F_s \cdot F_w \cdot F_g \tag{5.4}$$

where

F_e = elliptical crack shape correction

F_s = free surface correction

F_w = finite width correction

F_g = stress concentration correction

The crack shape correction factor, F_e, is given by the following equation:[55]

$$F_e = \frac{1}{E(k)} \tag{5.5}$$

where $E(k)$ is the complete elliptical integral of the second kind as given by:

$$E(k) = \int_0^{\pi/2} [\ 1 - k^2 \sin^2\theta\ ]^{1/2}\ d\theta \tag{5.6}$$

where

$$k^2 = \frac{c^2 - a^2}{c^2}$$

a = minor semidiameter (surface crack depth)

c = major semidiameter (one-half the crack width)

For a semicircular crack in a semi-infinite plate subjected to a uniform stress, the free surface correction is given by:[52]

$$F_s = 1.211 - 0.186 \sqrt{\frac{a}{c}} \tag{5.7}$$

For a central crack in a plate of finite width the finite width correction factor is given by:[52]

$$F_w = \sqrt{\sec \frac{\pi a}{2t}} \tag{5.8}$$

A general approximation for the stress gradient correction factor, F_g, can be given in the form:[56]

$$F_g = \frac{K_{tm}}{1 + G\alpha^\beta} \tag{5.9}$$

where G and β are dimensionless constants, α is the ratio of crack size to plate thickness, a/t, and K_{tm} is the maximum stress concentration factor at the weld toe. This approximation has been found to be applicable to several different structural details including coverplates and web attachments. For the toe of an end-weld coverplate termination, Zettlemoyer developed from finite element analysis the following stress gradient correction factor:[57]

$$F_g = \frac{K_{tm}}{1 + 6.789(a/t_f)^{0.4348}} \tag{5.10}$$

where

K_{tm} = stress concentration factor

a = crack depth

t_f = flange thickness

The stress concentration factor was calculated at the toe of the weld for an uncracked section with the following equation:

$$K_{tm} = -3.539 \log\left(\frac{Z}{t_f}\right) + 1.981 \log\left(\frac{t_{cp}}{t_f}\right) + 5.798 \qquad (5.11)$$

where

Z = weld leg size

t_{cp} = coverplate thickness

t_f = flange thickness

For the web attachment detail, finite element analysis[58] indicated that the stress gradient correction factor could be approximated by the following equation:

$$F_g = \frac{K_{tm}}{1 + 0.88\ a^{0.576}} \qquad (5.12)$$

where the stress concentration factor, K_{tm}, was determined to be approximately 8.0 by finite element analysis when the attachment thickness exceeded 1.0 in.

5.2 Crack Size and Shape

The initial discontinuities that exist along a fillet weld toe are generally the result of the inclusion of nonmetallic material in the weld metal as it cools. Since these discontinuities exist in the high stress concentration region of the weld toe, they act as crack initiation sites. The initial size or depth of a discontinuity at the toe of transverse coverplate welds has been found to range from 0.001 to 0.03 in. For the web attachment detail, the range in initial crack sizes has been measured to be from 0.002 to 0.02 in.

Limited crack shape measurements for various welded details have resulted in a wide variety of estimates and are plotted in Fig. 5-1 as a function of the two semidiameters: a and c. As given by Eq. (5.7), the free surface correction factor and hence the crack propagation rate is influenced by the shape of the crack as given by the ratio of the minor semidiameter to the major semidiameter, a/c. Measurements of crack shapes in large-scale coverplated beam test specimens has provided a lower bound approximation given by:[57]

$$c = 5.462\ a^{1.133} \tag{5.13}$$

For the web attachment detail, similar measurements have provided the following relationship:[59]

$$c = 3.247\ a^{1.241} \tag{5.14}$$

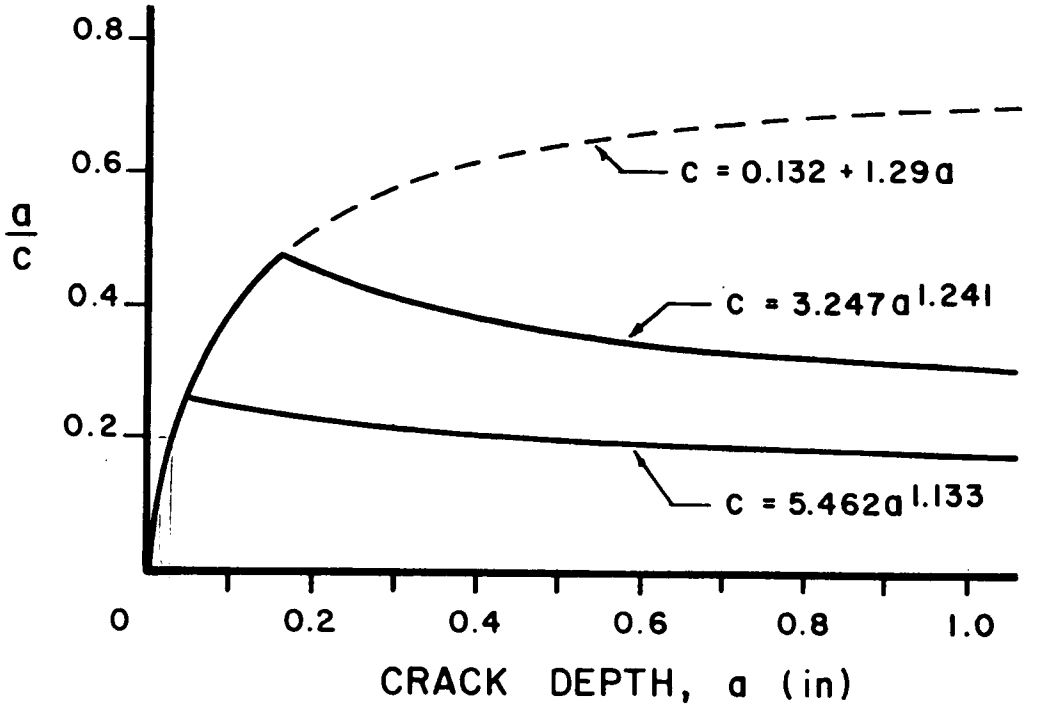

Figure 5-1: Measures crack shape variations with crack depth

5.3 Stress Spectra

In several NCHRP supported fatigue research programs a Rayleigh-type stress range spectrum was used to simulate variable amplitude loading. This includes NCHRP Project 12-12[9] and 12-15(4),[16] as well as the current NCHRP Project 12-15(5). The general shape of this type of skewed stress range spectrum is shown in Fig. 5-2.

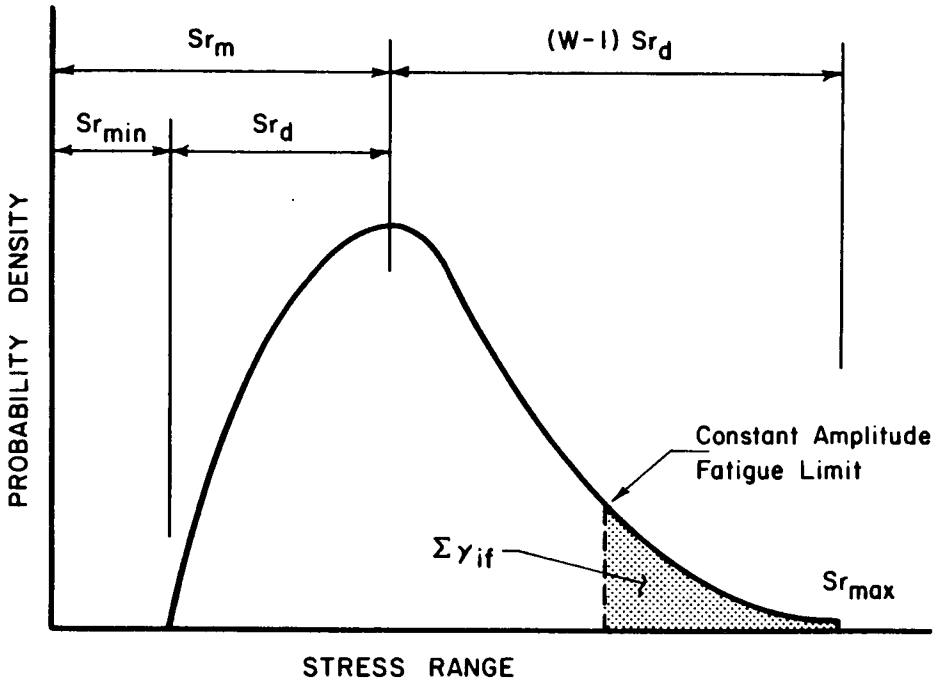

Figure 5-2: Rayleigh-type stress range spectrum

For the Rayleigh-type distribution, the probability density curve, P, is defined as follows:

$$P = \frac{p'}{Sr_d} \tag{5.15}$$

where

$$p' = 1.011\ x'\ e^{1/2\ x'^2} \tag{5.16}$$

$$Sr_d = \frac{Sr_{max} - Sr_{min}}{Sr_e} \tag{5.17}$$

in which

$$x' = \frac{Sr - Sr_{min}}{Sr_d} \tag{5.18}$$

where W is the width of the assumed distribution. The Rayleigh distribution provides a value for the effective stress range, Sr_e, that is:

$$Sr_e = Sr_{min} + 1.5 \cdot Sr_d \tag{5.19}$$

Two Rayleigh-type stress range spectra were used for the crack propagation models. Figure 5-3 is one of the stress range distributions used in NCHRP Project 12-15(4). The distribution has been normalized with the constant amplitude fatigue limit at the eight highest stress range interval. The Root-Mean-Cubed (RMC) average of the distribution is 0.55 percent of the constant amplitude fatigue limit. Figure 5-4 gives the distribution used in NCHRP Project 12-15(5). This distribution is normalized with the tenth highest stress range interval. Overloads were introduced into the distribution at an exceedance rate of 0.1 percent of the constant amplitude fatigue limit. The RMC effective stress range is given as 58 percent of the constant amplitude fatigue limit. For the series of experimental results used in this study, the overloads had a maximum value of 7/6 of the constant amplitude fatigue limit.

In addition to the Rayleigh-type distributions, three other stress range spectra were used to evaluate the influence of spectrum shape on fatigue life estimates. These include: a constant distribution, a linear distribution, and a geometrically varying distribution. The three normalized distributions are shown in Fig. 5-5

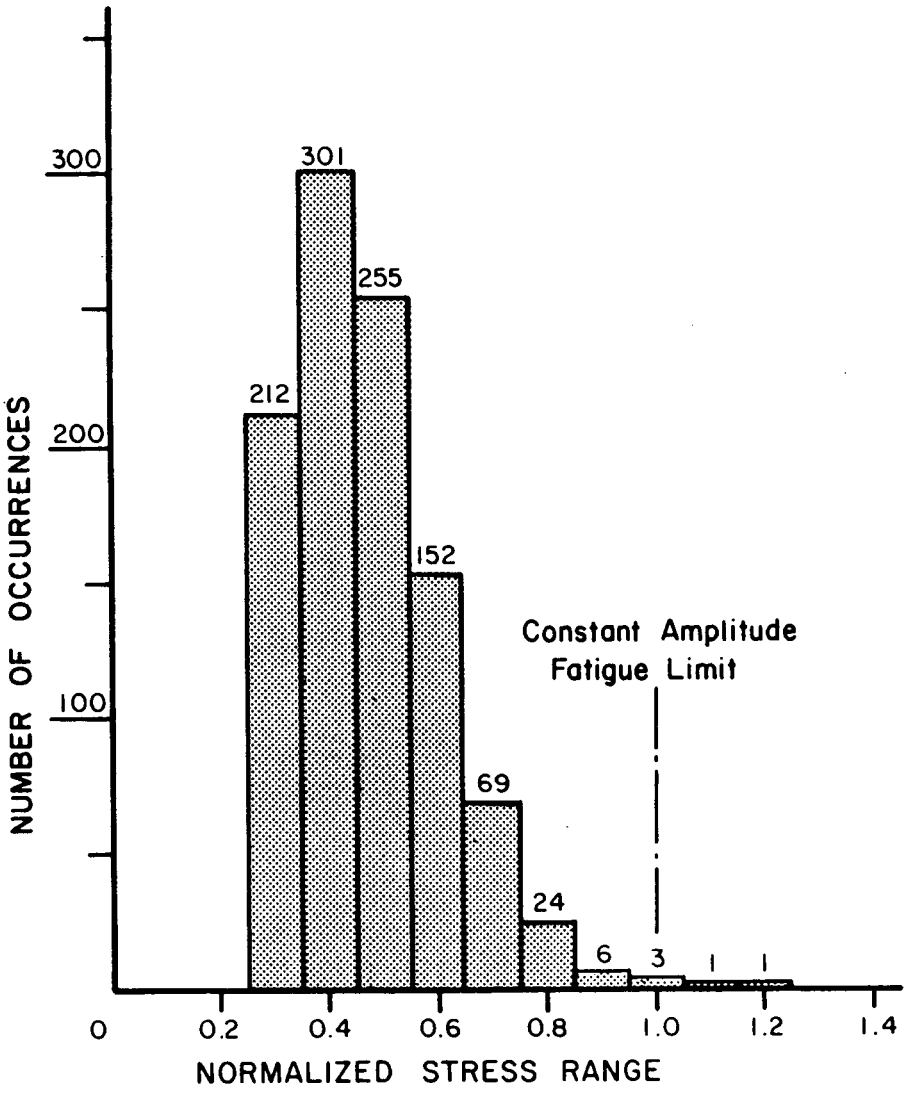

Figure 5-3: Stress range spectrum for NCHRP Project 12-15(4)

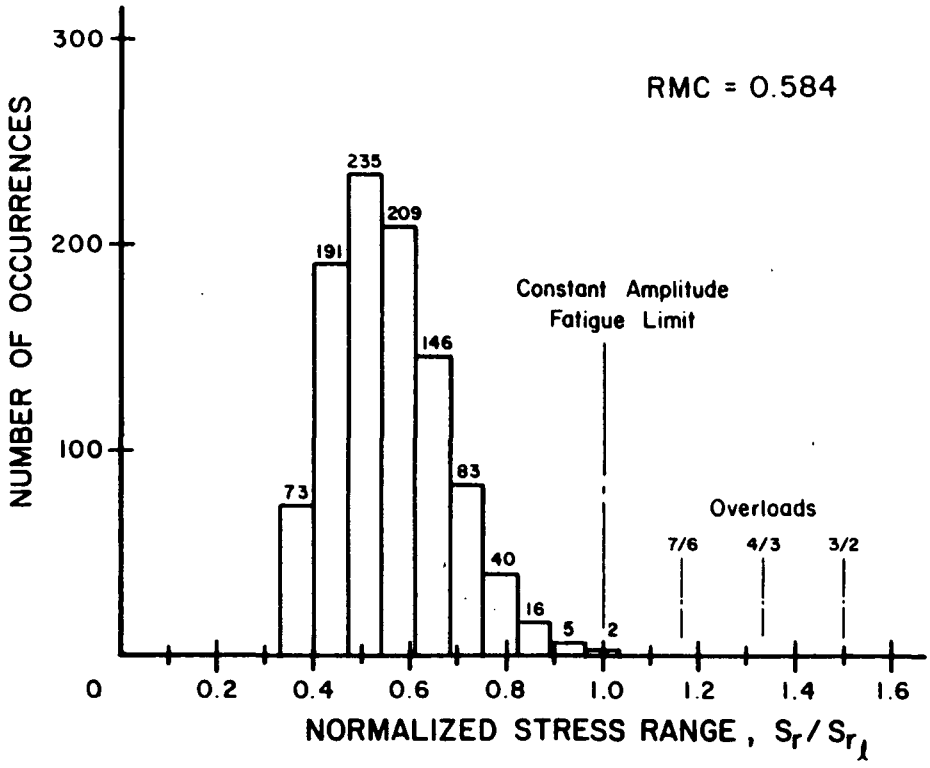

Figure 5-4: Stress range spectrum for NCHRP Project 12-15(5)

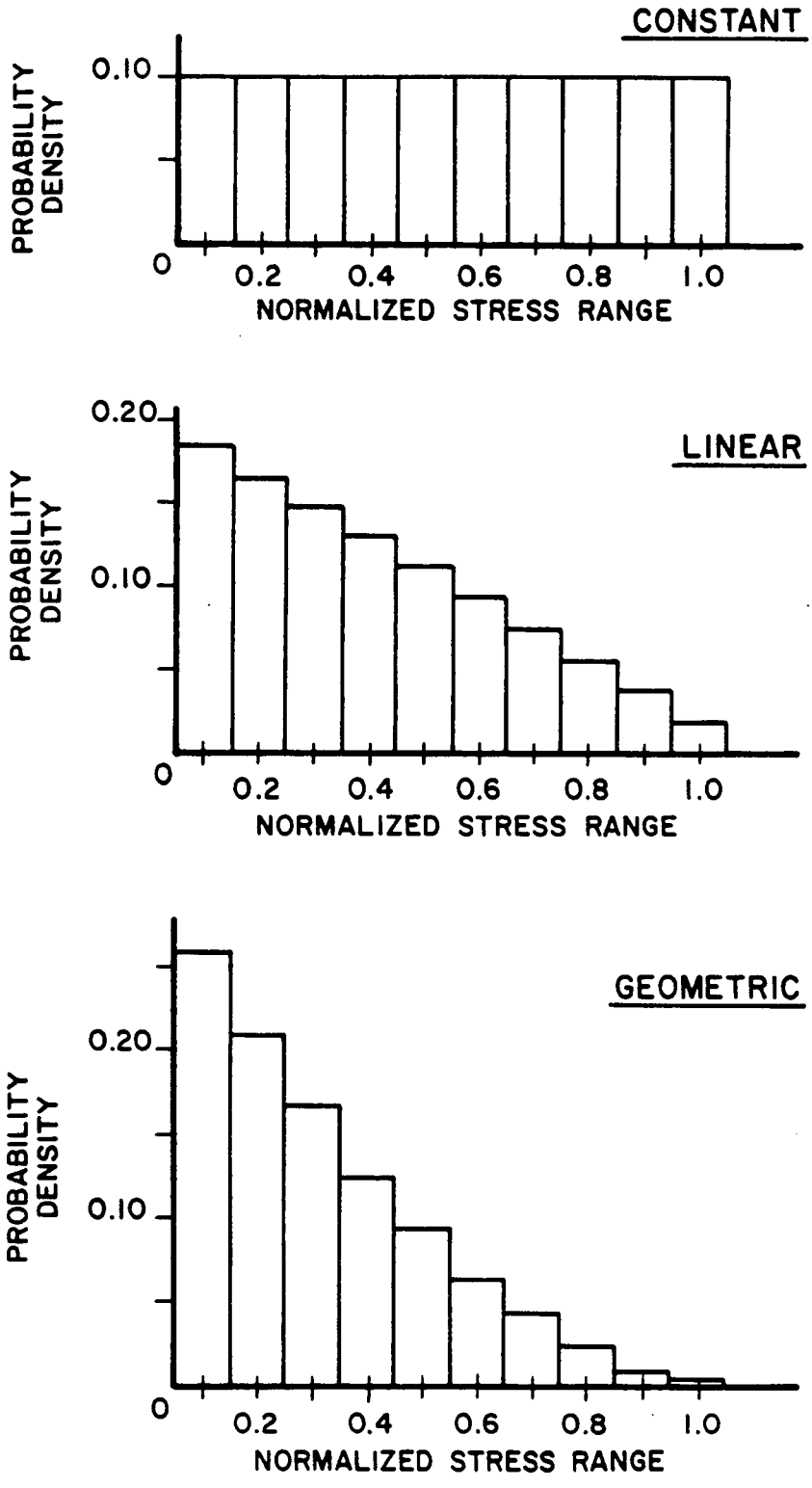

Figure 5-5: Stress spectrum shapes

5.4 Factors Influencing Fatigue Behavior

The main focus of this chapter is to examine the factors that influence the fatigue behavior of welded bridge details subjected to variable amplitude loading. Examination of Eq. (5.3) for the stress intensity factor, ΔK, shows that it's value is dependent on three parameters: the crack size, a; the stress range, S_r; and the stress field correction factors grouped together as $F(a)$. All three interrelated parameters contribute to the variability that exists in fatigue test data and have an effect on actual in-service performance as compared to design expectations. The variability of each parameter will be discussed as it pertains to the variable amplitude fatigue behavior of the coverplate detail of NCHRP Project 12-15(4).

5.4.1 Crack size

Fatigue life calculations for both constant amplitude and variable amplitude loading are sensitive to the initial crack size. As the initial crack size increases, the fatigue life will decrease due to the inverse relation between the stress intensity range and the total number of cycles to failure in the integration of fatigue life. Based on measurements of initial crack sizes in coverplated beams, a reasonable lower bound estimate of 0.03 in. will be assumed for the coverplate detail under study. Figure 5-6 shows the fatigue resistance curve developed from the fatigue life calculations with an assumed crack size of 0.03 in. This resistance curve coincides with the Category E resistance curve. Also shown in Fig. 5-6 are the fatigue resistance curves corresponding to initial crack sizes of: 0.005, 0.01, and 0.05 in. As these curves illustrate, the sloping fatigue relationship decreases as the initial crack size increases. In addition, the fatigue limit is reached at lower stress range levels.

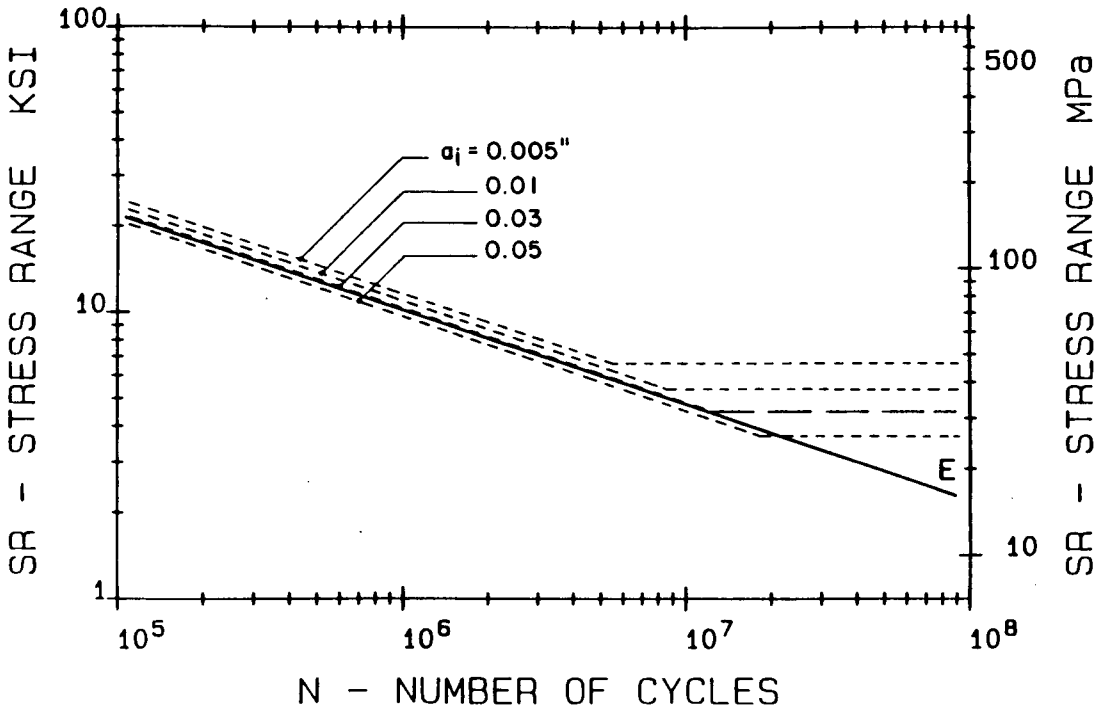

Figure 5-6: Fatigue resistance curves as a function of initial crack size

5.4.2 Stress field correction factors

Of the four stress field correction factors, the stress concentration correction, F_g, provides the largest contribution to variability in fatigue behavior. As given in Eq. (5.9), the numerator of the stress field correction factor is given by the stress concentration factor, K_{tm}. For the coverplate detail under study, the value of the stress concentration factor is calculated as 6.14 from Eq. (5.11). However, the development of Eq. (5.11), by finite element analysis, was based on the assumption that the fillet weld angle was 45°. Gurney has shown that a deviation of the weld angle significantly affects the stress concentration at the weld toe.[60] As the weld angle increases (increasing the steepness of the profile), the stress concentration factor increases. Conversely, a more shallow profile will

have a tendency to reduce the stress concentration and will thereby increase fatigue strength. For the purposes of this study, increased stress concentration factors of 7.0 and 8.0 were also analyzed.

As shown in Fig. 5-7, the fatigue resistance curves for the coverplate detail decrease as the stress concentration factor, K_{tm}, increases.

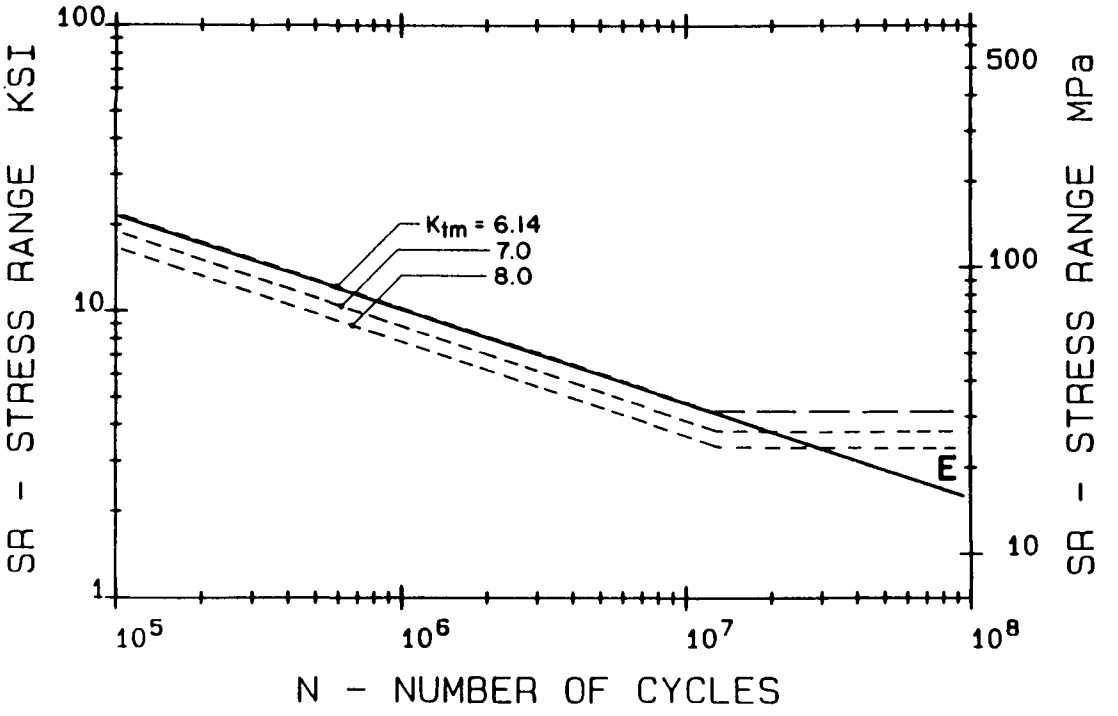

Figure 5-7: Fatigue resistance curves as a function of stress concentration factor

The stress concentration of 6.14 corresponds to a fatigue resistance of AASHTO Category E classification. As the stress concentration factor increases to 8.0 the fatigue resistance approaches the resistance provided by the AASHTO Category E′ detail classification.

5.4.3 Stress range

In fatigue experimentation the estimation of the nominal stress range at a detail is usually known to a high degree of accuracy. Given strain gage readings at a detail location, the stress range can be estimated within a few percent of the actual value. In variable amplitude testing, properly controlling the experiment can insure that each desired stress range interval is obtained. In any event, an error on one stress range value will not significantly change the value of the effective stress range when all cycles in the spectrum are considered.

However, for design and in-service performance, variability of the stress range spectrum can occur. Any increase in truck weight distribution will cause an upward shift in the stress range spectrum. Even if the maximum load level does not change, a greater concentration of trucks near the legal limit will result in a higher weighted average, resulting in an increase in fatigue damage. More accurate analysis and design methods, such as those associated with finite element analyses, result in the actual stress range being much closer in value to the calculated design value. This again results in an upward shift of the stress range spectrum and results in an increase in fatigue damage.

5.4.4 Fatigue crack thresholds

As discussed in Chapter Four, the lower bound estimate for the fatigue crack growth threshold in steel weldments is given by 2.75 ksi$\sqrt{\text{in.}}$ For the purposes of this study it will be assumed that this value is correct since it has been used to develop and correlate the crack growth models that are used in the current study. While values for the crack growth threshold have been observed below 2.75 ksi$\sqrt{\text{in}}$, they have been reported for variable amplitude

crack growth studies. These values are computed by either the root-mean-square or the root-mean-cube estimate of the stress intensity factors resulting from the variable load spectrum. A similar situation presents itself as found with the S-N fatigue limit under variable amplitude loading. While the effective stress intensity range may be below the threshold of 2.75 ksi$\sqrt{\text{in}}$, a portion of the load spectrum results in stress intensity ranges above the threshold, resulting in crack propagation.

While the value of the crack growth threshold can be taken as constant, two of the components that contribute to it's value are not. Both the stress concentration factor, K_{tm}, and the initial crack size, a_i, influence the stress range value for the constant amplitude fatigue limit. Figure 5-8 shows for the coverplate detail the relationship between the crack depth and the stress range for the crack growth threshold assuming a value of 2.75 ksi$\sqrt{\text{in}}$. The curves correspond to each of the stress concentration factors under study: 6.14, 7.0, and 8.0. For a given coverplate detail with one of these stress concentration factors, any combination of stress range and crack size that plots above the curve indicates that the fatigue crack threshold value has been exceeded and crack propagation occurs.

Figure 5-9 shows the fatigue crack threshold curves for the web attachment detail with stress concentration factors of 7.0 and 8.0. Though similar to the coverplate detail shown in Fig. 5-8, there is not as rapid a decay at the larger crack sizes. This is primarily due to the eventual crack propagation outside the high stress concentration field of the web attachment end.

Examination of Figs. 5-8 and 5-9 indicates that as the stress concentration

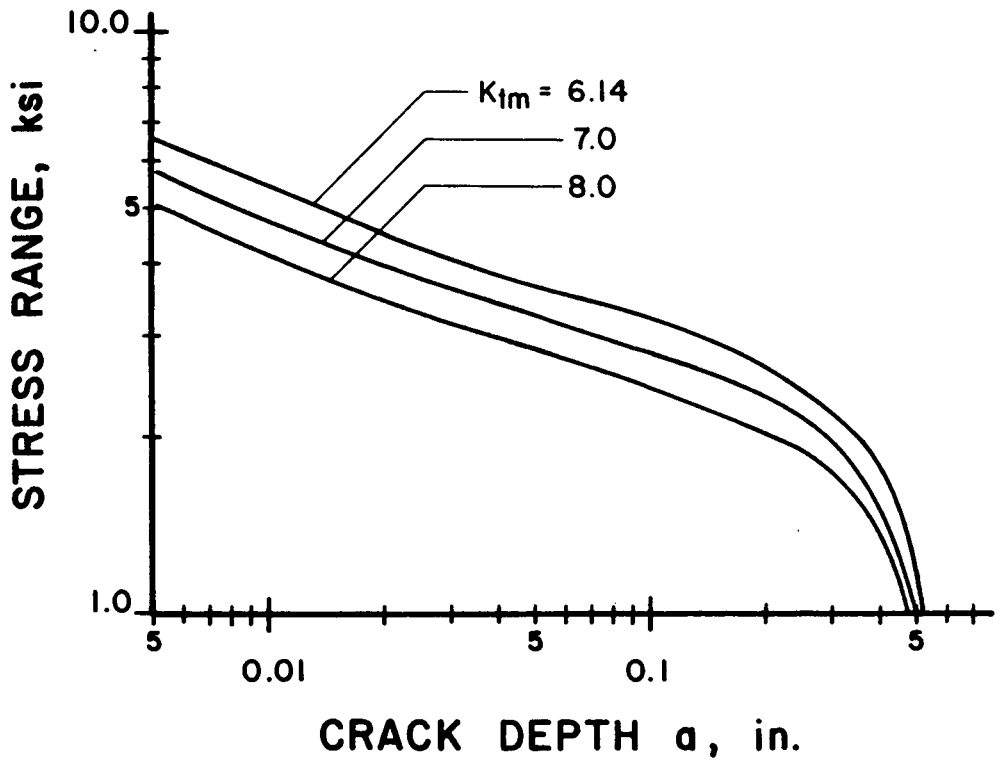

Figure 5-8: Fatigue crack threshold values, coverplate detail

increases, the constant amplitude fatigue limit decreases; although the differences decrease with large crack sizes. The curves also indicate that as the stress concentration increases, a smaller stress range is required for a given crack size in order to obtain the no-growth threshold. The smaller stress range at high stress concentrations gives rise to constant amplitude fatigue limits occurring at higher cycle lives as the severity of the detail increases.

More importantly, these curves indicate the crack growth threshold decay that will occur under variable amplitude loading. As the crack propagates under the higher stress range values of the stress spectrum, the crack size increases, resulting in a decrease in the stress range threshold value. This results in lower stress cycles contributing to fatigue crack propagation with time. The shape of the curve and hence the rate at which the smaller cycles

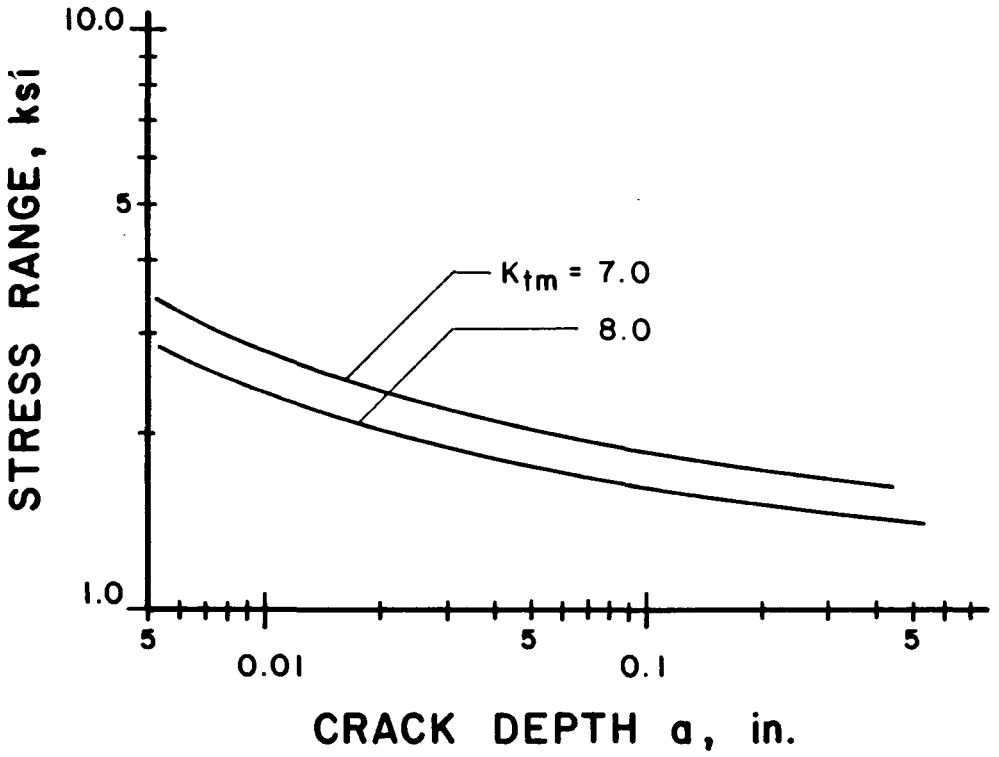

Figure 5-9: Fatigue crack threshold values, web attachment

begin to contribute to fatigue damage is a function of the stress field correction factors, $F(a)$.

5.5 Crack Propagation Simulation

Fatigue crack propagation under variable amplitude loading was simulated using the crack growth models in a step-wise fashion as governed by the crack growth threshold curves of Figs. 5-8 and 5-9. For each stress cycle in the spectrum, the threshold crack size was determined, since as the magnitude of the stress cycle increases, the threshold crack size decreases. The effective stress range (RMC) was then calculated from the stress cycles in the spectrum that had a crack threshold size below the assumed initial crack size for each detail (0.03 in. for the coverplate and 0.02 in. for the web attachment). A crack

propagation calculation was made with this effective stress range by integrating from the initial crack size to the threshold crack size of the next lowest stress cycle in the spectrum. This calculation gave the number of cycles required to propagate the crack to the next lowest non-contributing stress cycle. A new crack growth calculation was made with a lower effective stress range value determined from a new stress spectrum that included the next lowest stress cycle. The integration was performed from the crack threshold size of the smallest stress cycle in the new truncated spectrum to the threshold crack size of the next lowest stress cycle. This procedure was repeated until the crack size increased in magnitude enough to cause failure.

Although the full stress range spectrum is continuously applied to the detail, for the purpose of this study it is assumed that only a portion of the stress cycles in the spectrum may actually contribute to crack growth in the high cycle, long life regime as governed by the crack threshold. By integrating the crack growth model in increments, the number and distribution of stress cycles that contribute to crack propagation during the total life of the welded detail can be determined. The total number of contributing cycles is referred to as the effective cycle life, N_f'. The value of the effective cycle life is always less than the nominal cycle life, N_f, determined by the full spectrum. In addition, the effective stress range for the truncated spectrum results in a higher value, S_{re}'.

The fatigue crack propagation models were used to evaluate the variability that exists in the parameters that contribute to the crack growth threshold and the influence it has on fatigue behavior and total life. Each of the three parameters of the stress intensity range will be examined: initial crack size,

stress range, and stress concentration of the stress field correction factor. The results are compared with the AASHTO fatigue resistance curves and the test data from the two NCHRP test programs previously discussed.

5.5.1 Influence of stress spectrum shift

As discussed in sec. 5.3.3, a change in the stress spectrum can occur with time. While the general shape of the stress range distribution may not change, the entire spectrum may shift to higher stress range values as shown schematically in Fig. 5-10.

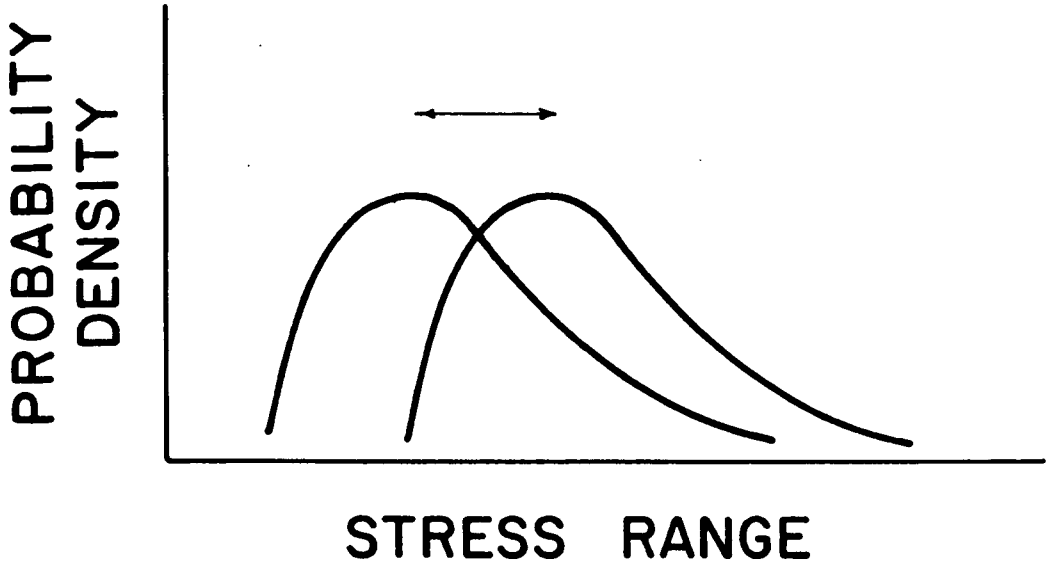

Figure 5-10: Shift of the stress range spectrum

This shift causes the effective stress range and both the minimum and maximum stress range values to increase. This results in a greater portion of stress cycles in the spectrum to be above the crack growth threshold (or the constant amplitude fatigue limit). Conversely, by shifting the stress spectrum to lower levels, the constant amplitude fatigue limit exceedance rate, $\Sigma\gamma_{if}$, decreases. This simulates high cycle, variable amplitude testing performed on

specimens in order to define a variable amplitude fatigue resistance curve below the fatigue limit. Both the coverplate detail of NCHRP Project 12-15(4) and the web attachment detail of NCHRP Report 12-15(5) were used for this simulation.

The coverplate details were subjected to the stress spectrum shown in Fig. 5-3. The maximum stress cycle was increased from 5.5 ksi to 7.5 ksi in 0.5 ksi increments. This resulted in a range of exceedance rates of the estimated constant amplitude fatigue limit (4.5 ksi) from 0.5 percent to 25 percent. A summary of the five different stress spectra and their corresponding stress parameters are given in Table 5-1.

Sr_{min} (ksi)	Sr_{max} (ksi)	Sr_e (ksi)	$\Sigma\gamma_{if}$ (%)
1.0	5.5	2.1	0.5
1.5	6.0	2.6	1.1
2.0	6.5	3.0	3.4
2.5	7.0	3.5	10.2
3.0	7.5	4.0	25.0

Table 5-1: Stress range parameters for the spectra shift

The results of the crack propagation simulation with the shifting stress spectra are given in Figs. 5-11 thru 5-15. The shaded portion of each stress range interval defines the portion of the total number of applied stress cycles that contribute to fatigue crack propagation, the sum of which is equal to the effective cycle life, N_f'. All stress cycles at or above the constant amplitude fatigue limit (CAFL) contribute, whereas the cycle distribution below the fatigue

limit is truncated. The degree of truncation is a function of the exceedance rate. As the exceedance rate decreases, truncation of the smaller cycles increases.

Table 5-2 summarizes the fatigue lives calculated from the crack growth simulations. Both the nominal and effective fatigue lives are given as well as the ratio of these two life estimates. Also given are the effective stress range values calculated from both the full and truncated spectra. As the exceedance rate increases from 0.5 to 25 percent and the effective stress range increases, the nominal cycle life decreases from 553 to 19.5 million cycles, respectively. The effective cycle life decreases from 27.8 to 15.2 million cycles for these same exceedance rate changes. The ratio between the effective cycle life and the nominal cycle life also increases as the exceedance rate increases.

The cycle life estimates for the various exceedance rates are plotted in Fig. 5-16. Both the nominal cycle lives (open symbols) and the effective cycle lives (solid symbols) are plotted with the appropriate effective stress range. These results indicate that as the exceedance rate decreases, the fatigue life estimate deviates from the straight-line extension of the resistance curve at an increasing rate. This deviation results from the inclusion of the non-contributing stress cycles in the life estimate. The effective fatigue life estimates plot on the resistance curve, since the summation of variable amplitude fatigue damage by Miner's Rule can be derived from fracture mechanics and only those cycles that contribute to crack growth are included. Of particular interest is the fact that the nominal fatigue lives plot along a straight line with it's log-slope equal to -5.4.

The placement of the web attachments in the shear span of the test

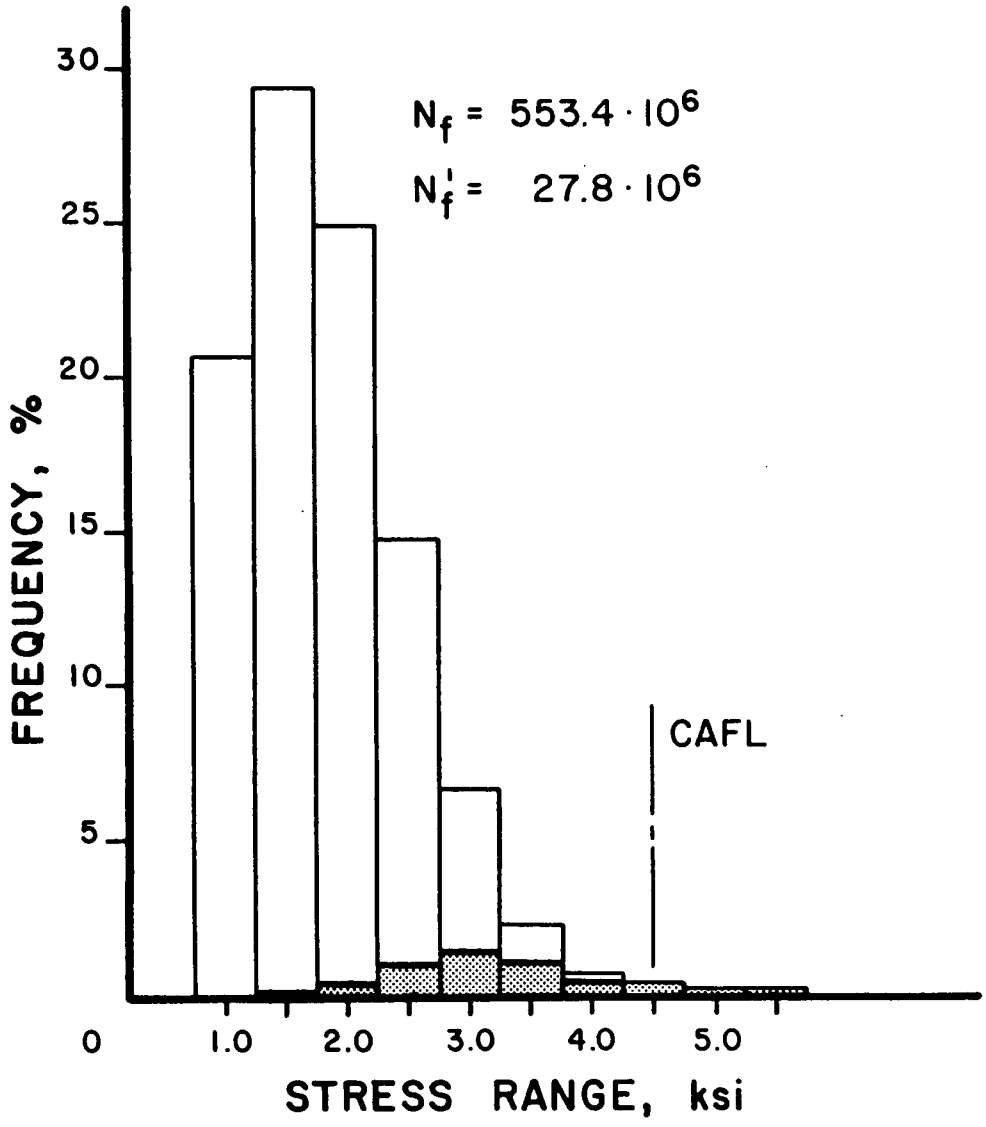

Figure 5-11: Coverplate cycle life with exceedance rate of 0.5 percent

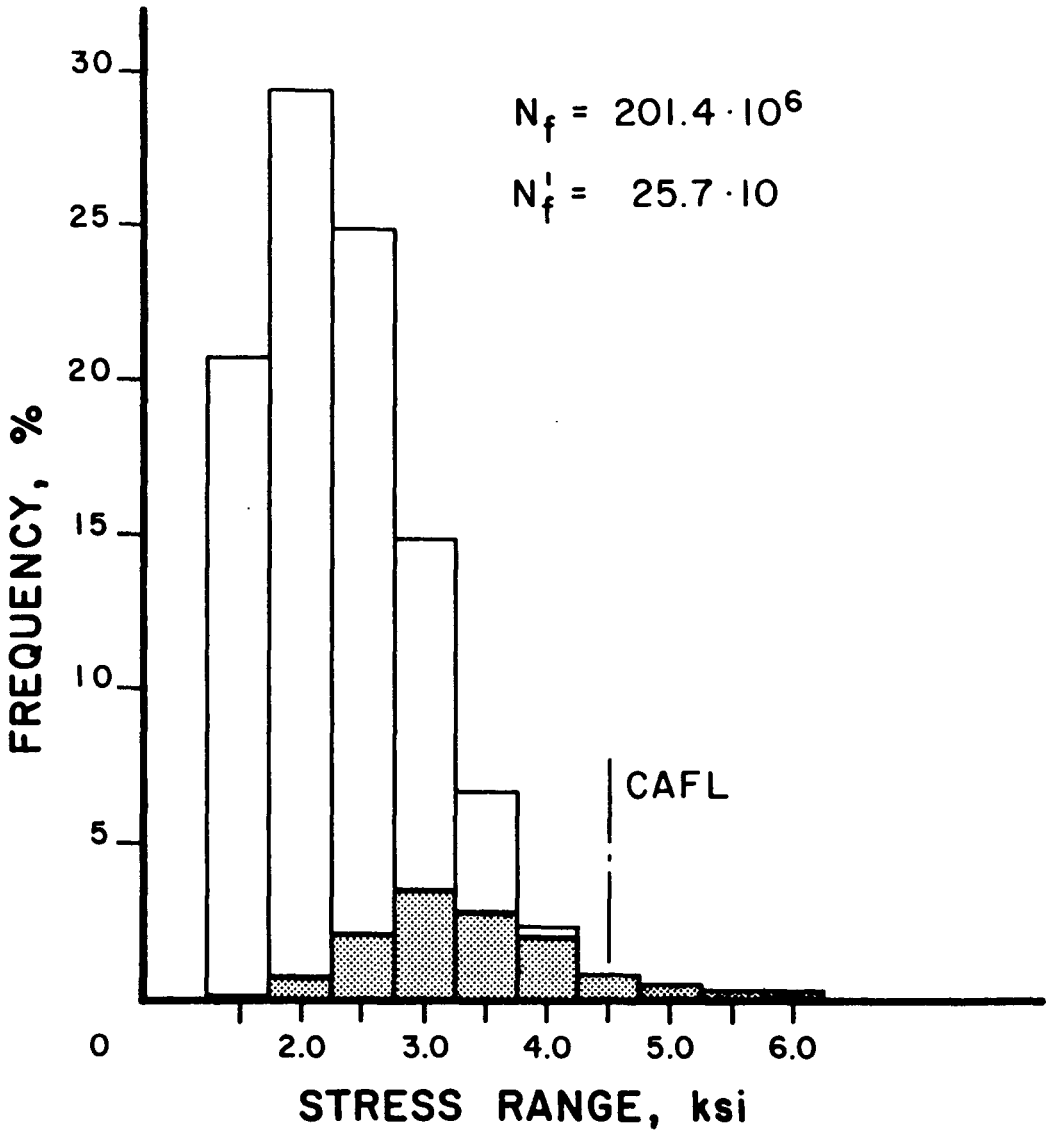

Figure 5-12: Coverplate cycle life with exceedance rate of 1.1 percent

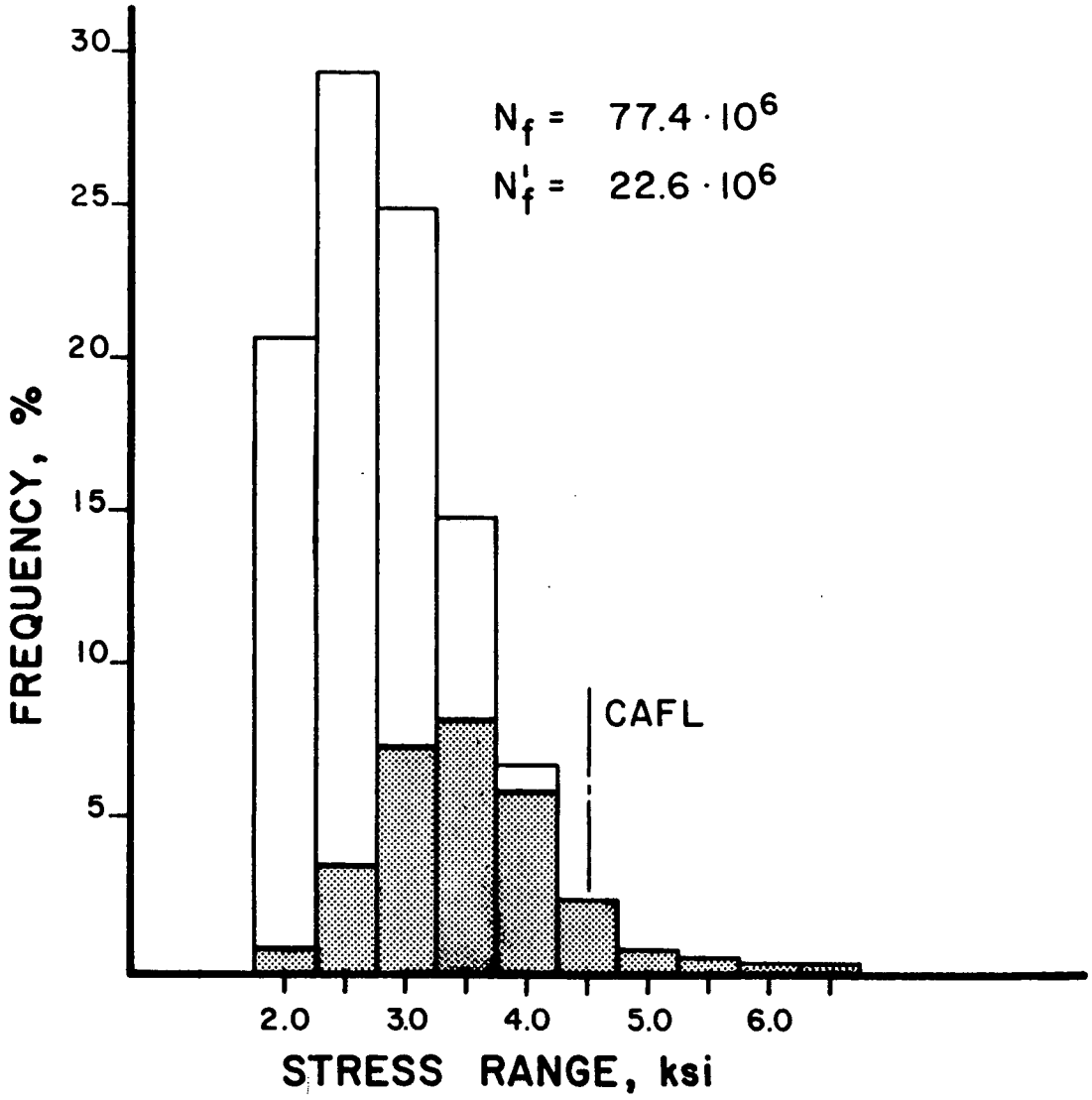

Figure 5-13: Coverplate cycle life with exceedance rate of 3.4 percent

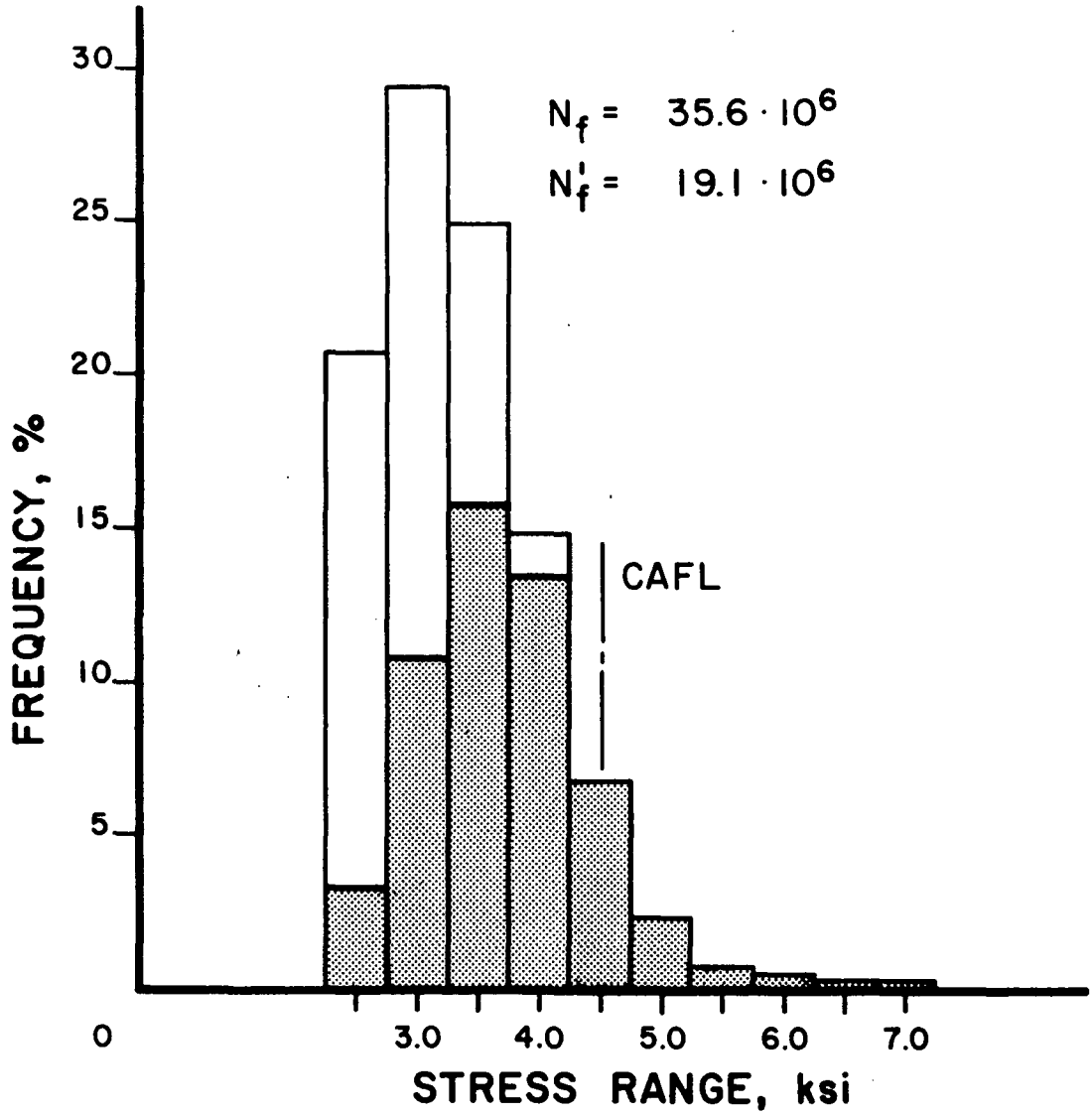

Figure 5-14: Coverplate cycle life with exceedance rate of 10.2 percent

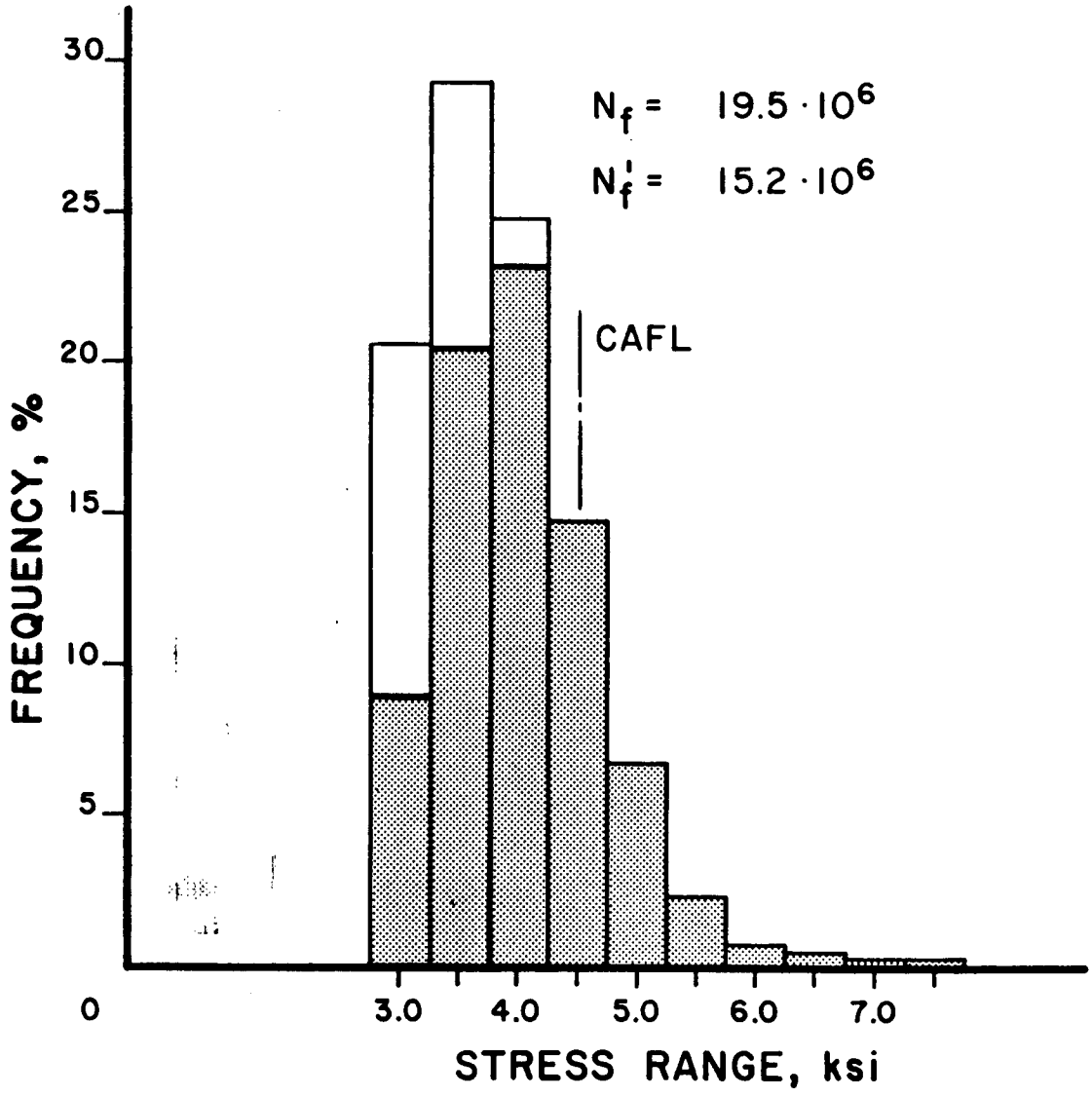

Figure 5-15: Coverplate cycle life with exceedance rate of 25 percent

$\Sigma\gamma_{if}$	Sr_e (ksi)	N_f ($\times 10^6$)	Sr_e' (ksi)	N_f' ($\times 10^6$)	N_f'/N_f (%)
0.5	2.1	553	3.37	27.8	5.0
1.1	2.6	201	3.47	25.7	12.8
3.4	3.0	77.4	3.61	22.6	29.2
10.2	3.5	35.6	3.83	19.1	53.7
25.0	4.0	19.5	4.13	15.2	77.9

Table 5-2: Spectra shift cycle life summary

girders provided detail failure locations with varying effective stress range values. This arrangement was used due to the uncertainty that exists for the constant amplitude fatigue limit of this type of detail. This provided a stress condition similar to that of a spectrum shift. The stress range parameters of the six different detail locations are given in Table 5-3.

The crack growth simulation was performed on four of the web attachment details. Three of the details cracked during the experimental program (Details 3, 6, and 7). Detail 7 with an effective stress range of 2.5 ksi failed after 43.6 million cycles. Detail 6 failed after 86 million cycles with an effective stress range of 2.2 ksi. A fatigue crack was detected at detail 3 after 100.7 million cycles at an effective stress range of 1.4 ksi.

The results of the crack propagation simulation are given in Figs. 5-17 thru 5-18 for Details 2, 3, 5, and 7 respectively. The shaded portion of each distribution represents the frequency of occurrence of each stress cycle that contributes to crack propagation. For Detail 3, assuming all cycles contribute,

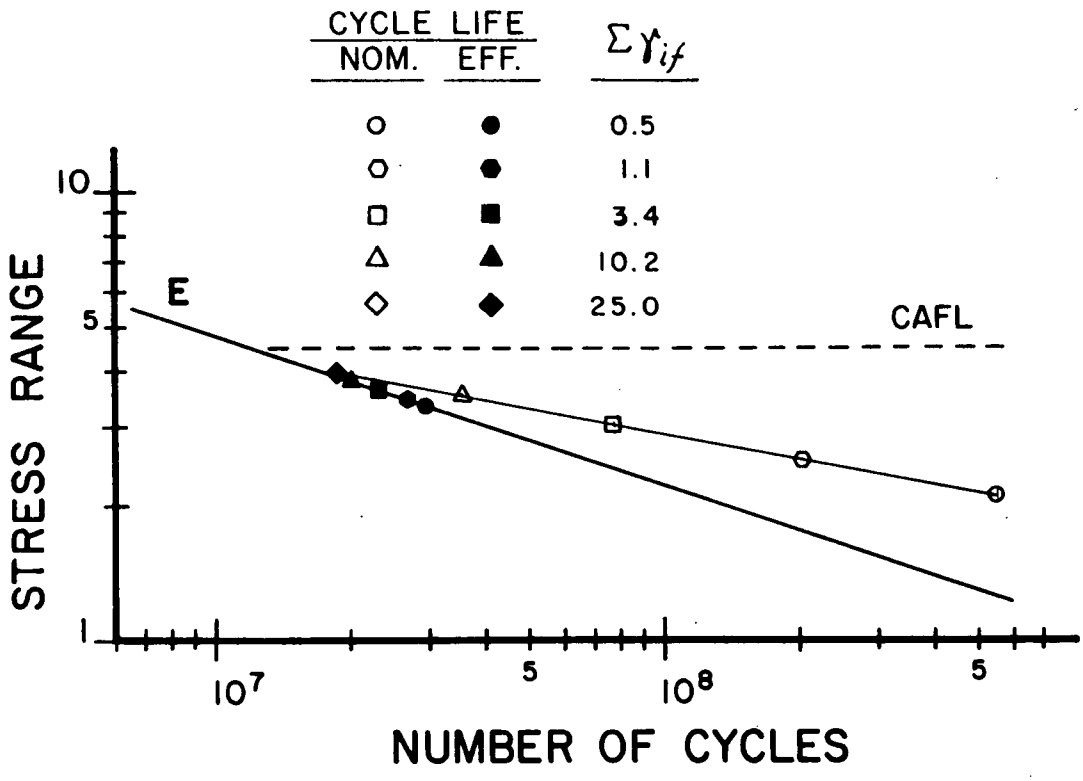

Figure 5-16: Nominal and effective cycle life estimates, coverplate detail with the spectra shift

the nominal fatigue life is estimated as 138 million cycles with an effective stress range of 1.7 ksi. When considering only the contributing cycles, the effective fatigue life was calculated as 54.4 million cycles with an effective stress range of 2.0 ksi. Correspondingly, for Detail 7, which resided in a higher stress field, the nominal fatigue life was estimated as 31.4 million cycles at an effective stress range of 2.5 ksi. The effective fatigue life was calculated as 28.2 million cycles. Both the experimental and simulated results are given in Table 5-4.

The stress range, cycle life relationships for the three web attachment test

Detail	Sr_{min} (ksi)	Sr_{CAFL} (ksi)	Sr_e (ksi)	$Sr_{overload}$ (ksi)
2	0.9	2.3	1.4	2.7
3	1.1	3.0	1.7	3.5
4	1.1	3.0	1.8	3.5
5	1.3	3.6	2.1	4.1
6	1.4	3.7	2.2	4.3
7	1.6	4.2	2.5	4.8

Table 5-3: Stress range parameters, web attachment detail

Detail	N_{f-exp} ($\times 10^6$)	N_f ($\times 10^6$)	Sr_e (ksi)	N_f' ($\times 10^6$)	Sr_e' (ksi)
2	---	392.0	1.3	85.6	1.8
3	100.7	138.0	1.8	54.4	2.0
6	86.0	66.8	2.1	42.6	2.3
7	43.6	31.4	2.5	28.2	2.6

Table 5-4: Web attachment cycle life summary

data points and the four crack growth simulation results are plotted with the AASHTO Category E and E′ resistance curves in Fig. 5-21. The test data is in reasonable agreement with the lower bound estimate of the Category E′ resistance curve.

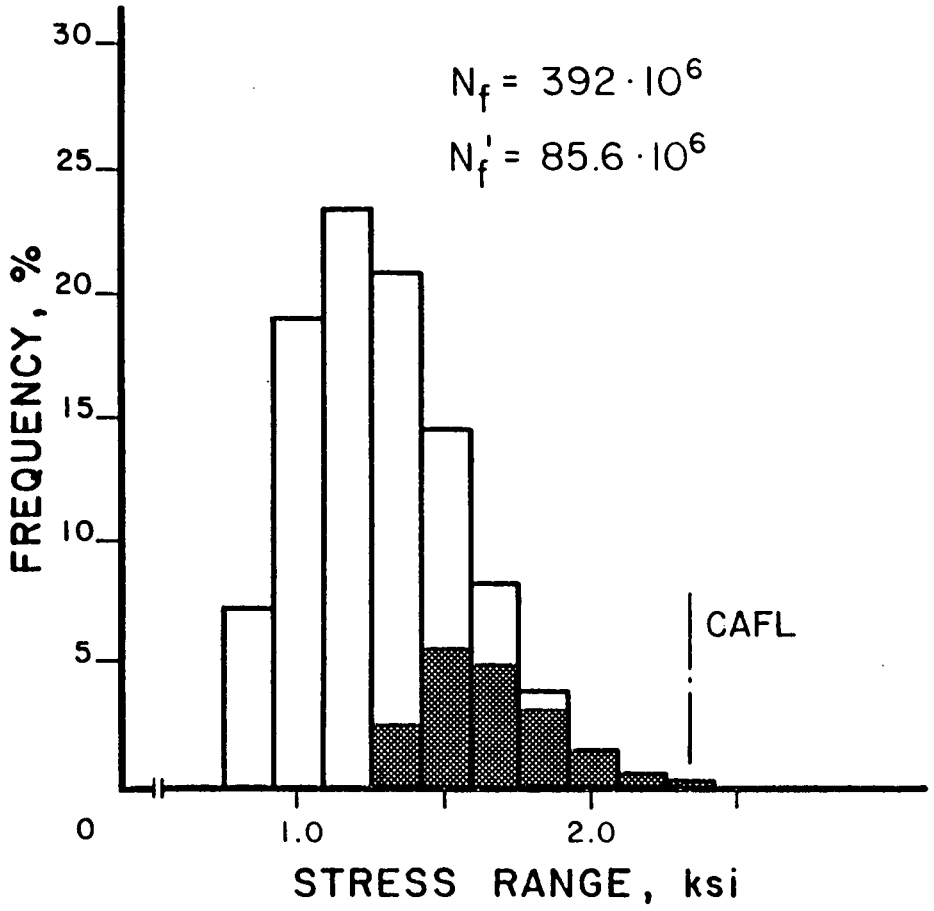

Figure 5-17: Web attachment cycle life, Detail 2

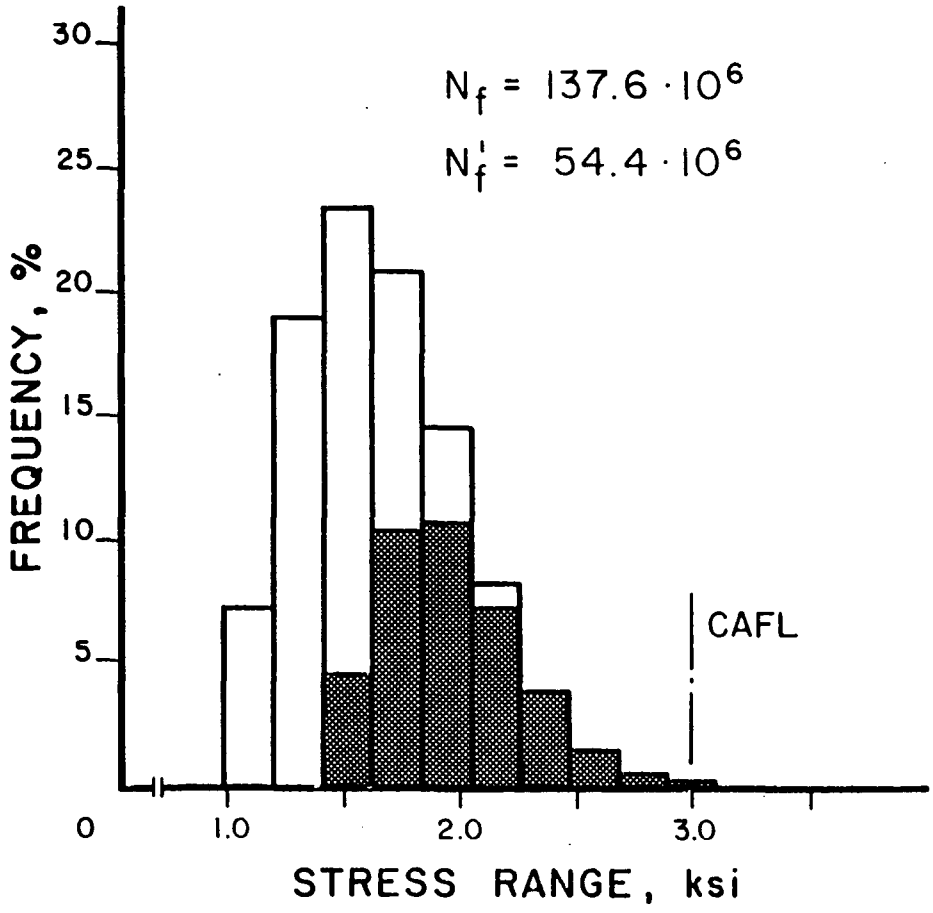

Figure 5-18: Web attachment cycle life, Detail 3

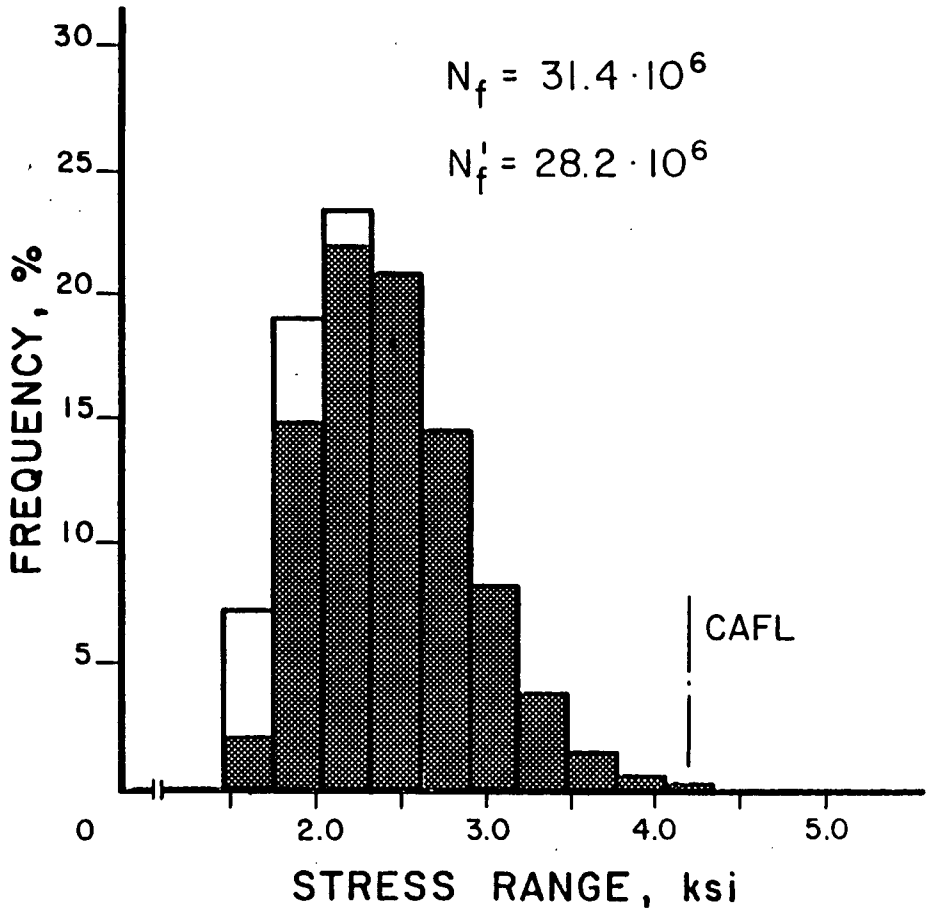

Figure 5-19: Web attachment cycle life, Detail 5

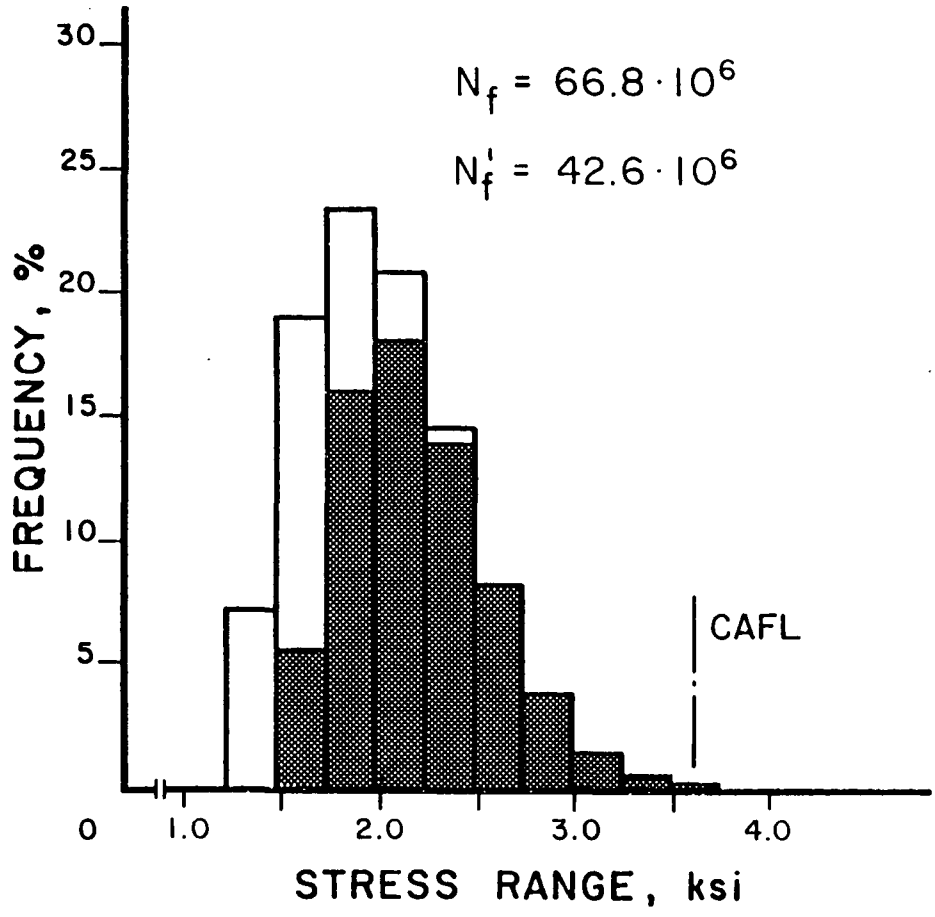

Figure 5-20: Web attachment cycle life, Detail 7

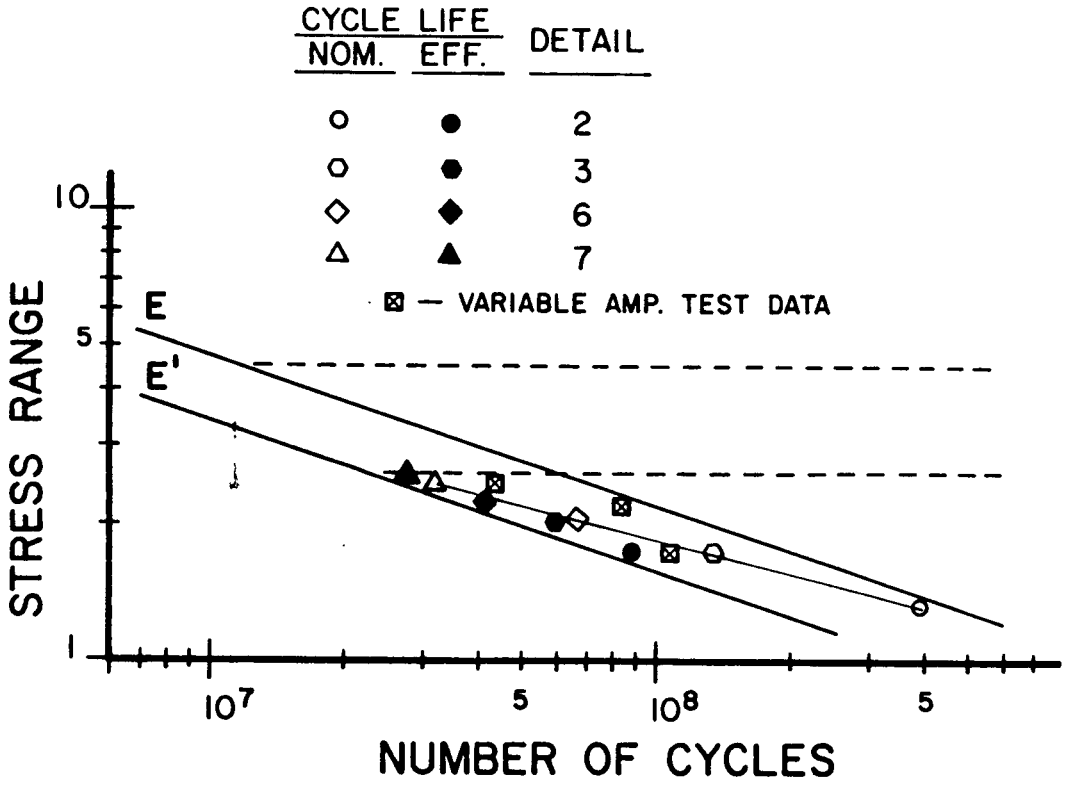

Figure 5-21: Web attachment detail cycle life estimates with the the AASHTO Category E and E′ resistance curves

5.5.2 Influence of stress concentration factor

The effect of changes in the stress concentration factor on variable amplitude fatigue life was studied for the coverplate detail. The results for the coverplate detail are given in Figs. 5-22 to 5-24. The identical stress range distribution was used to examine all three stress concentration factors. The fatigue limit exceedance rate was 1.1 percent, and the effective stress range for the full spectrum was 2.55 ksi. As is consistent with fracture mechanics, the nominal fatigue life decreased significantly as the stress concentration factor increased from 6.14 to 8.0. This behavior is similar to that exhibited by a

spectrum shift. While the stress range values remain constant, the increase in the stress concentration causes a decrease in the crack size threshold and, hence, a decrease in the constant amplitude fatigue limit. The constant amplitude fatigue limit decreases from 4.5 ksi for a stress concentration factor of 6.14 to 3.5 ksi for a factor of 8.0. The full spectrum is predicted to be truncated below the fatigue limit for all three cases so that only a portion of the smaller magnitude stress cycles contribute to crack propagation.

Table 5-5 summarizes the cycle life estimates from the coverplate growth simulations with the varying stress concentration factors. As the stress concentration factor increased from 6.14 to 8.0, the nominal fatigue life decreased from $201 \cdot 10^6$ cycles to $41.4 \cdot 10^6$ cycles. The ratio between the effective and nominal cycle life increased from 0.128 to 0.430 for the same range of stress concentration factors.

The predicted cycle lives for the three different stress concentration factors are given in Fig. 5-25. Both the nominal cycle life and effective cycle life estimates are plotted with the appropriate effective stress range and compared to the AASHTO Category E and E′resistance curves. The stress concentration factor of 6.14 corresponds closely with the Category E resistance curve. Deviation of the nominal fatigue life from the resistance curve for the factor of 6.14 is due to the inclusion of the non-contributing stress cycles. As the stress concentration factor was increased to 7.0, the nominal fatigue life approached the Category E resistance curve. However, the actual resistance curve is defined by the dashed line and and is consistent with the effective fatigue life estimate, as the plot of the solid square data point indicates. As the stress concentration factor increased to 8.0, the nominal fatigue life falls below the Category E

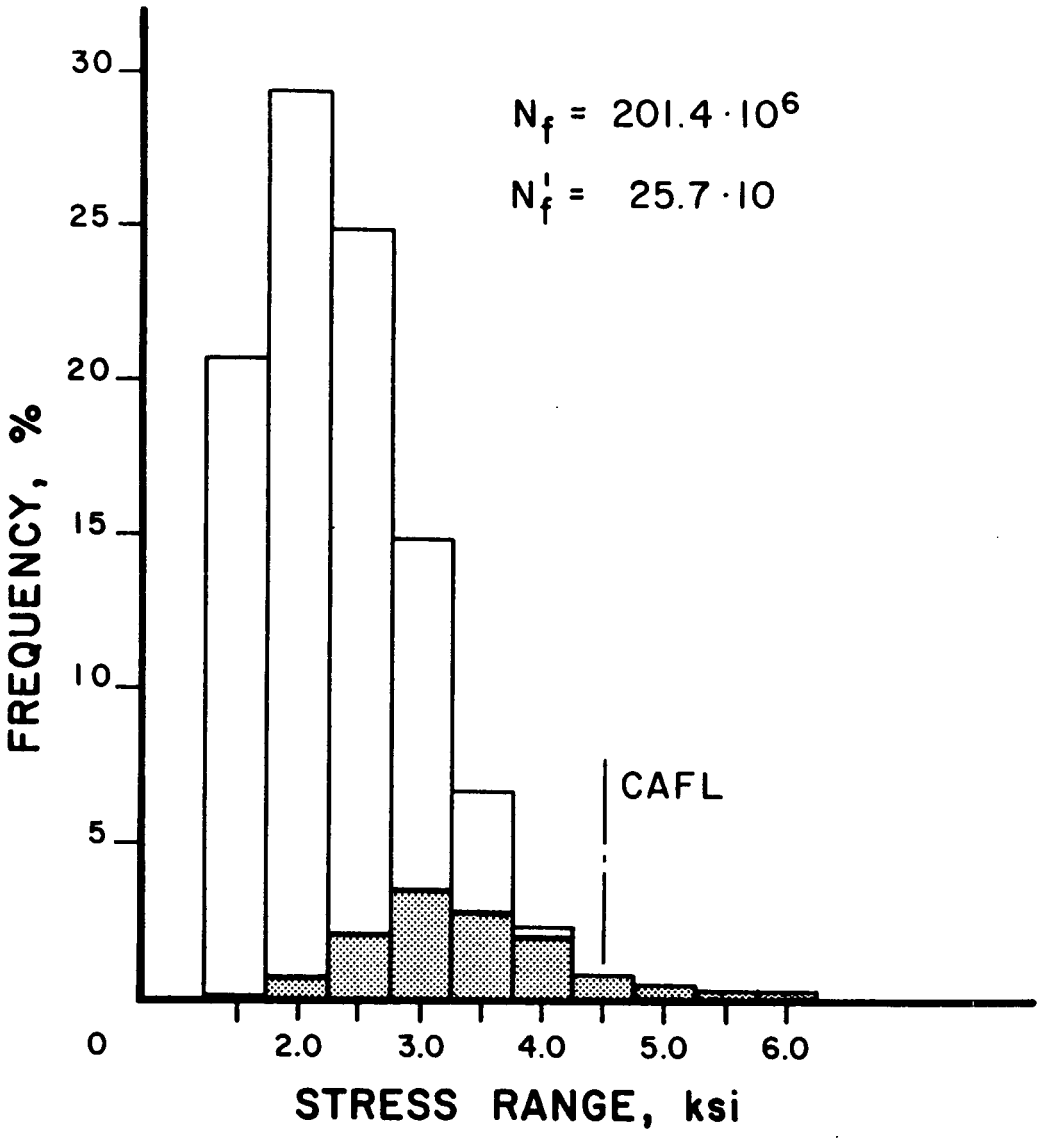

Figure 5-22: Coverplate cycle life with stress concentration factor of 6.14

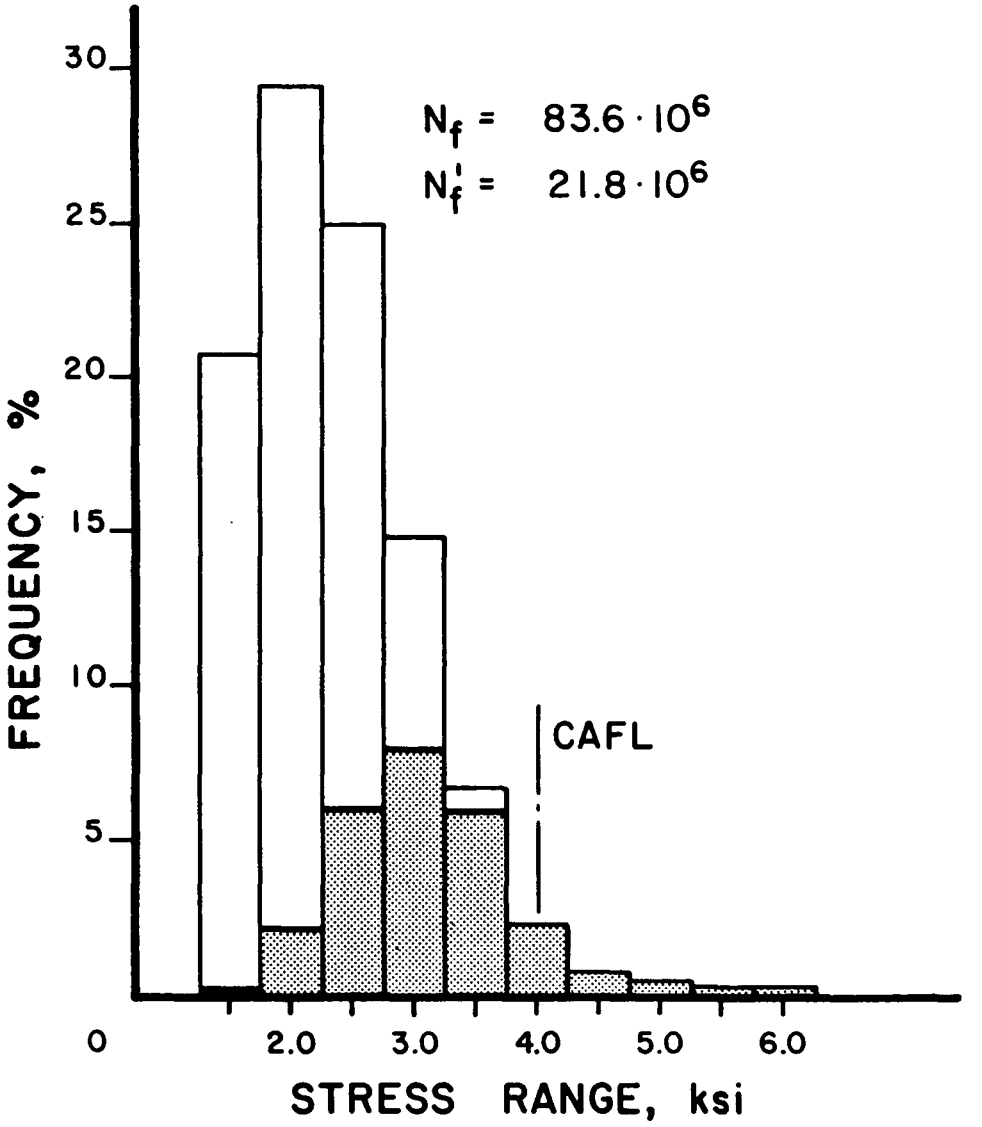

Figure 5-23: Coverplate cycle life with stress concentration factor of 7.0

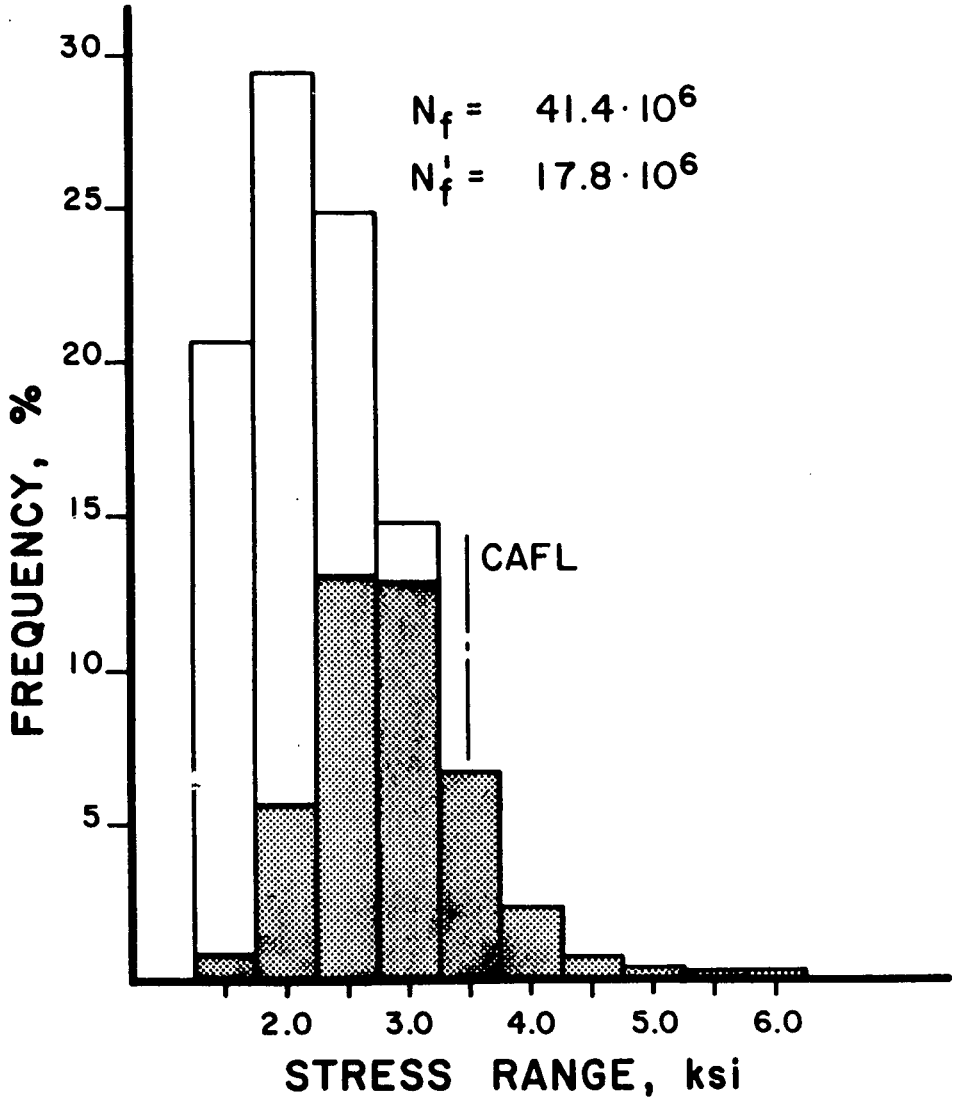

Figure 5-24: Coverplate cycle life with stress concentration factor of 8.0

K_{tm}	Sr_e (ksi)	N_f ($\times 10^6$)	Sr_e' (ksi)	N_f' ($\times 10^6$)	N_f'/N_f (%)
6.14	2.55	201	3.47	25.7	12.8
7.0	2.55	83.6	3.21	21.8	26.1
8.0	2.55	41.4	3.01	17.8	43.0

Table 5-5: Stress concentration factor fatigue life summary

fatigue life prediction and corresponds more closely with Category E′. The actual fatigue resistance curve is also plotted as a dashed line. The effective fatigue life estimate is plotted as a solid triangle.

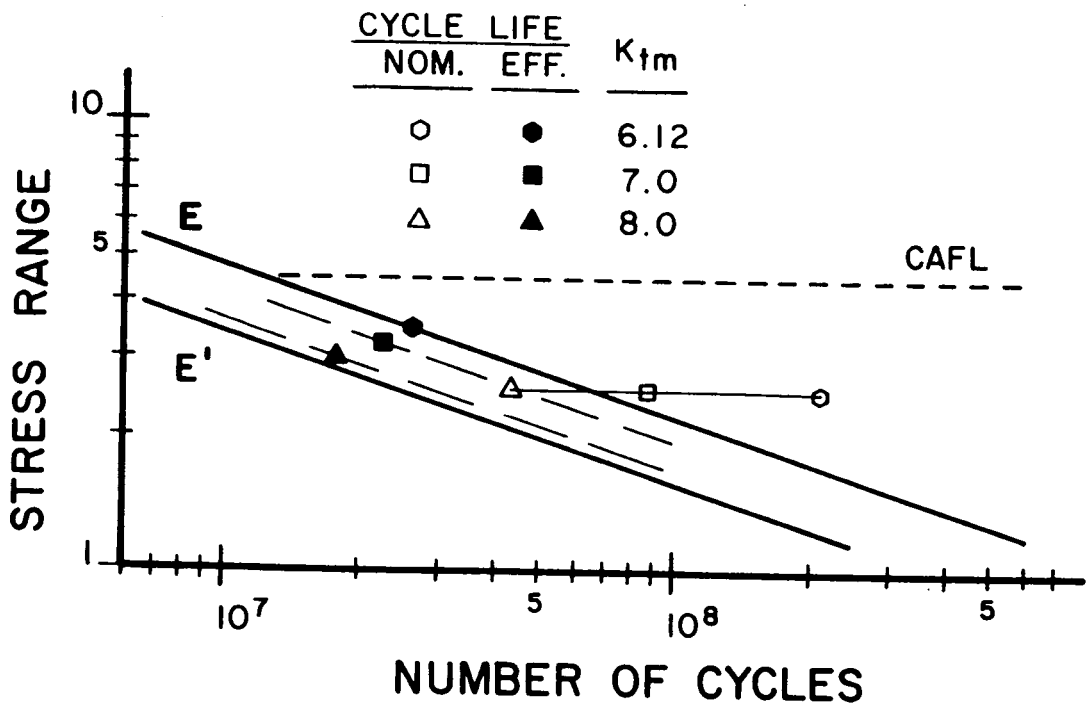

Figure 5-25: Cycle life estimates for varying stress concentration factors

5.5.3 Influence of stress range spectrum

The effect of the stress range spectrum shape was studied for the coverplate detail with a stress concentration factor of 6.12. Four different types of stress spectrum shapes were used for the crack propagation model: constant, linear, geometric, and the Rayleigh-type distribution of NCHRP 12-15(4). The stress range interval values were kept constant for the four different spectrum shapes. The maximum stress cycle, Sr_{max}, was identical for each spectrum and was taken as 6.0 ksi. Since the distribution of stress cycles differed, the fatigue limit exceedance rates differed for each spectrum. As the skewness of the spectrum increased (increasing number of smaller cycles), the effective stress range and the fatigue limit exceedance rate decreased. As summarized in Table 5-6, the exceedance rate was greatest for the constant spectrum at 40 percent and decreased to a value of 1.1 percent for the Rayleigh-type skewed distribution.

Spectrum Shape	Sr_e (ksi)	$\Sigma\alpha_{if}$ (ksi)
Constant	4.2	40.0
Linear	3.5	18.2
Geometric	3.0	7.8
Rayleigh	2.6	1.1

Table 5-6: Stress parameters for spectrum shapes

The results of the crack propagation simulation with the different spectrum shapes are given in Figs. 5-26 to 5-29. The shaped portion of each stress range interval defines the portion of the total number of applied stress cycles that are

predicted to contribute to fatigue crack propagation. The same results are summarized in Table 5-7. As the skewness of a spectrum increases to the right, the exceedance rate decreased and an increasing number of small stress cycles are then predicted to be non-contributing. For the constant stress spectrum, it is estimated that 65 percent of the total number of stress cycles cause fatigue damage. This decreased to approximately 13 percent for the Rayleigh-type distribution.

Spectrum Shape	Sr_e (ksi)	N_f ($\times 10^6$)	Sr_e' (ksi)	N_f' ($\times 10^6$)	N_f'/N_f (%)
Constant	4.23	15.1	4.78	9.8	64.6
Linear	3.46	31.1	4.26	13.8	44.4
Geometric	2.95	61.5	3.91	18.0	29.3
Rayleigh	2.55	201	3.47	25.7	12.8

Table 5-7: Stress range spectrum shape summary

Both the nominal and effective cycle life estimates for the four spectrum shapes are plotted with the AASHTO Category E resistance curve in Fig. 5-30. A stress concentration of 6.14 for the coverplate detail resulted in a fatigue resistance that is compatible with Category E. The effective cycle life for each spectrum (closed symbols) plot on the resistance curve since only contributing cycles are counted in the life estimate. As the skewness of the spectrum increases, the deviation of the nominal cycle life estimates (open symbols) from the resistance curve increased. For the constant stress range spectrum, the nominal cycle life is predicted to be 15.1 million cycles at an effective stress

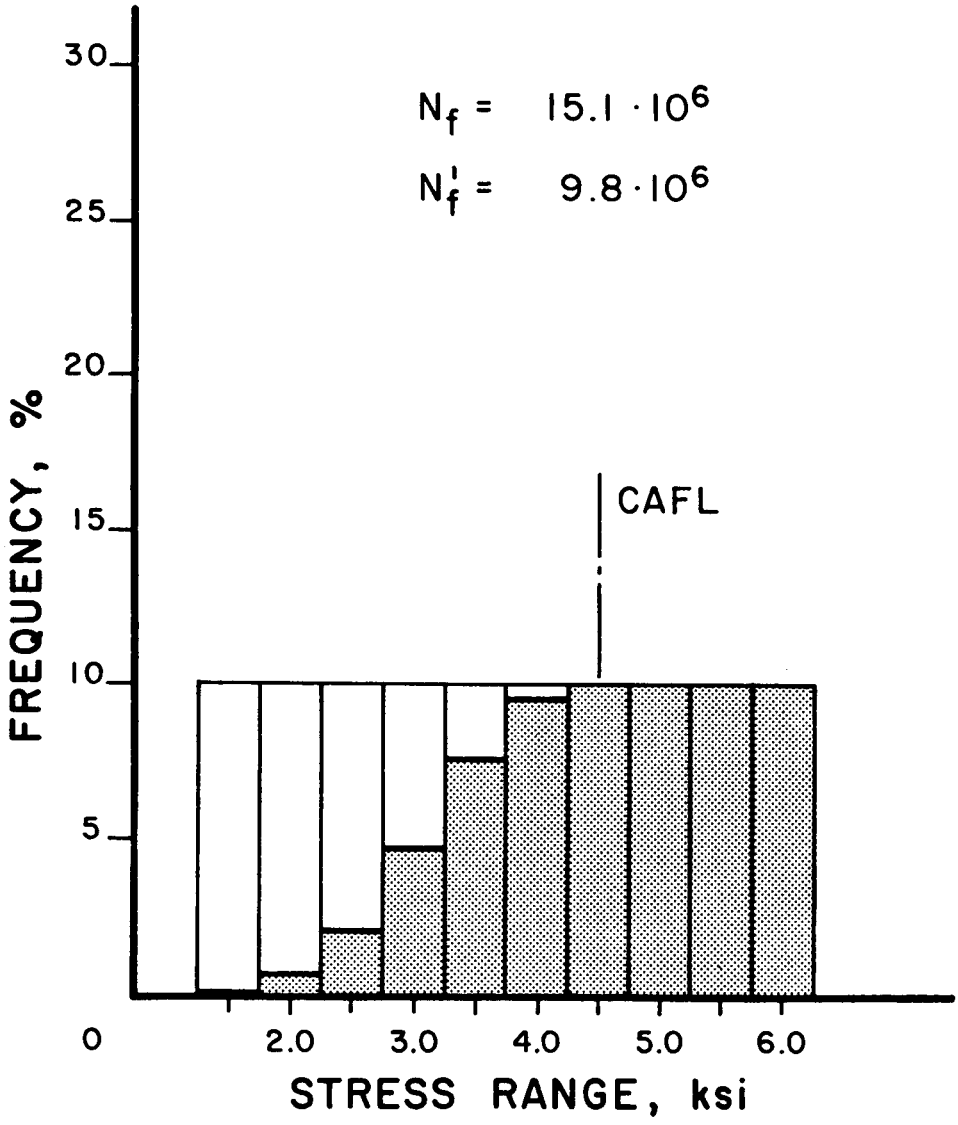

Figure 5-26: Coverplate cycle life with Constant stress range distribution

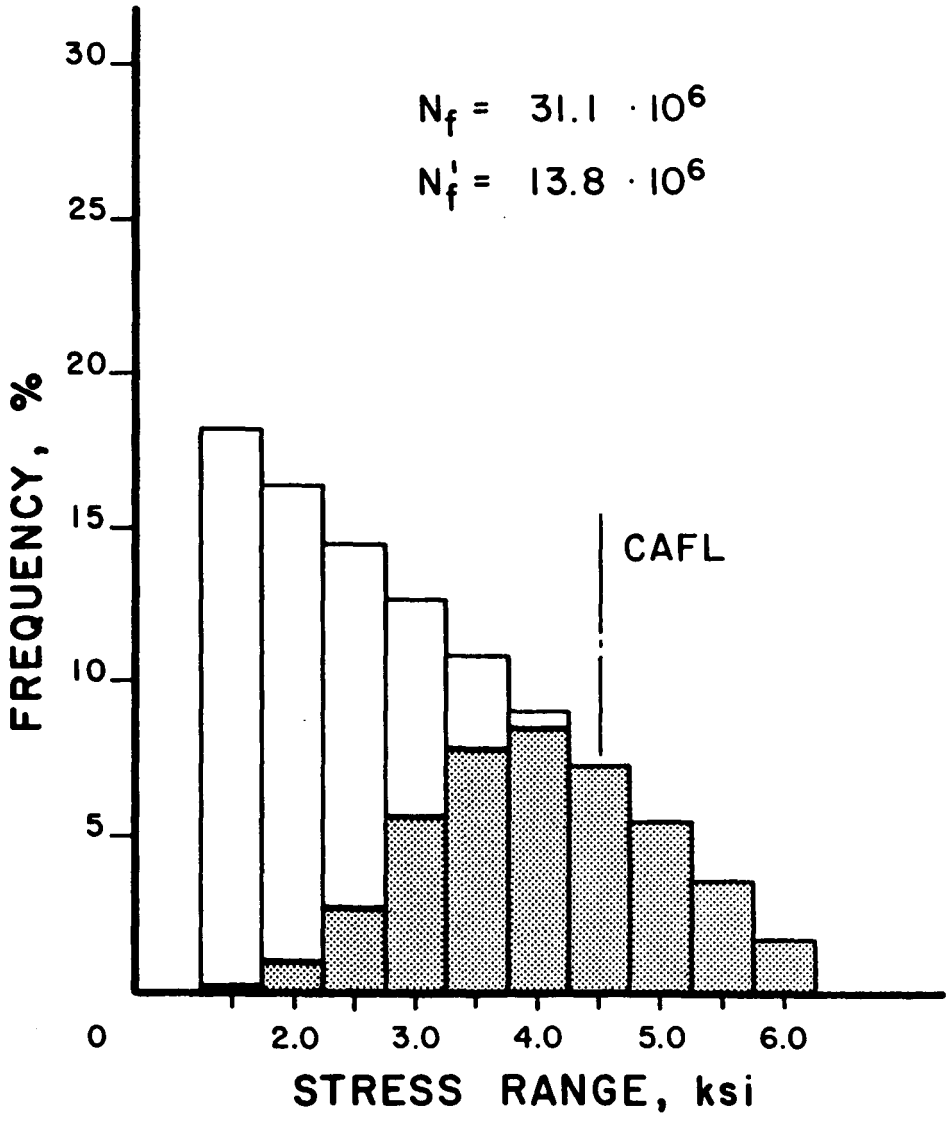

Figure 5-27: Coverplate cycle life with Linear stress range distribution

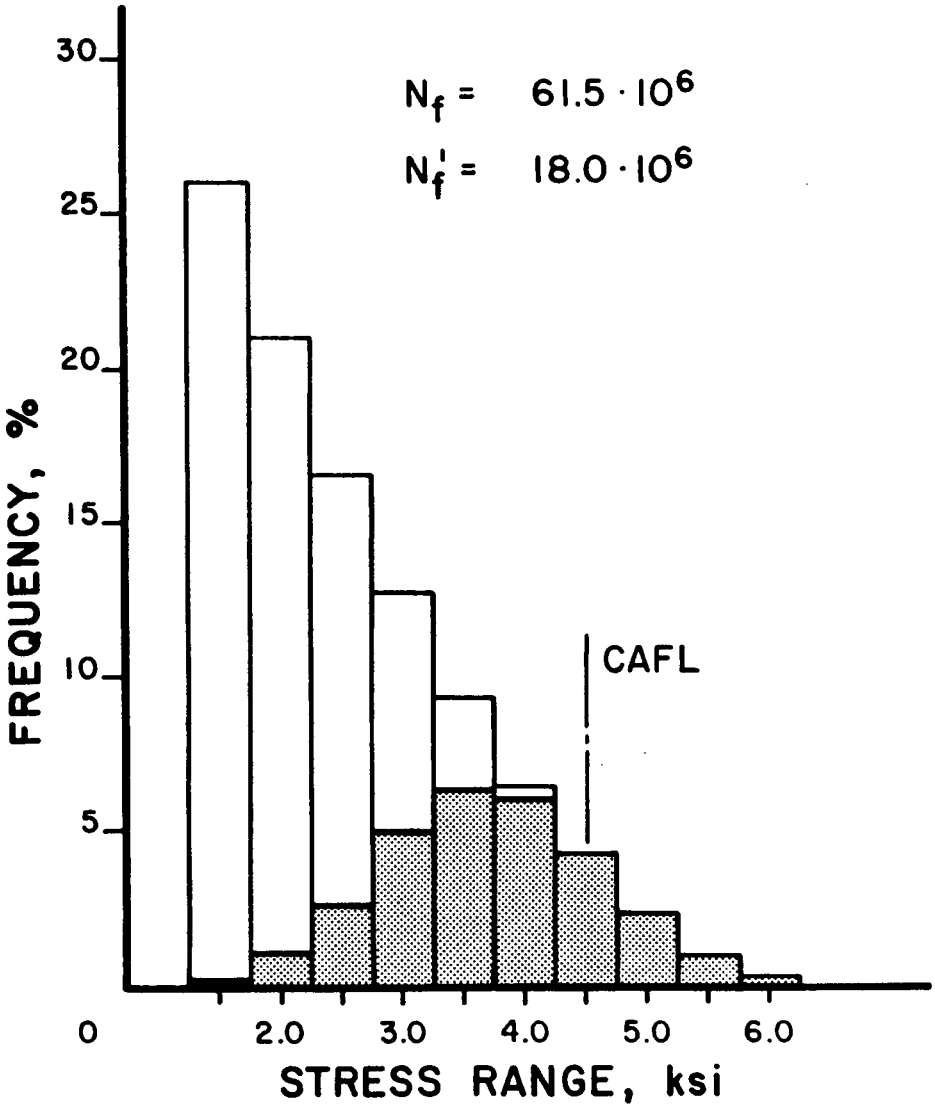

Figure 5-28: Coverplate cycle life with Geometric stress range distribution

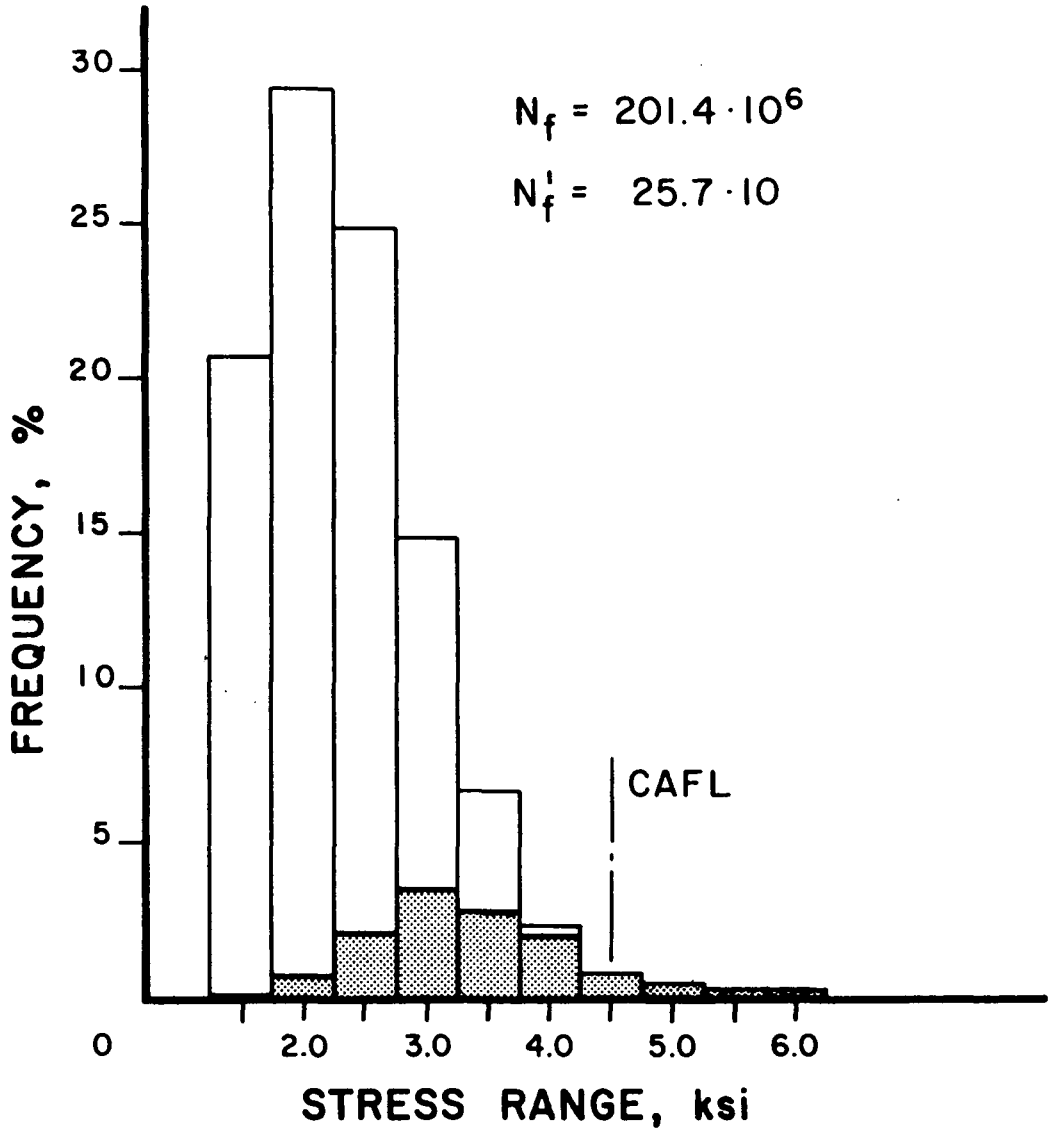

Figure 5-29: Coverplate cycle life with Rayleigh stress range distribution

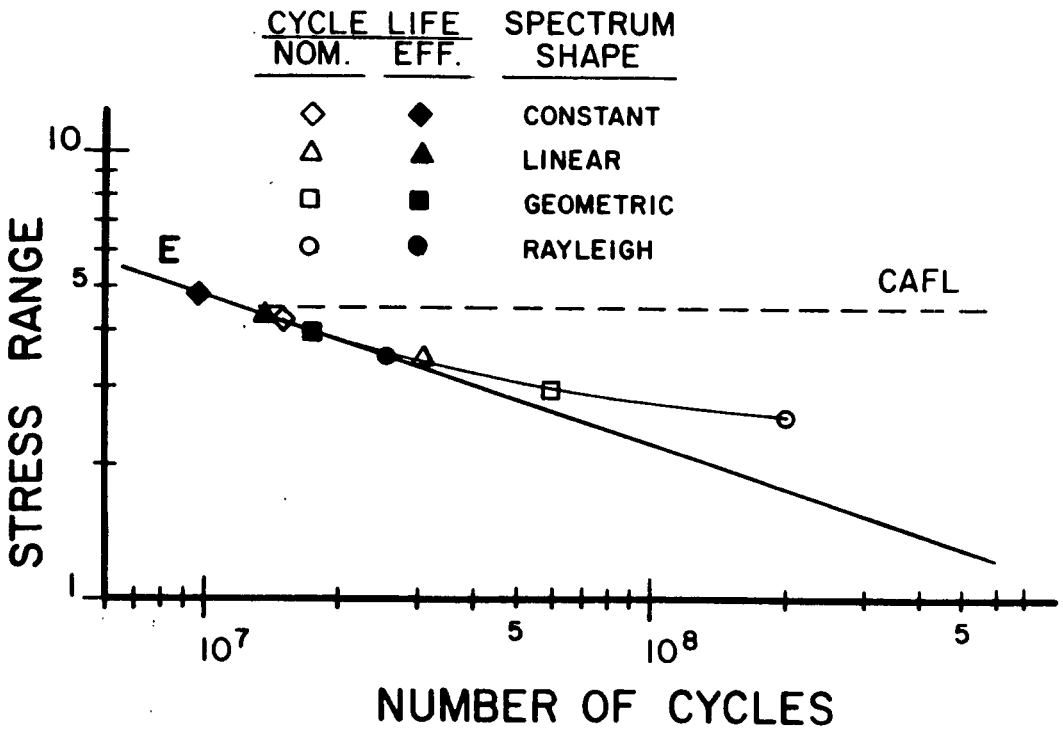

Figure 5-30: Cycle life estimates for varying spectrum shapes

range of 4.2 ksi. The cycle life estimate for Category E at 4.2 ksi is given as 14.6 million cycles. For the Rayleigh-type distribution, the nominal cycle life was predicted to be approximately 200 million cycles for an effective stress range of 2.6 ksi. For the same effective stress range, Category E provides a cycle life of 64 million cycles.

5.5.4 Interaction between variables

The previous discussion considered each parameter that contributes to fatigue and the variability in fatigue resistance independently. However, fatigue test results provides cycle life estimates that reflect the interaction of these effects. For the coverplate crack propagation simulation, the combined influence of a change in the fatigue limit exceedance rate and a change in the stress

concentration would result in a wide range of predicted cycle life estimates. Given in Fig. 5-31 is the estimated range in variability of the coverplate detail with the test data of NCHRP 12-15(5). The shaded area represents a variation of the exceedance rate from 0.1 to 15 percent and a stress concentration from 6.1 to 8.0. All but a few of the data points fall within the predicted range of cycle life estimates.

Figure 5-32 shows the test data for the web attachments with the predicted range of cycle life for stress concentrations between 7.0 and 8.0. As with the coverplate data, the majority of the experimental data fall within this range at the lower effective stress ranges. The data at the high stress range levels have effective stress ranges above the fatigue limit. Therefore, all cycles contribute to crack propagation and the cycle life estimates plot consistent with the Category E′ resistance curve.

5.6 Stress Cycle Truncation

In many variable amplitude fatigue resistance experiments and all fatigue life estimates, the problem of where to truncate the stress spectrum exists. Strain measurements of in-service bridges often provide a stress range spectrum that is similar to the distribution shown in Fig. 5-33, when the measured stress cycles above some finite limit are included in the distribution. The increasing number of smaller cycles are due to superimposed vibratory cycles, lighter vehicular traffic, or combination loading. Generally for practical considerations, the smaller stress cycles are truncated at a lower limit of 0.3 ksi to 0.5 ksi.

As was shown in the previous section, small stress cycles will influence fatigue life estimates in the higher cycle region. At the lower exceedance rates, a larger percentage of the small stress cycles do not significantly contribute to

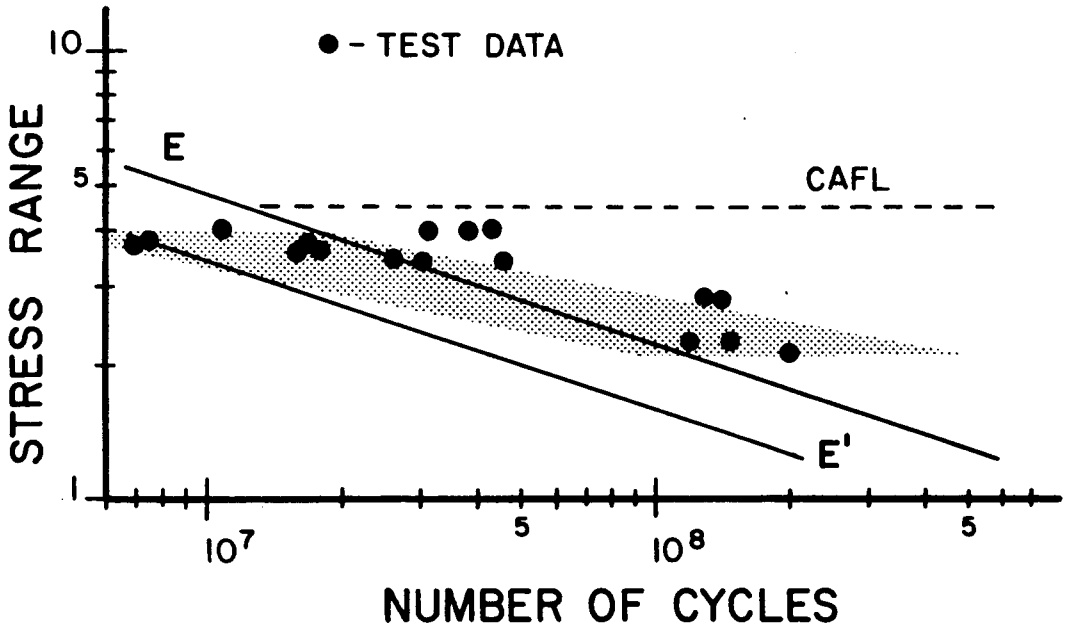

Figure 5-31: Predicted variation in coverplate cycle life

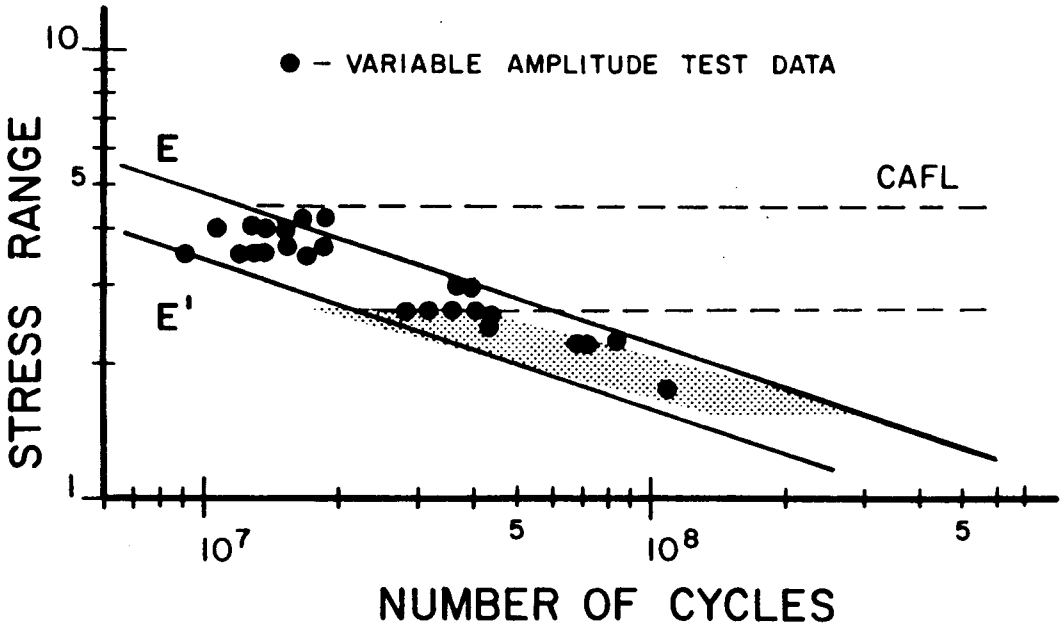

Figure 5-32: Predicted variation in web attachment cycle life

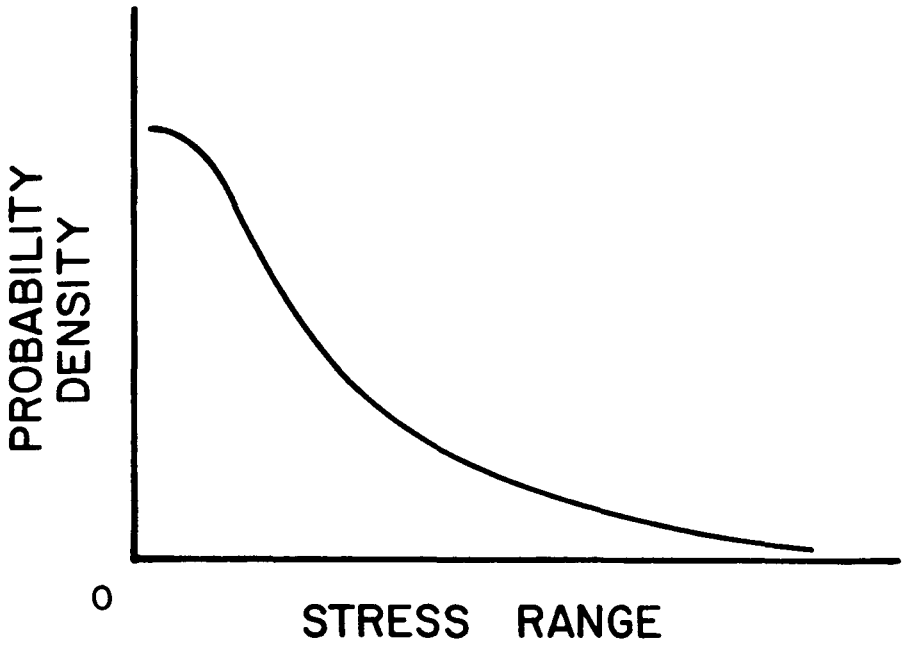

Figure 5-33: Idealized stress range histogram

fatigue crack propagation. The point at which the small stress cycles begin to contribute to fatigue damage is highly dependent on: the constant amplitude fatigue limit (crack growth threshold), the spectrum shape, and relative magnitude between the small stress cycle and the peak stress range in the spectrum. The analysis indicates that including the non-contributing cycles into the fatigue life calculation, causes the estimate to be conservative. This section will study the effect of stress cycle truncation on both fatigue test results and fatigue life assessments.

5.6.1 Fatigue test stress spectrum truncation

The two Rayleigh-type stress range spectra used in the fatigue crack propagation models were truncated by approximately 50 percent of the original number of cycles. For the coverplate detail spectrum, the lower two stress range intervals were eliminated. This eliminated 513 stress cycles from the original 1024, resulting in 511 remaining cycles. This caused the effective stress range (RMC) to increase from 43 percent of the peak stress to approximately 50 percent. The spectrum used for the web attachment with 1000 stress cycles defining the distribution was truncated by 498 cycles. The lowest three stress cycle intervals were eliminated.

The results from the crack growth simulation of the coverplate detail with the spectrum shift are given in Table 5-8. Although the stress range spectrum has been truncated, thus approximately doubling the exceedance rate, the values for $\Sigma\gamma_{if}$ are the original exceedance rates for the full spectrum so that comparison can be made with the results given in Table 5-2. Comparison of the two tables shows that at the lower exceedance, the truncated spectrum gives a nominal fatigue life that is approximately one-half of the full spectrum and the effective fatigue lives are approximately equal. At the higher exceedance rates, where a greater portion of smaller stress cycles contribute to crack growth, the effective fatigue lives are significantly less for the truncated spectra.

The coverplate stress range, cycle life relationships for both the full and truncated spectrum shift are shown in 5-34. As the plot of the results indicate, the fatigue life is reduced by the stress cycle truncation, although the effective stress range increases. This results in a movement along the same resistance curve that defines the resistance of the detail subjected to the full spectrum.

$\Sigma\gamma_{if}$ (%)	Sr_e (ksi)	N_f ($\times 10^6$)	Sr_e' (ksi)	N_f' ($\times 10^6$)	N_f'/N_f (%)
0.5	2.5	276	3.4	27.4	9.9
1.1	3.0	101	3.5	24.6	24.4
3.4	3.5	39.7	3.6	20.4	51.4
10.2	4.0	19.7	4.0	15.9	80.7
25.0	4.5	12.2	4.5	11.9	97.5

Table 5-8: Truncated spectra shift cycle life summary

The predicted results from the crack propagation simulation for the web attachment detail with the truncated spectrum are summarized in Table 5-9. The greatest variation in the nominal fatigue life, N_f, occurs at the lower peak stress levels (lower exceedance rates). However, the effective fatigue lives are similar in value. At the higher stress spectra, truncation of smaller contributing stress cycles occurs and the effective fatigue life, N_f', decreases.

The truncated stress range distributions for the web attachment Details 3 and 7 are given in Figs. 5-35 and 5-36 respectively. At the higher stress range level provided by Detail 7, almost all of the stress range intervals that remain are above the constant amplitude fatigue limit. Therefore, all cycles contribute to crack growth. At the lower stress level provided by Detail 3, a significant portion of the spectrum is initially below the constant amplitude fatigue limit resulting in the variation between the nominal cycle life and the effective cycle life. Comparison of these two figures with Figs. 5-18 and 5-20 gives a proper perspective on cycle truncation.

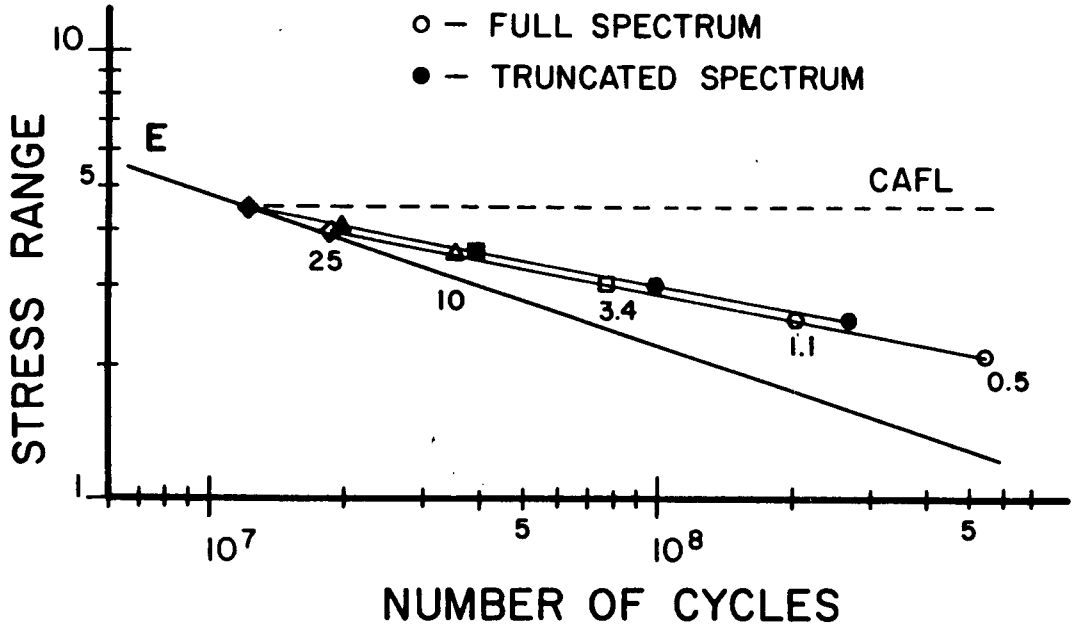

Figure 5-34: Comparison of fatigue life estimates between full and truncated spectrum, coverplate spectra shift

Detail	Sr_e (ksi)	N_f ($\times 10^6$)	Sr_e' (ksi)	N_f' ($\times 10^6$)	N_f'/N_f (%)
3	1.7	72.0	2.1	51.5	72.0
7	2.4	20.4	2.4	20.4	100

Table 5-9: Truncated test spectrum, web attachments

The results for the three different coverplate stress concentration factors are summarized in Table 5-10. The nominal cycle lives are approximately one-

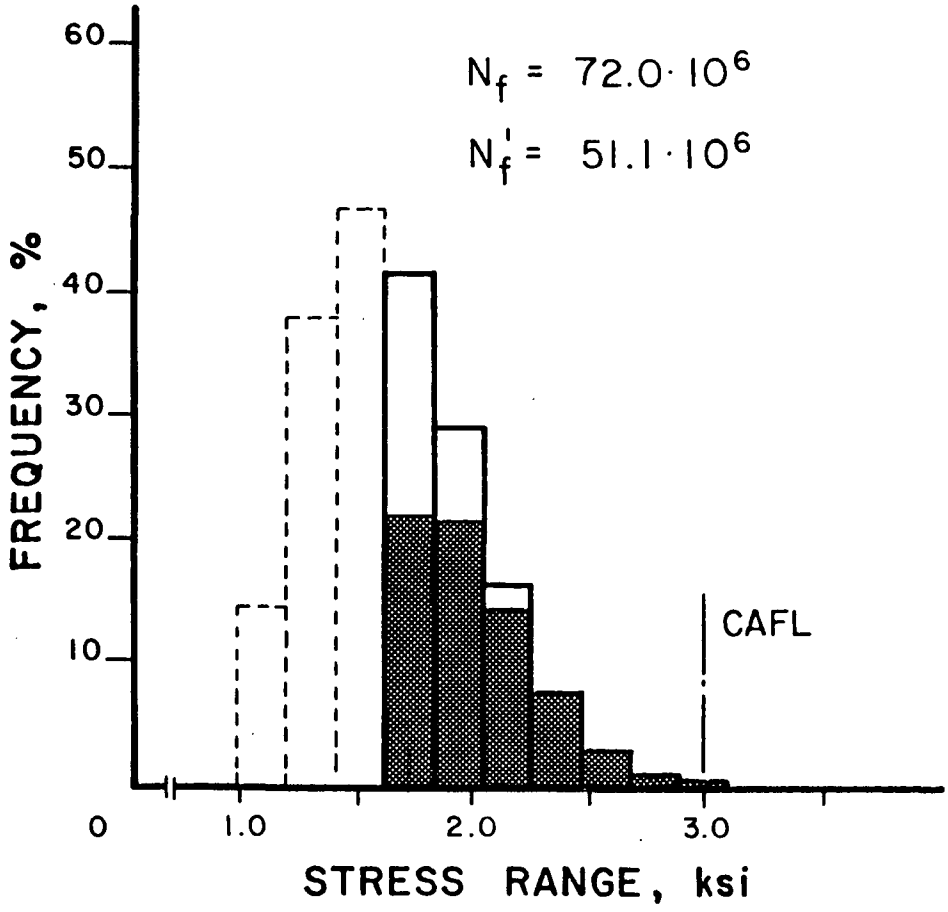

Figure 5-35: Web attachment Detail 3, stress cycle truncation

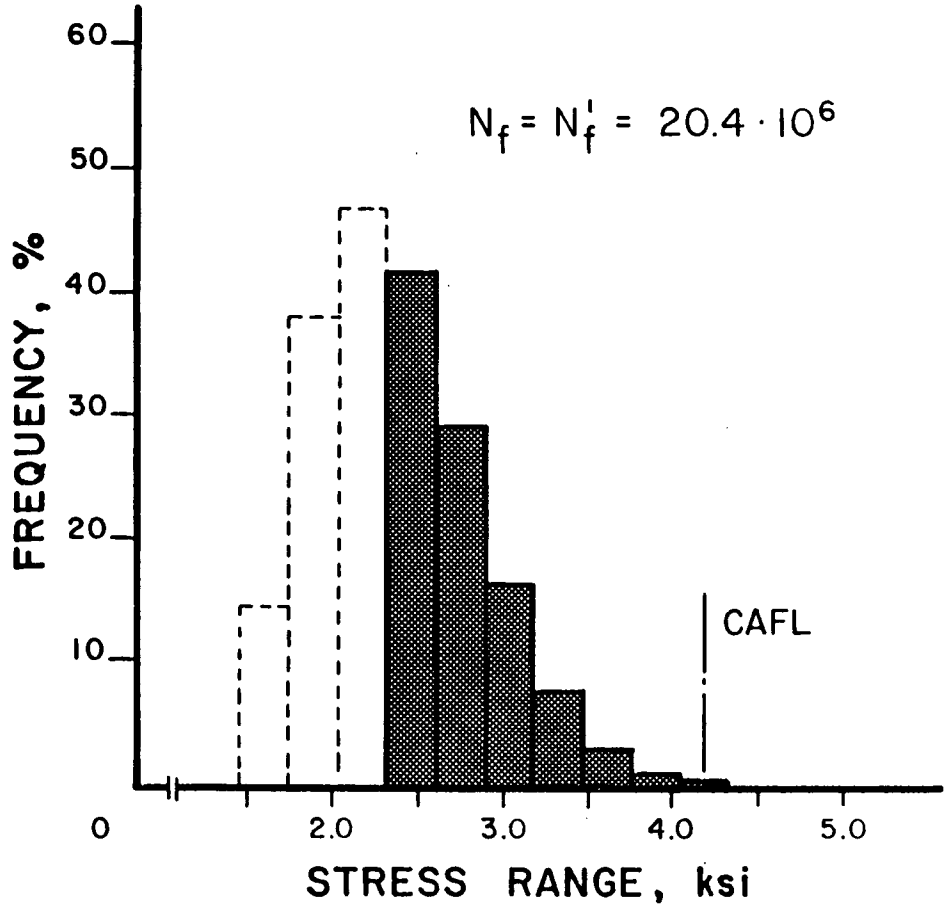

Figure 5-36: Web attachment Detail 7, stress cycle truncation

half of those with the full spectrum. The effective cycle lives are only slightly reduced. The largest reduction in cycle life occurs at the largest stress concentration. The stress range, cycle life relationship for both the full and truncated spectrum are compared in Fig. 5-37. For all three stress concentration factors, the full and truncated cycle life N_f, plot along the resistance curve. No significant error would result in the estimation of the fatigue resistance from test generated with a truncated stress spectrum.

K_{tm}	Sr_e (ksi)	N_f ($\times 10^6$)	Sr_e' (ksi)	N_f' ($\times 10^6$)	N_f'/N_f (%)
6.14	3.0	101	3.5	24.6	24.4
7.0	3.0	42.3	3.3	20.2	47.8
8.0	3.0	21.4	3.1	15.7	73.4

Table 5-10: Stress concentration factor cycle life summary, truncated spectrum, coverplate detail

5.6.2 Fatigue life estimate cycle truncation

The effect of stress cycle truncation on cycle life estimates was studied using the coverplate fatigue crack propagation model. This allowed for the evaluation of stress cycle truncation on significant experimental database for that particular detail. The stress cycle truncation was performed on: the spectra used for the spectrum shift, the varying stress concentration, and the spectrum shape studies.

Each stress range spectrum was evaluated for stress cycle truncation in the following manner. The lowest stress cycle interval was eliminated from the spectrum and the effective stress range was computed on the basis of the

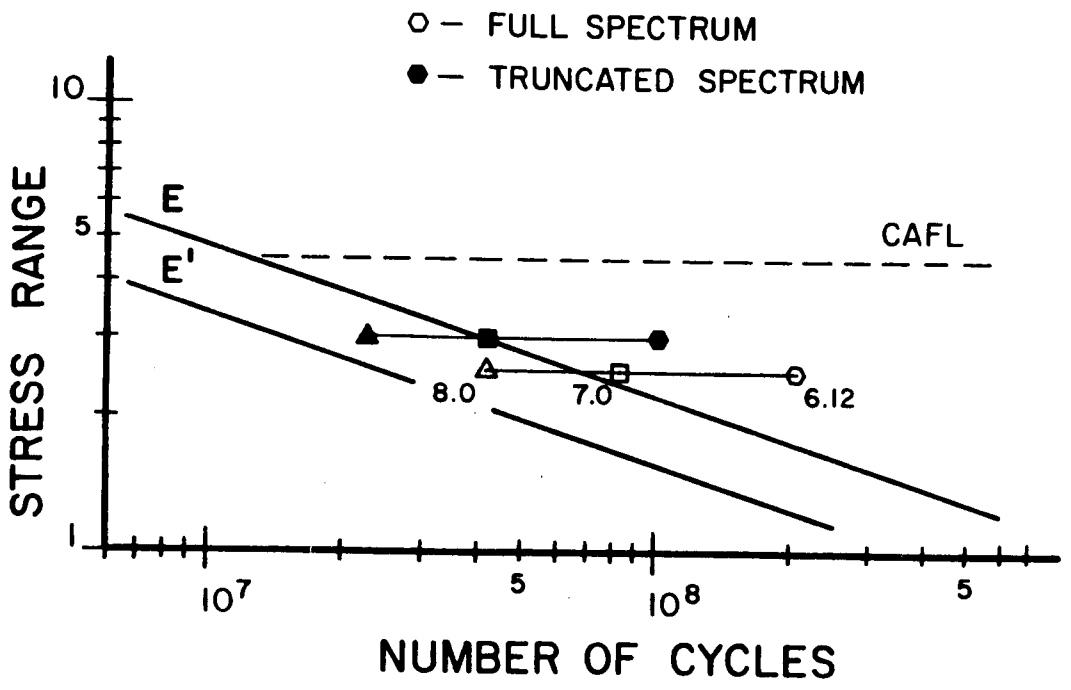

Figure 5-37: S-N relationships for coverplate stress concentrations, truncated spectrum

remaining stress range intervals. From the results of the full spectrum propagation model, the number of cycles corresponding to the frequency of occurrence of that stress range interval were eliminated from the nominal cycle life, N_f. This gave an effective stress range, number of cycles to failure relationship that is slightly less than the full spectrum fatigue life as determined from the fatigue crack propagation model. The next lowest stress cycle interval in the remaining spectrum was truncated and the calculations repeated for the effective stress range and cycle life. repeated. By plotting the effective stress range, life estimates at each truncation level, a failure curve can be established for each spectrum studied.

Figure 5-38 gives the fatigue life curves for the stress range distributions

used in the spectrum shift analysis. As illustrated in the plot, each curve generally follows the same path. The lower the exceedance rate, the higher the full spectrum nominal cycle life estimate. Generally, the lower exceedance rates result in estimates that are still conservative with respect to the straight-line extension of the resistance curve. At the higher exceedance rates, where almost all stress cycles in the full spectrum contribute to fatigue crack propagation, any stress cycle truncation will result in a non-conservative estimate for cycle life due to the truncation of damaging stress cycles.

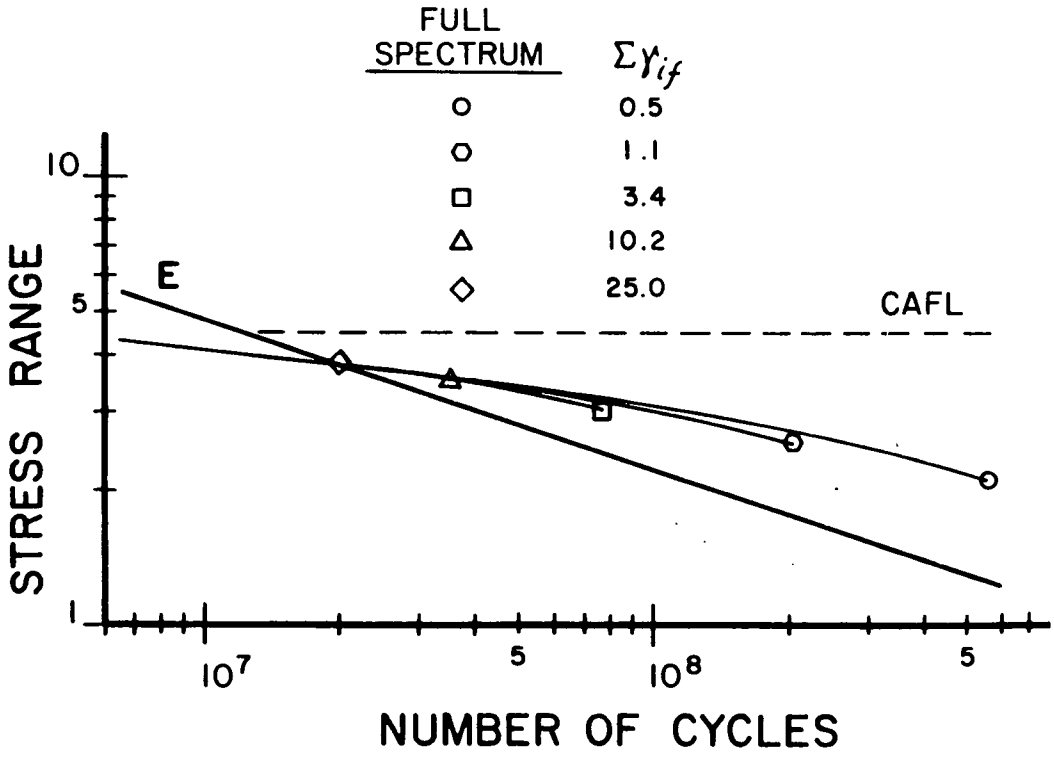

Figure 5-38: Cycle life truncation, coverplate spectra shift

Results of the stress cycle truncation for the varying stress concentrations are plotted in Fig. 5-39. While the life estimates do not overlap as is the case with the spectra shift they do run parallel to one another. As the stress

concentration decreases, fewer numbers of stress cycles need to be truncated to cause the life estimate to be non-conservative. At the stress concentration of 8.0, the full spectrum provides a fatigue life that is overestimated by the assumed fatigue resistance of Category E and any truncation is non-conservative. At a stress concentration of 6.12, the truncated life estimate does not become non-conservative until more than half of the full spectrum has been eliminated.

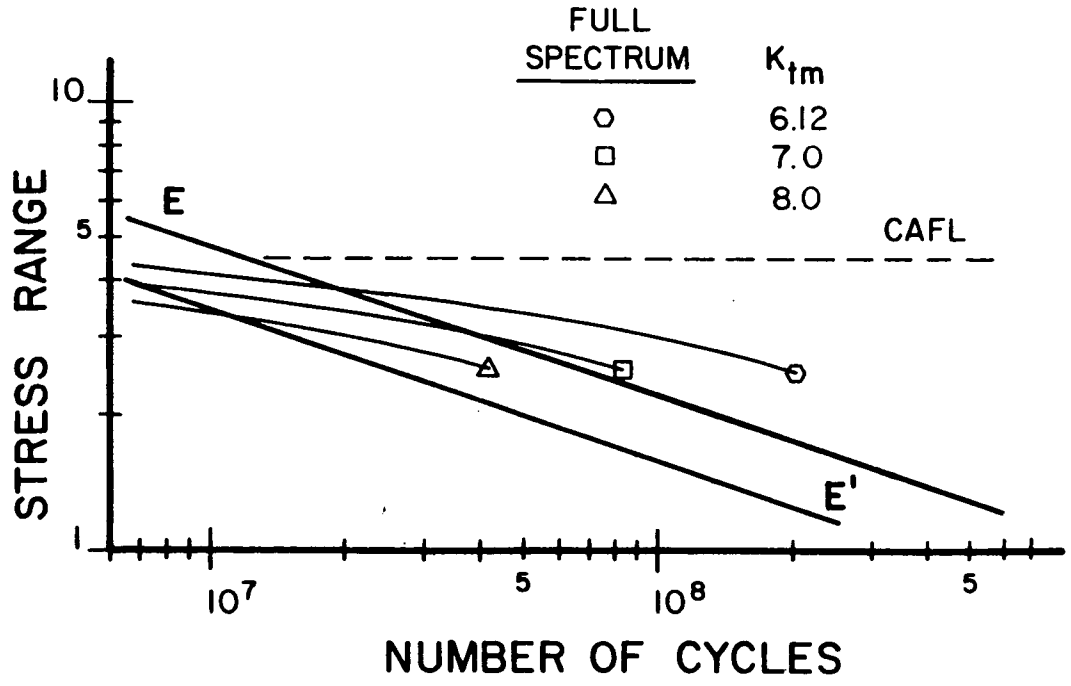

Figure 5-39: Cycle life truncation, coverplate stress concentration

The truncated cycle life estimates for the various stress range spectrum shapes are plotted in Fig. 5-40. The results for the constant, linear varying, geometric, and Rayleigh distributions are given. Three of the curves plot close together while the Rayleigh-type distribution curve is shifted into the higher life region. This is due to the fact that this distribution gave the highest nominal cycle life estimate. Again, the degree of non-conservativeness in the truncated fatigue life estimate is a function of the percentage of non-contributing cycles in

the nominal cycle life.

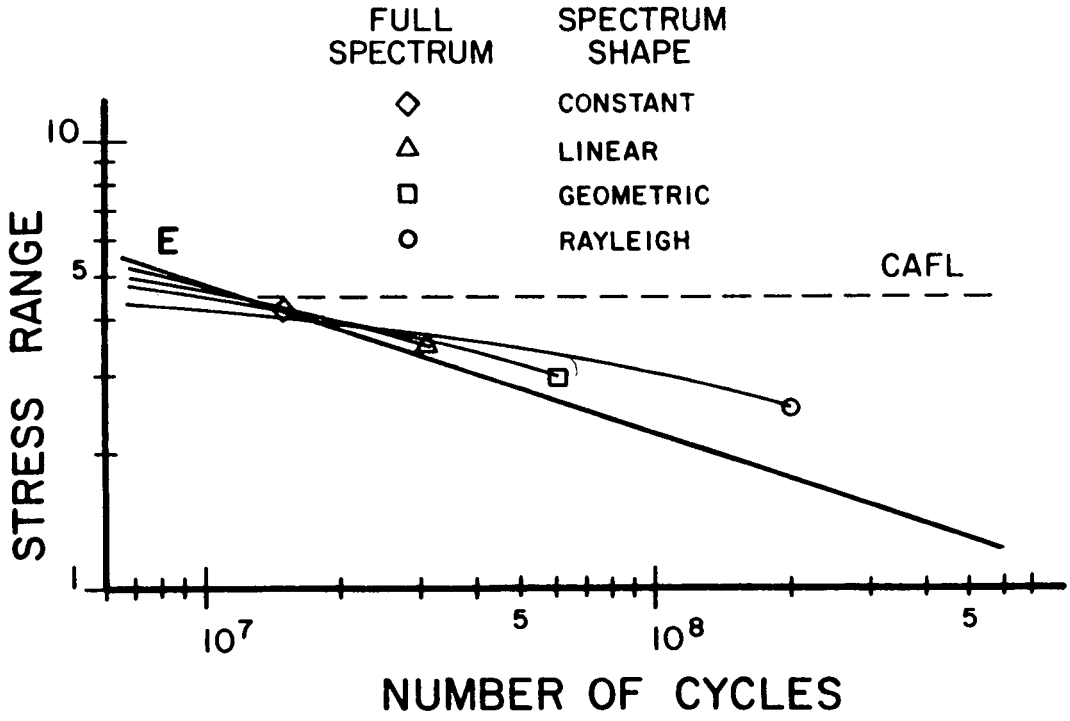

Figure 5-40: Truncated fatigue life estimates, spectrum shapes

5.7 Summary

A parametric study involving fatigue crack propagation models of welded steel details has been conducted. For variable amplitude loading, it has been shown that variability that exists in fatigue analysis and design has a significant effect on fatigue life estimates in the high cycle, long life regime. Specifically, the following conclusions have been reached.

5.7.1 Variable amplitude fatigue resistance

The variability in the parameters of the stress intensity range (initial crack size, stress range spectrum, and stress concentration factor) can cause a wide variation in the fatigue life estimates in the high cycle, long life regime.

A deviation of the fatigue resistance from the straight-line extension below the constant amplitude fatigue limit is partially due to the inclusion of non-contributing stress cycles in the fatigue life estimate. The variable amplitude fatigue data shows a definite spread in cycle life below the constant amplitude fatigue limit; indicating the summation of non-contributing stress cycles.

Experimental observations that for small exceedance rates (one percent or less), all variable amplitude load cycles contribute to fatigue damage can be partially related to the variability associated with the fatigue resistance of a detail. If no variability exists, all cycles to contribute to crack propagation would require the complete absence of a crack growth threshold or one that would completely decay upon the first application of an overload. If no threshold exists, then no fatigue limit exists. However, experimental results indicates that a portion of the details fatigue tested do not fail, thus indicating the existence of a limit. Rapid decay of the threshold would require an accelerated growth rate significantly above any observed in order for the smaller cycles to begin contributing early in fatigue life.

5.7.2 Fatigue test cycle truncation

The truncation of small stress cycles in a fatigue test spectrum will have an effect on the fatigue life estimates. This in turn will influence the establishment of a variable amplitude fatigue resistance curve based on the test data. As a greater portion of smaller stress cycles are included in the test spectrum, the effective stress range decreases and the number of cycles to failure increases. The resistance curve then becomes a function of the stress range spectrum and the cycle counting method. Therefore, the established fatigue behavior becomes unique to the test conditions.

5.7.3 Fatigue life cycle truncation

The significance truncating smaller stress cycles when determining fatigue life is a function of the true exceedance rate of the detail's constant amplitude fatigue limit. At high exceedance rates, stress cycle truncation will result in unconservative estimates of fatigue damage. At the lower exceedance levels, cycle truncation results in the removal of noncontributing stress cycles and can provide a fatigue life estimate closer to the true resistance of the detail.

Chapter 6
Application of Results

This chapter outlines the restrictions and limitations that must be placed on fatigue test data in order that the fatigue behavior of welded steel details subjected to variable amplitude loading can be accurately defined. As noted in the preceding chapters, the various stress distributions and geometrical conditions that full-scale welded steel details are subjected to in service must be fully accounted for during fatigue testing and in the evaluation and application of the test results. The recent revisions of the AASHTO fatigue design curves shown in Fig. 6-1 reflect four significant characteristics that make these curves applicable when determining the fatigue resistance of welded bridge details:

- The fatigue resistance is based on fatigue test results obtained from large-scale test specimens.

- The resistance curves are parallel to one another and all have a slope of -3.0.

- The variable amplitude fatigue resistance has been correlated with Miner's Cumulative Damage Rule.

- High cycle, long life fatigue resistance is defined by the straight-line extension below the constant amplitude fatigue limit.

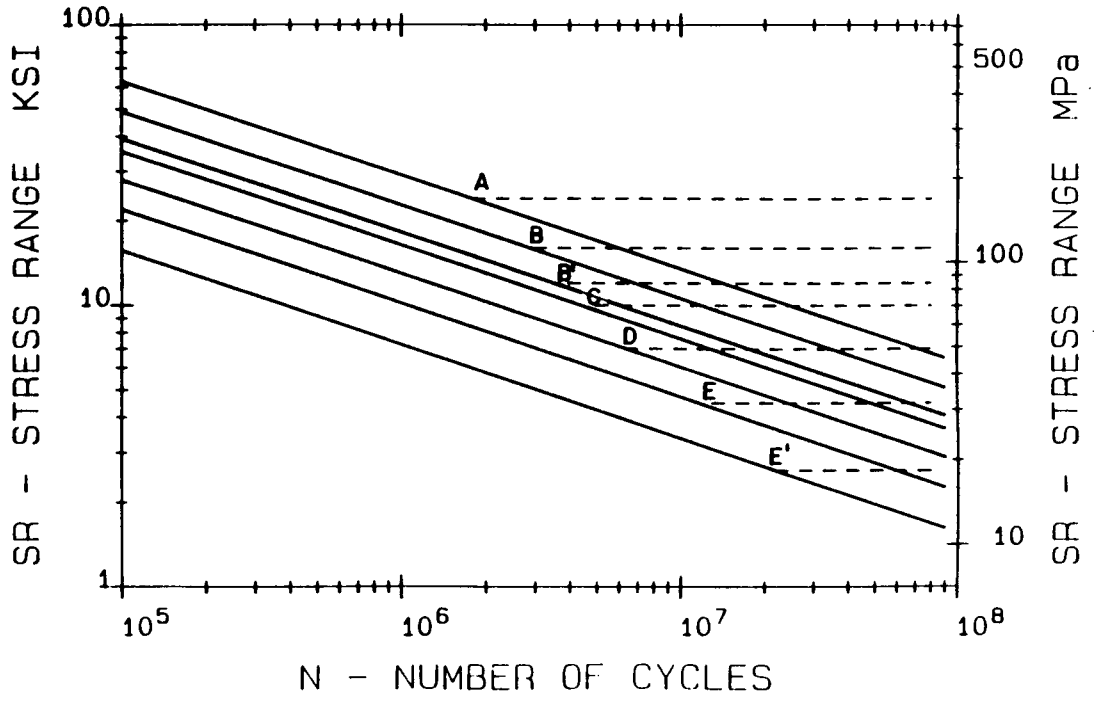

Figure 6-1: Revised AASHTO Fatigue Design Curves

6.1 Application of Fracture Mechanics to Full-Scale Welded Steel Details

Previous studies have shown that fatigue cracks in large welded structures will form and propagate in zones of high residual stresses. These stresses are present throughout all but an insignificant portion of the total fatigue life. The experimental results have demonstrated that no appreciable redistribution or relaxation of the residual stresses occurs. The existence of residual stresses throughout the useful life of the detail means that fatigue crack propagation always occurs under high stress ratios.

Crack growth at high stress ratios does so in the relative absence of crack tip closure. Therefore, fatigue crack propagation rates applicable to the fatigue behavior of structures and simulated test details must be obtained from tests

performed at high stress ratios. Results from this type of testing under both constant and variable amplitude loading have shown the growth rate to be:

$$\frac{da}{dN} = 3.6 \cdot 10^{-10} \, \Delta K^{3.0} \tag{6.1}$$

for the upper bound estimate of fatigue crack propagation in structural steels.

A second consequence of growth under high stress ratios and in the absence of crack tip closure is the decrease in stress cycle interaction effects. As a result, each stress cycle results in fatigue crack propagation that can be approximated by a single growth rate curve, as defined in Region II by Eq. (6.1). When fatigue crack propagation is defined by a single growth rate relationship throughout the entire fatigue life, then and only then is Miner's Rule valid. At lower stress ratios where increased crack tip closure is encountered, the resulting fatigue crack propagation is occurring on a series of different growth curves. The growth curve of any particular stress cycle is dependent upon the effective stress intensity range (function of crack closure) and is dictated by the past load history.

6.2 Effect of Specimen Size on Fatigue Behavior

When fatigue test experiments are carried out with test specimens that are not large enough to retain high residual stresses, then crack growth will not occur at the growth level defined by Eq. (6.1). This will always result in a higher fatigue life. Small-scale specimens do not provide the three dimensional constraint that exists in full-scale details and therefore, do not develop residual stress magnitudes as high as those found in the large specimens or actual in-service details. The lack of fully developed residual stress fields may be compensated to a degree in small-scale specimens by performing the tests at

high minimum or mean stress levels. However, this is seldom done due to a lack of understanding of the significance of residual stresses, the limitation of equipment load capacity, or the yield strength of the steel.

Finite element analyses of welded detail geometries revealed a three-dimensional effect on the stress field correction factor.[61] Limited detail size can not fully simulate the stress state that would be expected in large-scale details due to the geometry.

In addition, the size and distribution of flaws in small-scale test specimens are seldom representative of full-scale structural details. Often, the smaller specimens are cut from larger pieces welded together under more ideal fabricating conditions. This has a tendency to reduce defect size and to improve other factors that affect the fatigue strength such as the variation in the weld profile. Geometrical conditions that can result in increased flaw size, such as gaps between plates, will only be present in large-scale test specimens.

An example of the effect of specimen size on fatigue test data occurred during an experimental program that was conducted by the Honshu-Shikoku Bridge Authority in Japan to develop fatigue design specifications for long-span bridges.[62, 63, 64, 65] The principal structural elements of the bridges were box-type members. A series of fatigue tests were conducted to determine the fatigue strength of longitudinal groove welds that would be used to join the web and flange plates together. The first specimen types tested were small rod specimens machined out of the longitudinal groove welds as shown in Fig. 6-2. The second series of specimens were flat plate specimens as shown in Fig. 6-3. Finally, a third series was carried out on large-scale box type specimens.

Test results from these three specimen types are compared with the

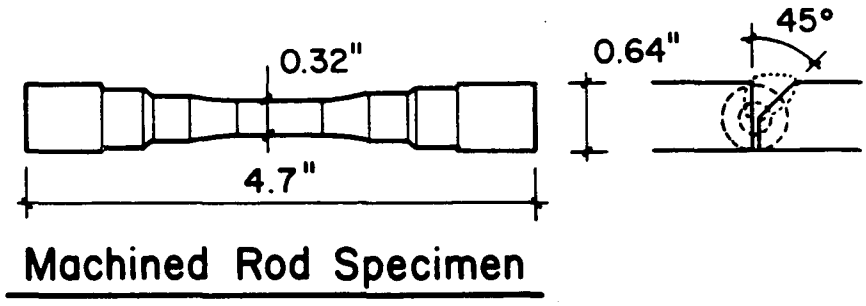

Figure 6-2: Small-scale machined rod specimens

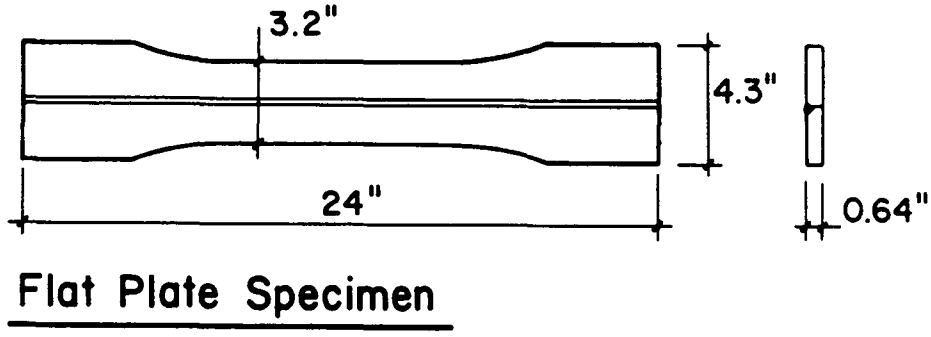

Figure 6-3: Flat plate specimens with longitudinal groove welds

AASHTO Category B′ resistance curve in Fig. 6-4. The small machined rod specimens clearly result in the highest fatigue strength. Although these specimens were machined from flat plate specimens their short length diminishes the probability that they will contain similar defect size distributions and their residual stress field had been substantially relaxed. The flat plate specimens were large enough to contain a greater portion of the residual stresses found in full-scale specimens and may contain more or larger defects. Hence, this results in lower fatigue lives as compared to the machined rod specimens. However, these welds were not fully constrained as was the case with the large-scale specimen welds, nor were the defect sizes as large. In the large-scale specimens

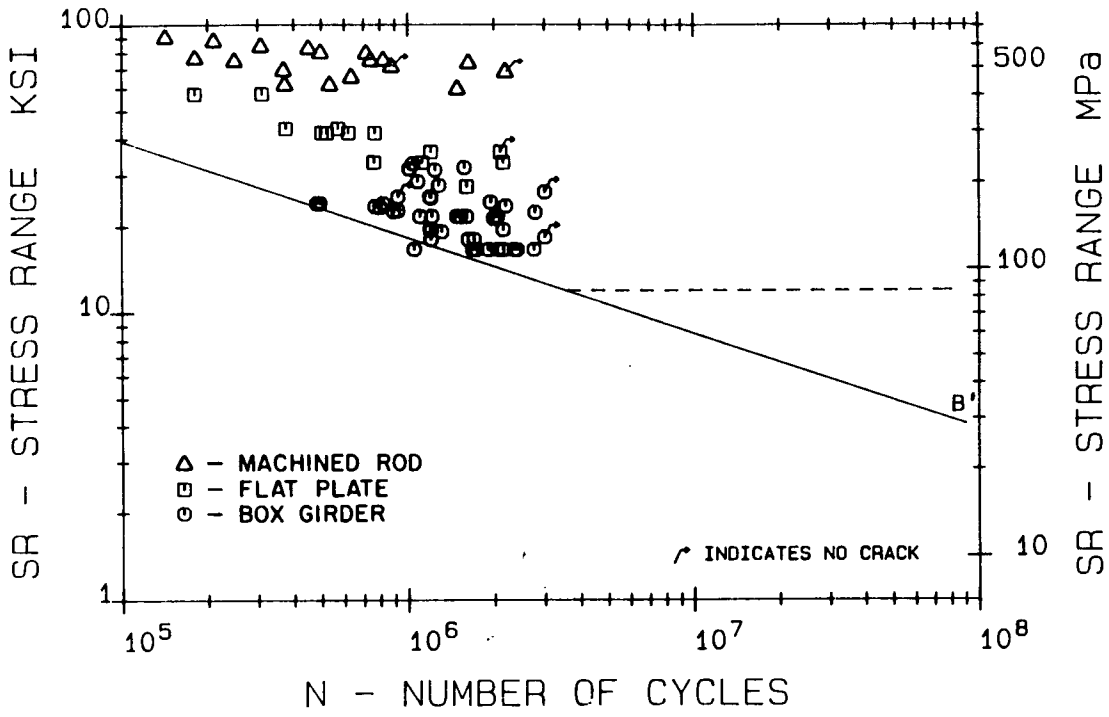

Figure 6-4: Japanese longitudinal partial penetration groove weld data

it was found that the gap length between the two plates influenced fatigue life. This gap increased with the increase in member size due to fit-up problems during fabrication. As a result, larger weld defects reside in these gaps and were impart responsible for the lower bound fatigue resistance provided by the box member specimens. It is apparent that the fatigue behavior of in-service longitudinal partial penetration groove welds could not have been accurately defined without the examination of data from large-scale test specimens.

A second example of the effect of specimen size on fatigue strength was observed during NCHRP Project 12-12.[9] Small-scale specimens, as shown in Fig. 6-5, were fabricated to simulate a coverplate detail. These specimens were subjected to both constant and variable amplitude loading. The variable amplitude loading consisted of Rayleigh-type distributions similar to those used in the larger-scale beam specimen test program. The small-scale plate specimen

test data are plotted in Fig. 6-6. As shown by the distribution of the data, the data points are well above the Category E resistance curve defining a welded coverplate that the small-scale specimens were intended to simulate. Because of the size limitations, mainly the 4 in. length of the attachment plate, these specimens behave more like an intermediate attachment and are therefore better described by the Category D resistance curve. Nevertheless, most of the data plots well beyond the Category D resistance curve. This was true for both the constant and variable amplitude test data.

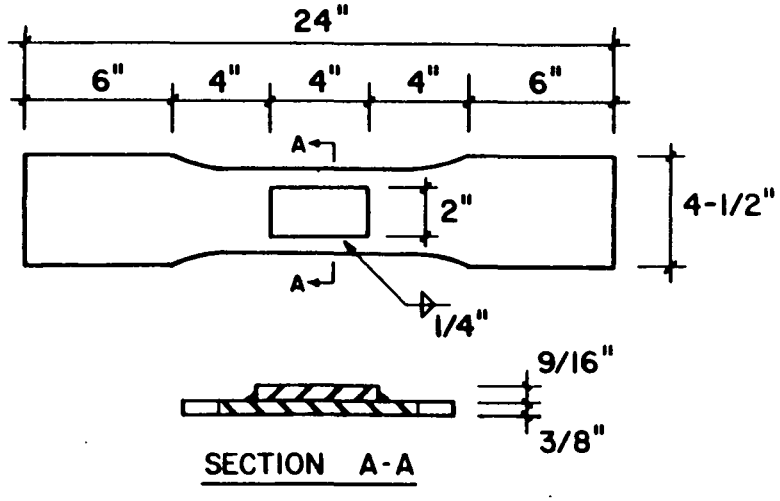

Simulated Coverplate Specimen

Figure 6-5: Simulated coverplate detail test specimens

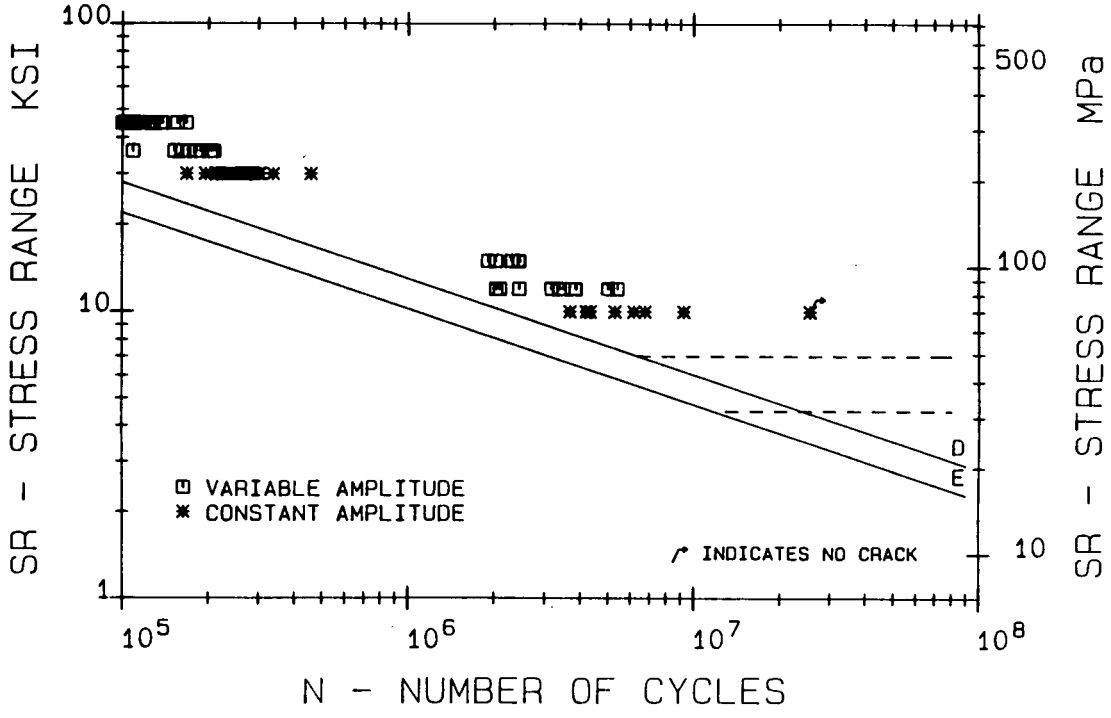

Figure 6-6: Fatigue test data for simulated coverplate detail NCHRP 12-12 test program

6.3 Limitations of Regression Analyses of Fatigue Test Data

Regression analysis of laboratory test data has demonstrated that stress range is the only significant stress parameter controlling the fatigue resistance of welded steel details (Sec. 2.2.2). The original AASHTO Fatigue Design Curves (Fig. 2-3) were developed from tests on one detail type for each design category. Although separate regression analyses of detail types for the same design category yielded similar regression coefficients, combining all data sets for a particular design category results in coefficients statistically different from those shown in Table 2-1. For example, when the original data for AASHTO Category C are combined (web stiffeners and short flange attachments), a regression analysis yields a slope of -3.42 and an intercept value of 10.13.

When compared to the values given in Table 2-1 for Category C, it can be seen that a significant difference exists between the slope and intercept coefficients. The original values, computed from short flange attachment data, are -3.25 and 10.038 for the slope and intercept, respectively. In a Japanese study,[62] separate regression analyses on each series of fatigue test results yielded a slope near -3.0. When the tests were combined, major deviations existed between the test series as the test data was not well distributed over many stress range levels. This resulted in a wide variation of the test results and also caused the slope provided by the regression analysis of all data to change.

The regression analyses on the original NCHRP fatigue test data[13, 14] was appropriate since the data was well distributed throughout the different levels of stress range by the factorial experimental design and the data resulted from only one experimental program. The fatigue experiments on each detail type resulted from factorial experiments with stress levels and steel type as the design variables. Each cell of the factorial for a particular stress parameter contained at least three specimens or replicates, permitting the variance of each cell to be estimated. When the test data was analyzed in terms of stress range, most stress range levels had more than twenty data points for a given detail type. The test specimens for the experimental program were all fabricated at the same shop using normal fabrication techniques, workmanship, and inspection procedures. This provided a large set of specimens which were similar in quality and configuration. This resulted in a reasonable distribution of the initial flaws, residual stress fields, and weld profiles and produced consistent results.

When test data is clustered in one region of fatigue life, the regression

analysis tends toward instability and any number of regression lines can be used to describe the fatigue resistance. This behavior can be observed in the evaluation of large-scale longitudinal partial penetration groove welds. The test data, and its correlation with the initial flaw sizes and crack growth rates, indicated a lower bound fatigue resistance defined by the Category B′ classification. However, the limited distribution of the data resulted in the mean regression analysis resistance curve shown in Fig. 6-7.

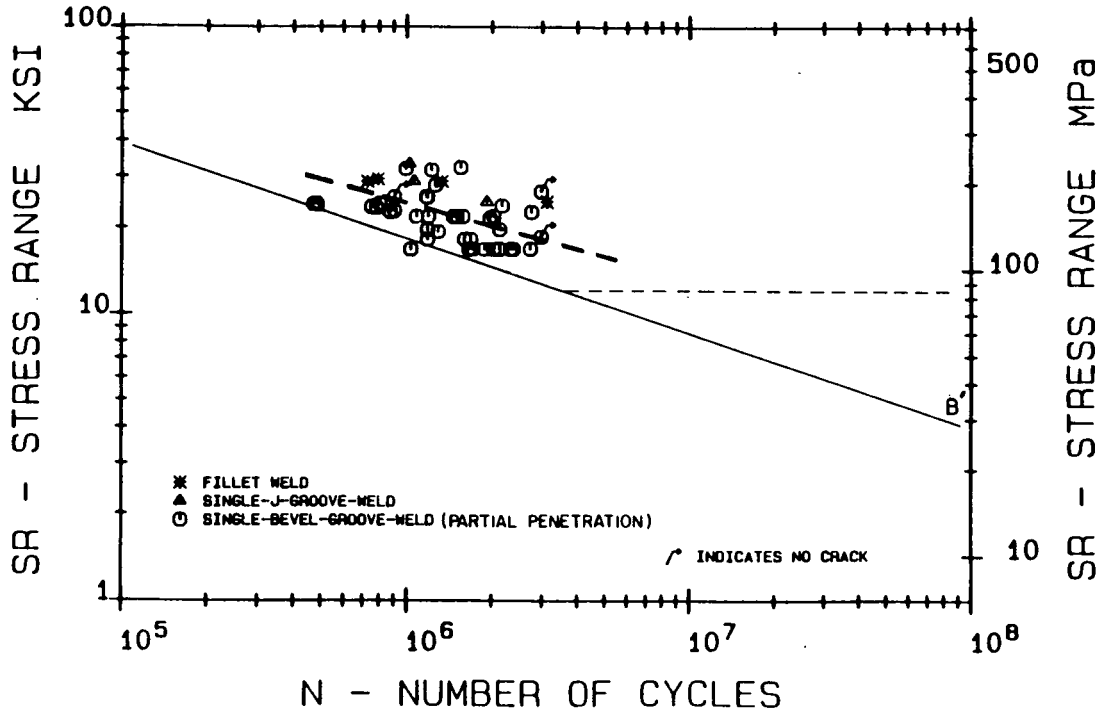

Figure 6-7: Fatigue test data for longitudinal partial penetration groove welds

A log-linear regression analysis of both constant amplitude and variable amplitude fatigue test data can have a tendency to be biased or skewed due to the influence of the crack growth threshold or constant amplitude fatigue limit. The scatter in the test data tends to increase as the constant amplitude limit is approached. The scatter existing in the data for a given stress range level is primarily due to variations in initial defect sizes and stress concentration factors.

As the initial defect size and/or the stress concentration increases, the failure point will occur at a lower number of stress cycles. When fatigue life begins in Region II, regardless of the stress range, the scatter band width will remain constant assuming the defect distribution and all other factors remain the same. However, as the stress range is decreased for a given test specimen, crack growth will begin in Region I for the smaller defect sizes and will therefore deviate from the power law of Region II crack growth. The larger sized defects will still commence growth in Region II. This increases the fatigue lives of specimens with smaller defects disportionately due to the lower, non-linear crack propagation rates of Region I.

As a consequence of the increased scatter near the constant amplitude fatigue limit, a regression analysis will be biased and will yield a slope that is skewed from -3.0. This effect is graphically shown in Fig. 6-8 for transverse web stiffeners. Regression analysis of all data results in a mean fatigue life represented by the heavy solid line. Data points, that represent failures in which a portion of the crack propagation was in Region I, are shown as solid circles. If these data points are excluded from the regression analysis, the slope will increase to approximately -3.0 and becomes parallel to the AASHTO Fatigue Design Curves.

Fatigue tests of welded details on beams and girders have an upper limit on maximum stress test levels by the yield stress of the steel. Therefore, as the detail fatigue strength increases and, consequently, it's constant amplitude fatigue limit, the distribution of test data over varying stress range levels decreases. This decreases the levels of stress range that can be evaluated, particularly for the lower yield point steels. This also magnifies the effect of

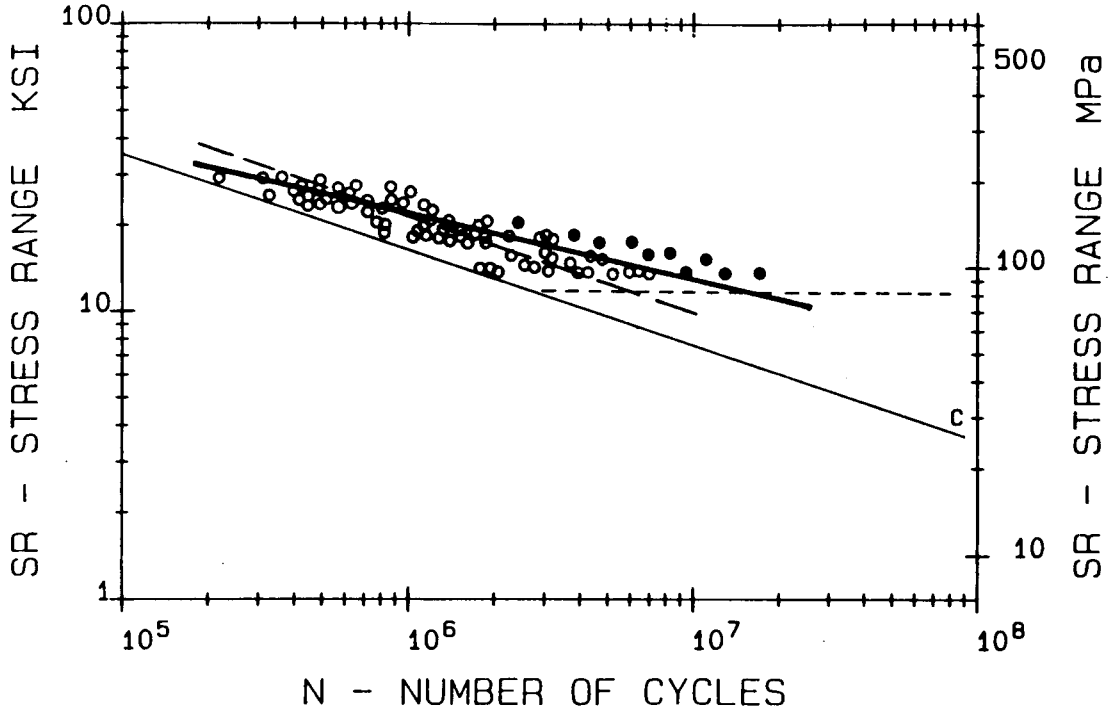

Figure 6-8: Fatigue test data and effect of the Constant Amplitude Fatigue Limit

the constant amplitude fatigue limit as tests near the fatigue limit will have more scatter and will therefore result in a greater deviation of the slope from -3.0. An examination of the regression coefficients for the original NCHRP test data reveals this tendency. Table 6-1 gives the slope coefficients obtained from the regression analysis of Categories A to E. When the data was well distributed over several levels of stress range, as was the case with Category E, the slope tends towards -3.0. The higher strength categories show a greater deviation from this slope.

Category	Slope
A	-3.178
B	-3.372
C	-3.25
D	-3.071
E	-3.095

Table 6-1: Regression slope coefficients

6.4 Cumulative Damage

As stated earlier, the most familiar and widely used cumulative damage rule was originally proposed by Palmgren and subsequently reformulated by Miner. Commonly referred to as Miner's Rule, this linear damage hypothesis estimates fatigue damage under variable amplitude loading based on the fatigue resistance developed from constant amplitude test data. According to Miner's Rule, fatigue failure will occur when the sum of cumulative cycle ratios for the various stress cycles equals unity. Therefore,

$$\sum \frac{n_i}{N_i} = 1.0 \tag{6.2}$$

where n_i is the number of cycles applied at a stress range Sr_i and N_i is the number of constant amplitude cycles to failure at Sr_i. The summation given in Eq. (6.2) is dependent on the fatigue resistance curve used to determine N_i. Normally, the Miner's Rule life estimate is compared with the mean fatigue resistance developed from constant amplitude test data. Given the inherent scatter in fatigue life associated with the data, it would be expected that

approximately 50 percent of the variable amplitude life estimates be less than 1.0. If a lower bound estimate of fatigue resistance is used, a summation less than 1.0 would be indicative of the rule's possible underconservativeness. Conversely, a summation greater than 1.0 would reflect the rule's overconservativeness. However, due to the scatter in the test data, precise evaluation of Miner's Rule is difficult. The summation of variable amplitude fatigue damage by Miner's Rule can be derived from fracture mechanics considerations as shown by Maddox.[66]

The two primary assumptions of Miner's Rule are:

- Fatigue life is defined by fatigue crack propagation only.
- Cycle by cycle interaction does not occur.

When crack growth occurs under high stress ratios, as is the case with full-scale welded steel details and the application of stress cycles is random in nature, then both of these assumptions are satisfied when the stress range spectrum is above the constant amplitude fatigue limit. At high effective stress ranges, most stress cycles are above the fatigue limit and all contribute to crack growth as defined by the Paris Power Law. As was noted in Chapter Four, fatigue crack propagation under high stress ratios and within the stress range limitations that bridge type structures are subjected to does so under reduced crack tip closure. This reduces cycle interaction effects due to overloads and underloads that result in a varied crack growth rate.

Implied in the assumption of Miner's Rule is that fatigue crack occurs along a single fatigue crack propagation curve, regardless of the magnitude of the stress cycle or it's occurrence with respect to time. Both the material constant, C, and the growth rate exponent, n, given in Eq. (4.7) remain

constant throughout fatigue crack propagation.

By providing an upper bound value on the fatigue crack propagation rate for use with Miner's Rule, fatigue life estimates made with the assumption that all cycles contribute to fatigue damage will result in a lower bound estimate for fatigue damage or correspondingly fatigue life. Correspondingly, developing fatigue resistance curves based on test results from large-scale test specimens will result in a lower bound estimate for both constant and variable amplitude loading.

The fatigue damage models proposed by Gurney[19] and Joehnk[4] attempt to account for interaction effects between stress cycles that cannot be adequately dealt with by Miner's cumulative damage rule. As discussed in Sec. (2.4), these non-linear damage rules modify the cycle life estimates provided by Miner's Rule. A correction factor is applied that increases the predicted number of cycles to failure for both design and analysis purposes. However, these experimental programs were based on results obtained from small-scale test specimens. The mean fatigue resistance curves for several details were established through constant amplitude fatigue testing at various stress range levels. Variable amplitude test results were then compared to the mean cycle life estimates of the constant amplitude data. Damage models were then developed based on this comparison to relate the damage produced by the variable amplitude stress cycles to that defined by the mean constant amplitude cycle life.

An examination of the constant amplitude test data used to establish the fatigue behavior of a particular detail indicates that the fatigue strength exceeds the lower bound resistance provided by the corresponding AASHTO fatigue

resistance curves. Figure 6-9 summarizes the constant amplitude test data used by Gurney. The axially loaded test specimens were flat plates with longitudinal non-load carrying attachment details. The attachments were approximately 6 in. in length and were welded either to the plate surface or the plate edge. These details are classified as AASHTO Category E. However, as the plot of the data indicates, the fatigue resistance of the two attachment details significantly exceeds the lower bound resistance of Category E and correspond more closely to Category B. The constant amplitude test data used by Joehnk are plotted in Fig. 6-10. The tee-shaped specimens used in the experimental program simulated an AASHTO Category C stiffener detail. Plate thicknesses were 1.0 in. with 0.6 in. fillet welds. These data also plot significantly above the appropriate resistance curve, exhibiting a relatively high fatigue strength that also exceeds Category B.

The deviation of the small-scale constant amplitude test results from the lower bound estimates provided by the AASHTO fatigue resistance curves cannot be adequately accounted for by differences in fabrication techniques, defect sizes and distributions, etc. Few large-scale stiffener detail specimens have approached the plate thickness or weld size used for the tee-shaped specimens. And yet, large-scale fatigue tests on similar type details have always resulted in lower cycle lives. The decreased fatigue life of the variable amplitude small-scale specimens can be attributed to the increase in stress cycle interaction that occurs at lower effective stress ratios. These small-scale specimens do not have the same stress states at fatigue crack initiation sites due to the decrease in specimens size and reduction in geometrical constraints. It can therefore be argued that the non-linear fatigue damage summation

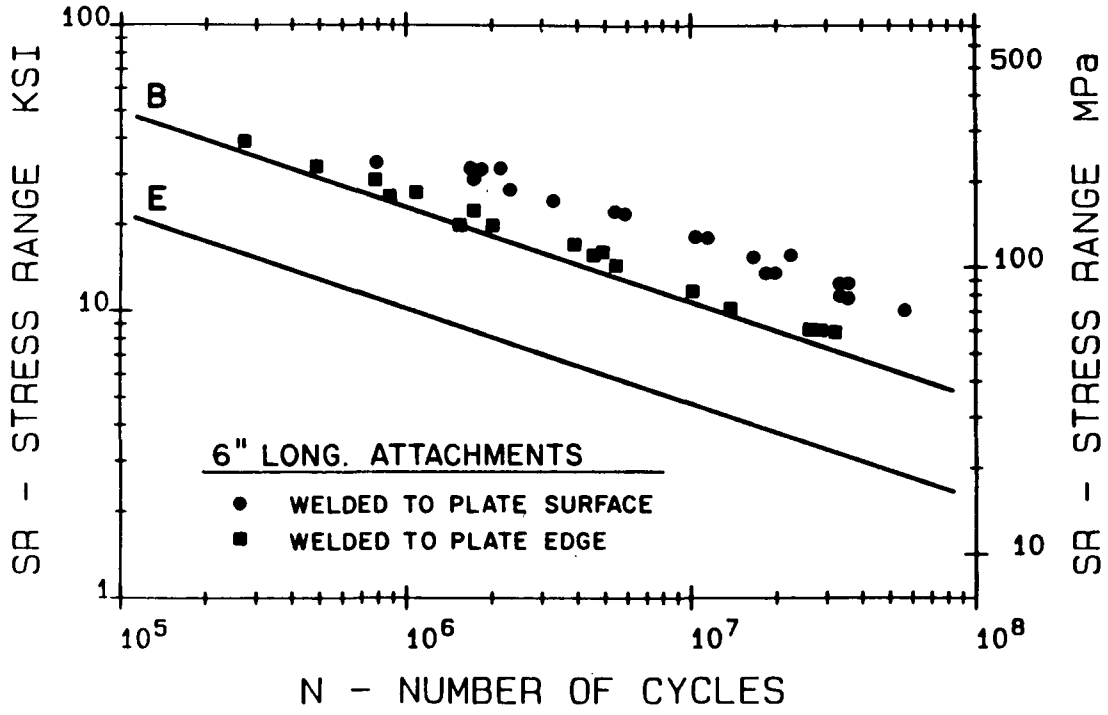

Figure 6-9: Constant amplitude test data used by Gurney

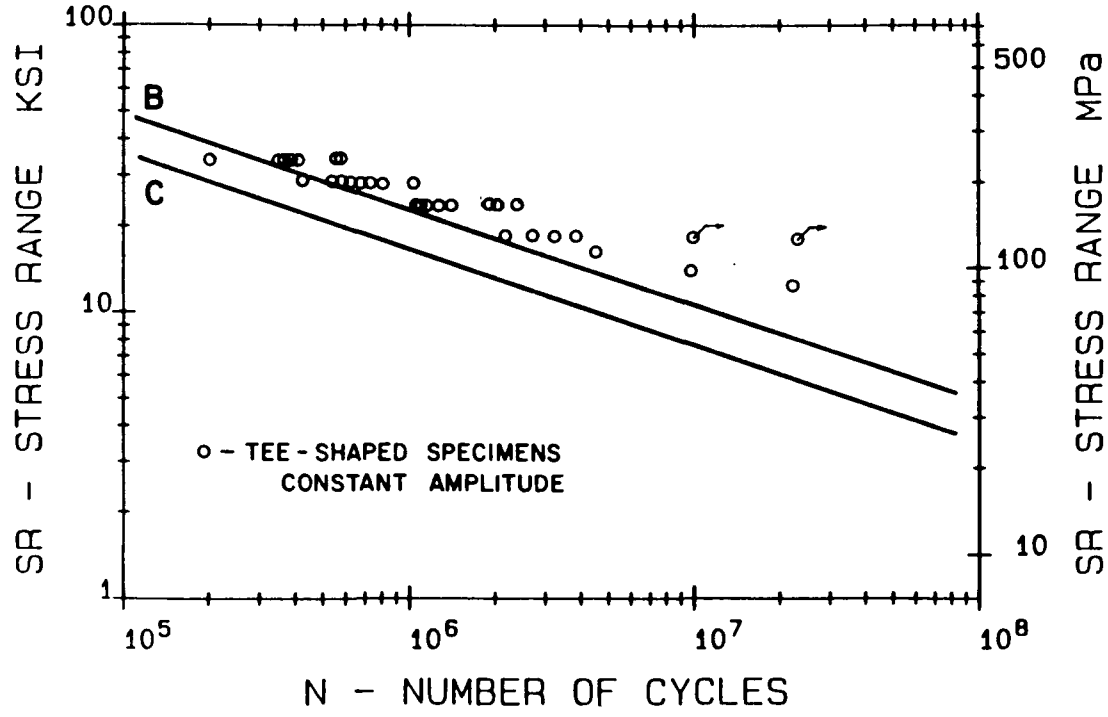

Figure 6-10: Constant amplitude test data used by Joehnk

observed in these small-scale specimens would not occur in large-scale welded bridge details. The fatigue resistance of the specimens under variable amplitude loading is reduced towards the lower bound estimate of large-scale details.

6.5 High Cycle Variable Amplitude Fatigue

Extensive fatigue testing of a single welded steel detail under both constant and variable amplitude loading will provide a well defined fatigue resistance curve for all cycle lives. Fatigue design S-N curves have been proposed[67] that take into account this behavior. Figure 6-11 indicated that as the effective stress range for a given stress spectrum approaches the constant amplitude fatigue limit, the resistance curve begins to deviate from the log-linear curve. As the effective stress range is reduced further, a limiting value is suggested that provides infinite life. This value, commonly referred to as the variable amplitude fatigue limit, is a function of the constant amplitude fatigue limit and the shape of the stress range spectrum. This fatigue behavior is based on limited test data that provides well conditioned knowledge of the fatigue resistance of the detail and it's constant amplitude fatigue limit. In design however, this condition seldom exists. Inherent to the fatigue design process is the variability of the constant amplitude fatigue limit. As discussed in Chapter Two, only a limited fatigue test database exists for the determination of these limits and, at present, does not allow for an adequate means of assessing fatigue limits for all possible bridge details and configurations that must be designed for fatigue.

The results of the crack propagation simulation model given in Chapter Five demonstrates that the value of the constant amplitude fatigue limit has a significant effect on fatigue life under variable amplitude loading. As the

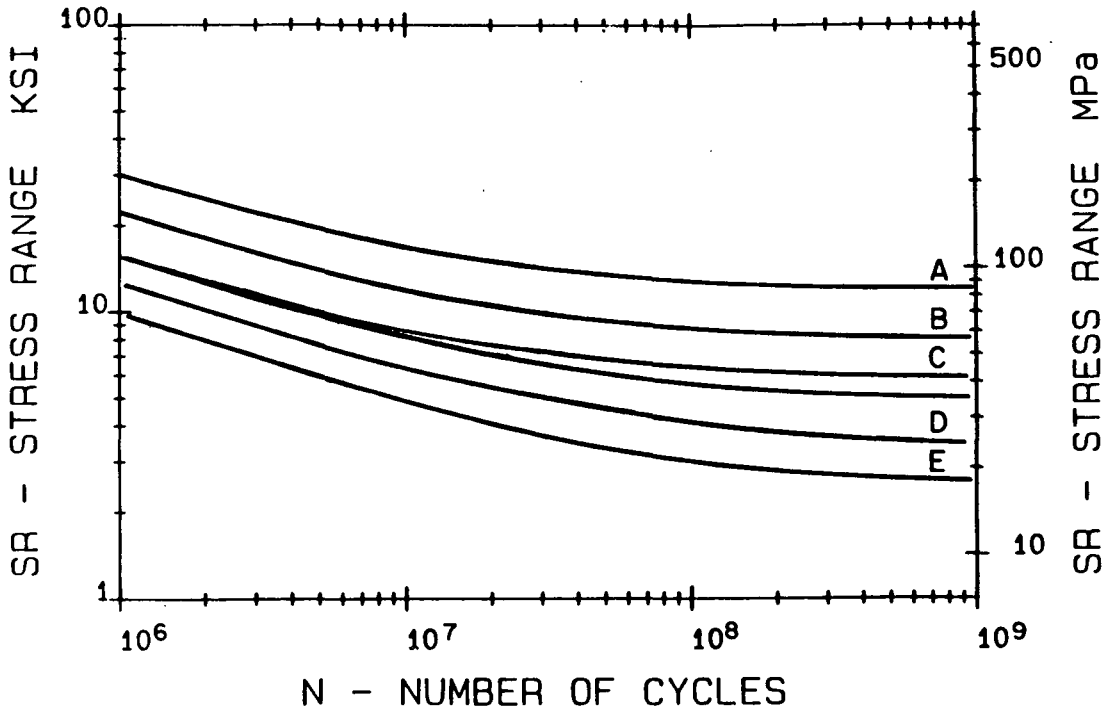

Figure 6-11: Variable amplitude fatigue design curves

fatigue limit is decreased for a given stress range spectrum, fatigue life is also decreased in the transition region due to the increasing number of stress cycles contributing to fatigue damage. This lowers the portion of the fatigue resistance curve as crack growth controls and extends the S-N curves toward the straight-line extension of the resistance curve as shown in Fig. 6-12

The fatigue design of most structural components is based on the intended design life and the ability to economically detect and repair fatigue cracking should it develop. When the inspection process is reliable, and repair or replacement of a fatigue damaged component is possible, fatigue designs can tolerate some crack growth and can be based on a finite life. The design variables for the required number of cycles (design life) are the effective stress range and the detail type. Highway bridges subjected to low traffic volumes are compatible with a finite life design. However, bridges designed for primary

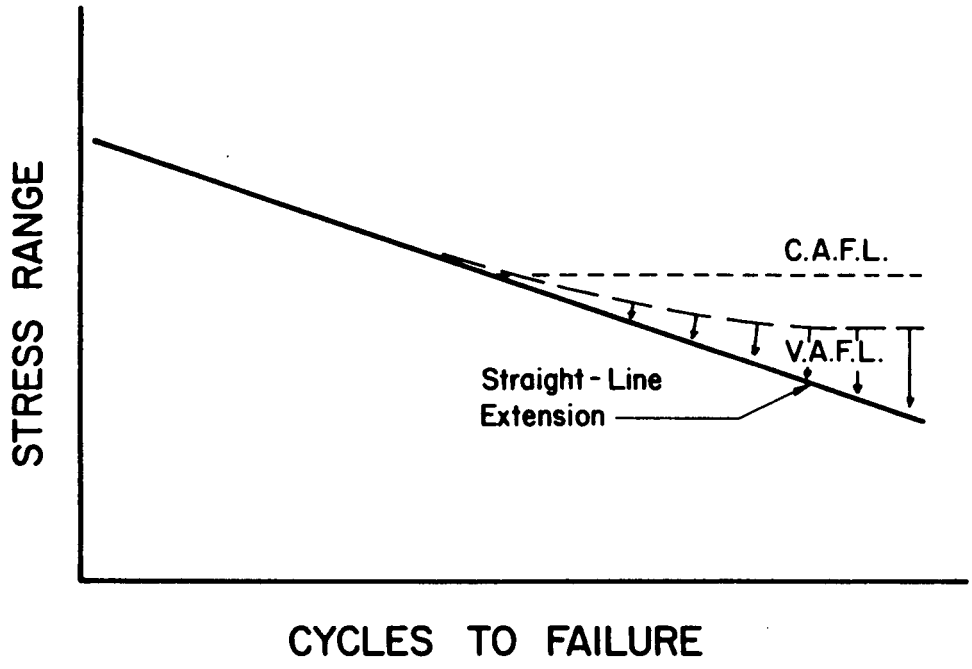

Figure 6-12: Effect of a decreased fatigue limit

highway systems will be subjected to moderate to heavy traffic volumes. This requires the design to be capable of resisting high cycle, long life conditions without premature failure and/or extensive crack growth.

The fatigue design of welded steel details subjected to variable amplitude loading in the long life, high cycle region can be dealt with in two ways. One approach is to design for infinite life assuring that no appreciable fatigue crack propagation occurs. The alternative is to design and permit crack growth but assure that the fatigue strength will permit achieving the desired life and variable stress cycles.

The finite fatigue design to a variable amplitude resistance curve in the high cycle region is a function of the following parameters:

- Effective stress range, Sr_e

- Maximum stress range, Sr_{max}
- Constant amplitude fatigue limit, Sr_l
- Detail type
- Spectrum shape
- Cycle counting method

Variability exists for each of these parameters and can therefore influence the detail's behavior. The variability in the stress range parameters, the constant amplitude fatigue limit, and the stress concentration (detail type) drive the variable amplitude fatigue resistance toward a straight-line extension of the resistance curve below the constant amplitude fatigue limit. This insures an adequate lower-bound resistance.

High cycle variable amplitude fatigue behavior is governed by the magnitude of the peak or maximum stress range. If a detail is subjected to a variable stress range spectrum whose peak stress cycle is below the true fatigue limit of the detail throughout the design life, then no fatigue crack propagation will occur. If a portion of the variable stress range spectrum exceeds the detail fatigue limit, cracking will occur. The maximum stress range is the only single parameter that determines the difference between a finite long life and infinite fatigue life.

The current AASHTO fatigue design procedure uses a peak stress range equal to the constant amplitude fatigue limit. The design procedure minimizes the possibility that the welded steel will experience stress cycles that exceed the fatigue limit. If it can be reasonably assured that the peak stress range remains below the constant amplitude fatigue limit, fatigue crack propagation will not occur and infinite life can be expected. Designing for crack growth

requires a more adequate definition of all of the parameters that influence fatigue resistance.

Chapter 7
Conclusions

7.1 Summary

This study has involved a broad-based assessment of the various parameters that influence the fatigue behavior of welded bridge details subjected to variable amplitude loading. Although the focus has been primarily on the resistance side of the design equation, it has been also shown that fatigue life is a function of the load (and stress range) spectrum at higher cycles lives. The large-scale structural components found in bridges and other similar type structures exhibit a uniqueness that requires their fatigue behavior to be analyzed within certain guidelines and limitations.

The most dominate parameters are the tensile residual stresses that are present in the vicinity of the fatigue crack initiation sites and the magnitude of stress range. Indirect measurements of the residual tensile stresses have indicated that these stresses are at, or near, to the yield stress, regardless of the steel type. The most common procedures used to establish the residual stress distribution is the method of sectioning and the hole drilling method. These methods result in average estimations due to the finite area of the section or hole. It is reasonable to assume that the actual stress values are higher due to the constraint and strength of full size weldments that tends to elevate the residual stresses above the nominal yield stress of the base metal. Analysis of large-scale welded specimens after cyclic loading has shown that no significant residual stress redistribution occurs at the weld toe even after millions of load cycles and at a constant stress range of 20 ksi. Therefore, it can be concluded

that fatigue crack propagation occurs under the influence of high tensile residual stresses throughout much of the fatigue life.

The loading to which bridges are subjected result in stress range spectrums that are usually more narrow than those that are used in fatigue testing. The possible combinations of dead load and live load stresses that can occur from bridge design considerations and constraints will always result in a relatively high stress ratio at a particular weld detail. This coupled with the presence of high tensile residual stresses results in an effective stress ratio that is high (greater than 0.8). This stress ratio exceeds the maximum value that can be obtained in fatigue crack propagation tests due to the limits on the nominal yield stress of the test specimen. Strain measurements on in-service bridges have demonstrated that extremely high load cycles do not result in high stress ranges but are attenuated in magnitude. Therefore, overload fatigue testing seldom simulates actual stress conditions.

The loads for the full service life are not precisely defined or constant with time. Bridge loadings have shown a consistent trend of increasing with time and there is little reason to believe that they will remain at their current level. Fatigue design procedures must consider this variable as it pertains to the high cycle fatigue life region.

7.2 Conclusions

One of the consequence of fatigue crack propagation at relatively high stress ratios (greater than 0.8) is that growth occurs with reduced crack tip closure. For variable amplitude loading the significance of this is two-fold. First, it means that the fatigue crack propagation rates for each stress range of the load spectrum will approach an upper bound limiting rate that corresponds

to the maximum possible value for crack growth. All stress cycles that exceed the crack growth threshold, regardless of their magnitude or time of application can be related to a single fatigue crack propagation curve. If cycle to cycle crack tip closure does not occur, then stress cycle interaction does not develop. As a consequence, there is no crack growth acceleration or retardation effects that influence the growth rate. Each cycle causes propagation along the same crack propagation curve. Therefore, the basic assumptions of Miner's Rule are satisfied.

In the high cycle region of fatigue behavior, the contribution of the lower cycles of a variable stress range spectrum to fatigue crack propagation is a function of the fatigue limit exceedance rate of the larger stress cycles. However, in the fatigue design process, the value of the constant amplitude fatigue limit is not known for many details and in some cases may differ from the assumed value. Therefore, it is not known at what level it is valid to truncate the smaller, noncontributing stress range values. In addition, as loads increase with time, they increase the peak stress range and also shift the spectrum upwards, causing smaller stress cycles to contribute that were previously truncated. Because of of the variability in the details' fatigue limits and the uncertainties of loading, the variable amplitude fatigue resistance of large-scale welded steel details is best defined by the straight-line extension of the S-N resistance curves. This curve provides a lower bound fatigue resistance for a given welded details.

7.3 Recommendations for Additional Research

The upper bound limit on fatigue crack propagation in large-scale welded structures must be clearly established. Test results from compact tension crack growth specimens cannot simulate the stress and strain conditions that exist in the vicinity of a crack in a large-scale welded structure. Due to the presence of residual tensile stresses in the weldment, the crack tip resides within a highly constrained tensile stress field that is at, or near, yield stress and is surrounded by a large low stressed elastic body. This results in an effective stress ratio that is higher than the conditions simulated by small-scale specimens. When this upper value of crack growth has been established, then its use in conjunction with Miner's Rule will provide the true lower bound for fatigue resistance.

Additional work is required to accurately determine crack growth threshold values and constant amplitude fatigue limits for welded steel details. The fatigue test database for these values continues to be sparse. The accurate determination of fatigue resistance under variable amplitude loading in the high cycle region can only be made with a precise knowledge of these limits. This study has indicated that fatigue life can be dramatically affected for a given stress range spectrum. In addition, current design procedures for bridges subjected to high traffic densities requires the design life to be infinite. This can only be provided when the fatigue limit for the detail used is accurately known.

The suggested research needs for the determination of the fatigue behavior of large-scale welded details subjected to variable amplitude loading are summarized as follows:

- Fatigue crack propagation studies that more accurately simulate the high stress ratios associated with welded structures.

- Overload/Underload fatigue crack growth studies at high stress ratios.

- Additional fatigue tests of large-scale welded details near the fatigue crack growth threshold.

- Experimental verification of the fatigue crack threshold decay under variable amplitude loading and it's effect on fatigue life estimates.

- Variable amplitude fatigue tests with truncated stress range spectra and comparison of the data with test data obtained from full stress range spectrum loading.

References

[1] Miner,M.A.
Cumulative Damage in Fatigue.
Journal of Applied Mechanics, ASME (12):159-164, September, 1945.

[2] Gurney,T.R.
Fatigue Tests Under Variable Amplitude Loading.
Research Report 220/1983, The Welding Institute, July, 1983.

[3] Gurney,T.R.
Fatigue Tests on Fillet Welded Joints to Assess the Validity of Miner's Cumulative Damage Rule.
Proceedings, Royal Society of London (A 386):393-408, 1983.

[4] Joehnk,J.M.
Fatigue Behavior of Welded Joints Subjected to Variable Amplitude Stresses.
Master's thesis, Department of Civil Engineering, The University of Texas at Austin, May, 1982.

[5] Swensson,K.D.
The Application of Cumulative Damage to Bridge Fatigue Design.
Master's thesis, Department of Civil Engineering, The University of Texas at Austin, May, 1984.

[6] Haibach,E.
The Allowable Stresses under Variable Amplitude Loading of Welded Joints.
In *Proceedings, Fatigue of Welded Structures Conference*, pages 328-339. The Welding Institute, 1971.

[7] Tilly,G.P. and Numm,D.E.
Variable Amplitude Fatigue in Relation to Highway Bridges.
Proc. Institute of Mechanical Engineers 194(27), 1980.

[8] Yamada,K and Albrecht,P.
Fatigue Behavior of Two Flange Details.
J. Structural Division, ASCE 103(ST4):781-791, April, 1977.

[9] Schilling,C.G., Klippstein,K.H., Barsom,J.M., and Blake,G.T.
Fatigue of Welded Steel Bridge Members Under Variable-Amplitude Loading.
NCHRP Report 188, National Cooperative Highway Research Program, 1978.

[10] Fisher,J.W., Slockbower,R.E., Hausamman,H., and Pense,A.W.
Long Time Observation of a Fatigue Damage Bridge.
Proc. ASCE 1(TC1):55-71, April, 1981.

[11] Highway Research Board.
The AASHO Road Test, Report 4, Bridge Research.
Special Report 61D, National Academy of Sciences - National Research Council, Washington,D.C., 1962.

[12] AASHO.
Standard Specifications for Highway Bridges, Nineth Edition.
American Association of State Highway Officials, 1965.

[13] Fisher,J.W., Frank,K.H., Hirt,M.A., and McNamee,B.M.
Effects of Weldments on the Fatigue Strength of Steel Beams.
NCHRP Report 102, National Cooperative Highway Research Program, 1970.

[14] Fisher,J.W., Albrecht,P.A., Yen,B.T., Klingerman,D.J., and McNamee,B.M.
Fatigue Strength of Steel Beams with Welded Stiffeners and Attachments.
NCHRP Report 147, National Cooperative Highway Research Program, 1974.

[15] AASHO.
Standard Specifications for Highway Bridges, Eleventh Edition.
American Association of State Highway Officials, 1974.

[16] Fisher,J.W., Mertz,D.R., and Zhong,A.
Steel Bridge Members Under Variable Amplitude Long Life Fatigue Loading.
NCHRP Report 267, National Cooperative Highway Research Program, 1983.

[17] Keating,P.B. and Fisher,J.W.
Full-Scale Welded Details Under Random Variable Amplitude Loading.
In *Proceedings, International Conference on Fatigue of Welded Constructions.* The Welding Institute, Brighton, UK, April, 1987.

[18] Dowling,N.E.
Fatigue Failure Predictions for Complicated Stress-Strain Histories.
Journal of Materials, JMLSA 7(1):71-87, March, 1972.

[19] Gurney,T.R.
Some Variable Amplitude Fatigue Tests on Fillet Welded Joints.
In *Proceedings, Internatinal Conference on Fatigue of Welded Constructions*, pages P65-1 to P65-19. The Welding Institute, Brighton, UK, April, 1987.

[20] Keating,P.B. and Fisher,J.W.
Evaluation of Fatigue Tests and Design Criteria on Welded Details.
NCHRP Report 286, National Cooperative Highway Research Program, 1986.

[21] Slockbower,R.F. and Fisher,J.W.
Fatigue Resistance of Full Scale Cover-Plate Beams.
Fritz Engineering Laboratory Report 386.9(78), Lehigh University, June, 1978.

[22] Keating,P.B., Halley,S.A., and Fisher,J.W.
Fatigue Test Database for Welded Steel Bridge Details.
Fritz Engineering Laboratory Report 488.2(86), Lehigh University, May, 1986.

[23] Schelling,D.
Effects of 90,000 Pound Seagoing Container Vehicles Carrying International Freight on I-70 West and I-95 North Bridges, Part I.
Technical Report, Department of Civil Engineering, University of Maryland, July, 1986.

[24] Keating, P.B., Fisher, J.W., Yen, B.T., and Frank, W.J.
Fatigue Behavior of Welded Wrought-Iron Bridge Hangers.
In *Second Bridge Engineering Conference, Volume 2*, pages 113-120. Transportation Research Board, September, 1984.
Transportation Research Record 950.

[25] Schilling,C.G.
Stress Cycles for Fatigue Design of Steel Bridges.
Journal of the Structural Division, ASCE 110(6):1222-1234, June, 1984.

[26] Tebedge,N.
Measurements of Residual Stresses - A Study of Methods.
Master's thesis, Lehigh University, May, 1969.

[27] Lozano,S.
Residual Stress Redistribution in Welded Beams Subjected to Repeated Bending.
Fritz Engineering Laboratory Report No. 358.17A, Lehigh University, May, 1970.
(M.S. Thesis).

[28] Tall,L.
Residual Stresses in Welded Plates - a Theoretical Study.
Research Supplement 43(1), Welding Journal, 1964.

[29] Irwin,G.W.
Analysis of Stresses and Strains Near the End of a Crack Transversing a Plate.
Journal of Applied Mechanics :361-364, September, 1957.

[30] Westergaard,H.W.
Bearing Pressures and Cracks.
Journal of Applied Mechanics (61):A49-53, 1939.

[31] Paris,P.C., Gomez,M.P., and Anderson,W.E.
A Rational Analytic Theory of Fatigue.
The Trend in Engineering (13):9-14, 1961.

[32] Paris,P.C.
The Growth of Fatigue Cracks Due to Variation in Load.
PhD thesis, Lehigh University, Bethlehem, PA, 1962.

[33] Paris,P.C.
The Fracture Mechanics Approach to Fatigue.
Proceedings, 10th Sagamore Conference :107, 1965.

[34] Irwin,G.P.
Fracture Handbuch der Physik.
Sprinjer, Berlin, 1958, pages 551-590.

[35] Elber,W.
Fatigue Crack Closure Under Cyclic Tension.
Engineering Fracture Mechanics 2:37-45, 1970.

[36] Elber,W.
The Significance of Fatigue Crack Closure.
In *Damage Tolerance in Aircraft Structures, ASTM STP 486*, pages 230-242. American Society of Testing and Materials, 1971.

[37] Barsom,J.M. and Noval,S.R.
Subcritical Crack Growth in Steel Bridge Members.
NCHRP Report 181, National Cooperative Highway Research Program, 1977.

[38] Barsom,J.M.
Fatigue-Crack Propagation in Steels of Various Yield Strengths.
Journal of Engineering for Industry, Transactions of the ASME 33(11):1190-1196, November, 1971.

[39] Bucci,R.J., Clark,W.G.Jr., and Paris,P.C.
Fatigue Crack Propagation Growth Rates under a Wide Variation of ΔK for an ASTM A517 Grade F (T-1) Steel.
In *Stress Analysis and Growth of Cracks, Proceedings of the 1971 National Symposium on Fracture Mechanics, Part I, ASTM STP 513*, pages 177-195. American Society for Testing and Materials, 1972.

[40] Barsom,J.M.
Fatigue Behavior of Pressure-Vessel Steels.
WRC Bulletin No. 194, Welding Research Council, New York, May, 1974.

[41] ASTM.
Standard Test Method for Measurement of Fatigue Crack Growth Rates.
ASTM Specification E647-86A.
1986

[42] Herman,W.A., Hertzberg,R.W., Newton,C.H., and Jaccard,R.
A Re-evaluation of Fatigue Threshold Test Methods.
Fatigue 87.
1987

[43] Wei,R.P. and Shih,T.T.
Delay in Fatigue Crack Growth.
International Journal of Fracture 10(1):77-85, 1974.

[44] Alzos,W.X., Shat,A.C.,Jr., and Hillberry,B.M.
Effects on Single Overload/Underload Cycles on Fatigue Crack Propagation.
In *Fatigue Crack Growth Under Spectrum Loads, ASTM STP 595*, pages 41-60. American Society for Testing and Materials, 1976.

[45] Abtahi,A., Albrecht,P., and Irwin,G.R.
Fatigue of Periodically Overloaded Stiffener Detail.
Journal of the Structural Division, ASCE 102(ST11):2103-2119, November, 1976.

[46] Jonas,O. and Wei,R.P.
An Exploratory Study of Delay in Fatigue-Crack Growth.
International Journal of Fracture Mechanics (7):116-118, 1971.

[47] Vecchio,R.S., Hertzberg,R.W., and Jaccard,R.
On the Overload Induced Fatigue Crack Propagation Behavior in Aluminum and Steel Alloys.
Fatigue of Engineering Materials and Structures 7(3):181-194, 1984.

[48] Hudson,C.M. and Hardrath,H.F.
NASA Technical Note D-960.
1961

[49] Elber,W.
Effects of Shot-Peening Residual Stresses on the Fracture and Crack-Growth Properties of D6AC Steels.
In *Fracture Toughness and Slow-Stable Cracking - ASTM STP 559*, pages 45-58. American Society for Testing and Materials, 1974.

[50] von Euw,E.F.J., Hertzberg,R.W., and Roberts,R.
Delay Effects in Fatigue Crack Propagation.
In *Stress Analysis and Growth of Cracks, Proceedings of the 1971 National Symposium on Fracture Mechanics, Part I, ASTM STP 513*, pages 230-259. American Society for Testing and Materials, 1972.

[51] Zwerneman,F.J.
Fatigue Crack Growth in Steel Under Variable Amplitude Load-Time Histories.
PhD thesis, The University of Texas at Austin, December, 1985.

[52] Tada,H., Paris,P.C., and Irwin,G.R.
The Stress Analysis of Cracks Handbook.
Del Research Corp., Hellertown, PA, 1973.

[53] Maddox,S.J.
Assessing the Significance of Flaws in Welds Subject to Fatigue.
Welding Journal (53), September, 1974.

[54] Albrecht,P. and Yamada,K.
Rapid Calculation of Stress Intensity Factors.
Journal of the Structural Division, ASCE 103(ST2):377-389, February, 1977.

[55] Irwin,G.R.
Crack Extension Force for a Part Through Crack in a Plate.
Transactions, American Society of Mechanical Engineers (E29), December, 1962.

[56] Zettlemoyer,N. and Fisher,J.W.
Stress Gradient Correction Factor for Stress Intensity at Welded Stiffeners and Cover Plates.
Welding Research Supplement, AWS (12):393s-397s, December, 1977.

[57] Zettlemoyer,N.
Stress Concentration and Fatigue of Welded Details.
PhD thesis, Lehigh University, October, 1976.

[58] Norris,S.N.
The Prediction of Fatigue Lives of Welded Web Attachments.
Master's thesis, Lehigh University, May, 1979.

[59] Zettlemoyer,N. and Fisher,J.W.
The Prediction of Fatigue Strength of Welded Details.
Fritz Engineering Laboratory Report No. 386-10, Lehigh University, May, 1978.

[60] Gurney,T.R.
Fatigue of Welded Structures, 2nd Edition.
Cambridge University Press, 1979.

[61] Smith,I.F.C. and Gurney,T.R.
Numerical Study of Geometrical Effects in Longitudinal Non-Load-Carrying Fillet Welded Joints.
Final Contract Report 3765/2/83, The Welding Institute, October, 1983.

[62] Miki,C., Nishino,F., Harabayashi,Y., and Ohga,H.
Fatigue Strength of Longitudinal Welded Joints Containing Blowholes.
Proceedings of JSCE (325):155-165, September, 1982.

[63] Miki,C., Nishino,F., Sasaki,T., and Mori,T.
Influence of Root Irregularity of Fatigue Strength of Partially-Penetrated Longitudinal Welds.
Proceedings of JSCE (337):223-226, September, 1983.

[64] Miki,C. Nishino,F., Tajima,J., and Kishimoto,Y.
Initiation and Propagation of Fatigue Cracks in Partially-Penetrated Longitudinal Welds.
Proceedings of JSCE (312):129-140, August, 1981.

[65] Tajima,J., Asama,T., Miki,C., and Takenouchi,H.
Fatigue of Nodal Joints and Box-Section Members in a Bridge Truss.
Proceedings, IABSE Colloquium - Lausanne, Fatigue of Steel and Concrete Structures :353-359, 1982.

[66] Maddox,S.J.
A Fracture Mechanics Approach to Service Fatigue in Welded Structures.
Welding Research Institute 4(2):1-30, 1972.

[67] Schilling,C.G. and Klippstein,K.H.
New Method for Fatigue Design of Bridges.
Journal of the Structural Division, ASCE 104(3):425-438, March, 1978.

Vita

The author was born in New York City on May 24, 1957. He is the fourth of five children of Dr. and Mrs. Richard P. Keating.

The author received his primary education in Ridgewood, New Jersey. In the fall of 1975 he entered Lehigh University. He earned the degree of Bachelor of Science in Civil Engineering from Lehigh University in June 1980 and the Bachelor of Arts in Arts and Sciences in January of 1981. After having completed one semester of graduate school at Lehigh University, he was employed by the New Orleans office of Modjeski and Masters, Consulting Engineers, from September 1981 to July 1982. After returning to Lehigh University in the fall of 1982, he received the degree of Master of Science in Civil Engineering in October of 1983. He continued his studies at Lehigh University towards the degree of Doctor of Philosophy in Civil Engineering.